Single-Particle Tracking of Proteins in Living Bacteria:

From Single Cells to a Mixed Community

by

Chanrith Siv

A dissertation submitted in partial fulfillment
of the requirements for the degree of
Doctor of Philosophy
(Biophysics)
in the University of Michigan
2017

Doctoral Committee:

Assistant Professor Julie S. Biteen, Chair
Associate Professor Matthew R. Chapman
Professor Victor J. DiRita, Michigan State University
Professor Ari Gafni
Assistant Professor Sarah L. Veatch

Chanrith Siv

csiv@umich.edu

ORCID ID: 0000-0002-9925-5120

To Grandma and my parents, whose sacrifices gave me an opportunity to come to America to have a chance at the American dream

Acknowledgements

This graduate school journey has been one of the most challenging experiences I have encountered thus far in my life. Though there were many hurdles to overcome, the rewards at the end of it all definitely outweighed all of the late nights spent in lab doing experiments. This academic pursuit was not something I would have ever imagined myself doing growing up, but I am truly grateful for all of the opportunities that I have received throughout my academic career. Everything that I have accomplished so far would not have been possible without the support of some important people in my life. I would like to express my sincerest gratitude towards everyone who have played a role in shaping my journey.

Finishing this dissertation would not have been possible if it wasn't for my amazing advisors, Professors Julie Biteen and Victor DiRita. To Julie, thank you for trusting and believing in me to take on risky, scary challenges in my projects and in my career endeavors. I would not have been able to receive the necessary tools to land this dream job if it wasn't for you supporting and allowing me to explore different, non-traditional avenues in graduate school. To Vic, thank you for letting me be a part of your lab and teaching me how to be more confident in science and in life. Thank you for the pep talks and thoughtful advice you have given me throughout the years. You two have always been there—even in the midst of your busy schedules—to reassure me that everything will be all right in the end. I am sorry that I will not be pursuing an academic career in the future, but I promise to make you both proud in some other ways. I will not let your many years of training me go to waste.

Next, I would like to thank my committee members, Professors Sarah Veatch, Ari Gafni, Kim Seed and Matt Chapman. Thank you for coming to all of the meetings and providing wonderful feedback. Though you were all hard on me at times, I appreciate the constructive feedback because it made me a better scientist in the end.

I am also indebted to the lab members who I have worked with during graduate school. You guys have taught me so much about science and about perseverance. You guys have provided me with wonderful work environments where I was allowed to be myself. I am definitely going to miss such a positive work environment. Thank you for all of the fun we have shared throughout the years; you guys definitely made work a lot easier. I especially want to thank Yi who have helped me tremendously in the past five years in the lab. To the members of the Seed and Chapman labs, I want to thank you all for welcoming me and allowing me to do experiments in your lab space.

I would also like to thank my closest friends. I'm sorry that I am not listing specific names of people, but I am sure you guys all know who you are. You guys have put up with my rants about life and have always kept me in check. If it wasn't for you guys listening and helping me get through this journey, I probably would've had more meltdowns.

Last but not least, I want to thank my family. To Mom and Dad, thank you for your unconditional love and support. It has been over 9 years since I first left home, but I have never once felt far away from you guys. To my brother Sotheara, thank you for everything you have done for me. Though I may be tough on you, just know that it is all coming from a very good place in my heart. To my older brother Sothearak and his family, thanks for the enjoyable memories for when I visited home. Though you all may not always understand everything that I have gone through to get this PhD, you guys were always there for me.

I am only where I am today because of the many people who have contributed to my success.

Chanrith Siv

Table of Contents

List of Tables

List of Figures

List of Appendices

Abstract

Bacteria consist of only a single cell, but these prokaryotes are amazingly complex. Bacteria are among the earliest forms of life that appeared on Earth billions of years ago; they are found in all types of environments including the human body. Understanding protein behavior in bacteria may provide new insights into their roles in shaping human health and disease. Owing to their small sizes, the diffraction limit of light has always limited subcellular imaging inside bacteria. With the advent of super-resolution microscopy, it became possible to visualize subcellular processes with very high sensitivity, specificity, and spatial resolutions. Coupled with single-particle tracking, it is now possible to detect and track macromolecules with tens-of-nanometers precision to understand the mode of motion of individual macromolecules, including confinement, restriction, and directed motion in real time. These modes of motion can be used to infer the activity of these macromolecules in biological processes happening inside living cells. The work in this thesis develops several novel approaches to studying microbial cell biology. In particular, I apply these methods to two non-model microbial systems: the pathogenic *Vibrio cholerae* and a set of human-gut anaerobes.

By investigating a transcription regulator in *V. cholerae*, I provide new knowledge about the expression systems typically used for understanding bacterial gene expression in the virulence regulation pathway. With advanced super-resolution imaging and single-molecule tracking methodologies, I probe changes in the subcellular dynamics of TcpP in live *Vibrio cholerae* in response to several growth conditions. I discover that differences in labeling, expression systems, and hosts can change the dynamics of TcpP, and thus these changes will

affect the toxin production in *V. cholerae*. Because single-molecule tracking is sensitive to the heterogeneous distribution of protein dynamics in live cells, the results reveal subcellular phenotypes that were previously hidden by bulk experiments. Furthermore, by fluorescently labeling another transcriptional regulator, ToxR, I show that ToxR and TcpP can be imaged simultaneously in the same bacterial cell. Based on this newly developed capability to obtain localizations and dynamics of these two proteins in a live cell, I present first explorations toward real-time, two-color super-resolution investigation of a regulatory pathway in a live pathogen. The findings in Chapter 2 and 3 suggest that single-molecule tracking of proteins provides a very sensitive assay to detect subtle differences in protein dynamics—and thus protein activities—that are hidden by *in vitro* measurements.

Additionally, I present the first imaging investigation of a co-culture of live, obligate anaerobes: *Bacteroides thetaiotaomicron* and *Ruminococcus bromii*. By developing several methods to characterize these two bacterial species with microscopy, I demonstrate in Chapter 4 the feasibility of growing and imaging multiple bacterial species from the same co-culture. Furthermore, I test the applicability of novel fluorescent proteins for use in anaerobic imaging conditions. This work on anaerobic co-culture systems shows the capability of high-resolution imaging at the nanoscale for future work addressing emerging questions related to the human gut microbiome. Overall, the results presented in this thesis demonstrate the capabilities of single-molecule imaging and single-molecule tracking in non-model bacterial systems to investigate unique questions regarding bacteria even bigger roles in human health and disease.

Chapter 1: Introduction

The work presented in this dissertation examines the applications of single-molecule fluorescence microscopy to two non-model bacterial systems: pathogens and anaerobic bacteria. In this chapter, I introduce optical microscopy and explain the importance of increasing spatial resolutions down to the nanometer-scale to unveil the inner workings inside live bacteria. I highlight available fluorescence labeling methods commonly used for bacterial imaging, as well as explain the drawbacks of these methods. Then, I review the body of literature regarding pathogenesis in *Vibrio cholerae* and the associated cholera disease. I introduce some examples of biological mechanisms occurring at bacterial cell membranes in *V. cholerae* and in other pathogens. Finally, I introduce the ongoing research to understand bacterial behavior in a microbiome.

1.1 Light microscopy in bacteria

The applications of light microscopy have been invaluable to modern cell biology. This instrument has allowed us to visualize living objects invisible to the naked eye, and enabled us to peek into subcellular structures in a non-invasive, minimally perturbing way. The resolution of a light microscope is well-matched to the cellular components of many eukaryotes, and thus makes this method a very useful tool in research and clinical settings. Even the smallest living objects like bacteria can be observed and cell shape recognized at only 100x magnification.

In brightfield microscopy, light from an incandescent source is aimed through the sample, causing the light to be absorbed, scattered or deflected by the sample. Brightfield micrsocopy has been used to visualize cells, but an additional staining process is often needed in order to enhance contrast in the microscope image **(Figure 1.1a)**[1] since cells are thin and transparent. Though stains and dyes are frequently used in biology and medicine to highlight structures in biological tissues for viewing, staining may destroy or introduce artifacts. Therefore, a phase-contrast microscope is more widely applicable for observing transparent, unstained, live cells. This optical microscopy technique converts phase shifts in light passing through a transparent specimen to differences in image contrast. As a result of making phases visible, biological processes can be observed and recorded with high contrast, sharp clarity, and minute specimen detail[2]. For bacteria, phase-contrast microscopy has been a useful tool for shape analysis, since a light-dark boundary around the entire cell makes it easy to determine by cell-segmentation algorithms **(Figure 1.1b)**[3]. However, phase-contrast microscopy is not ideal for thick samples as phase artifacts may distort details around the perimeter of the sample.

The technique of fluorescence microscopy has become an essential tool in biology due to attributes that are not readily available in other contrast modes with traditional optical microscopy. In this microscopy technique, fluorophores absorb one wavelength of light and emit light at a longer wavelength to produce a physical phenomenon described as fluorescence[4]. With the discovery of the green fluorescent protein[5] (GFP), virtually any non-fluorescent protein of interest can be made to fluoresce. Therefore, with an array of available fluorochromes, fluorescence microscopy has made it possible to identify cells and sub-microscopic cellular components with a high degree of specificity amid non-fluorescing material. By specific attachment of fluorophores to proteins of interest, selective proteins in live bacteria can be

localized and followed over time **(Figure 1.1c)**. Furthermore, with the right fluorescence filters, multi-color imaging can be achieved to visualize multiple macromolecules simultaneously to see protein complexes and cellular factories, resembling a more relevant depiction of the complexity of biology. Though fluorescence microscopy holds great promise for broad applications in biology, the sensitivity of fluorescence detection is compromised by background signals, either from cellular autofluorescence or from unbound and non-specific reagents[6,7], and by blurring, bleaching and bleedthrough of signals[8].

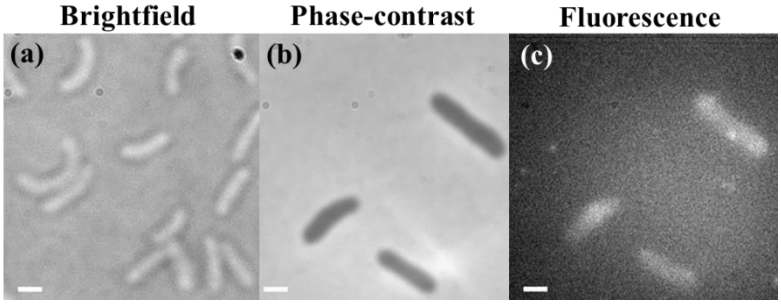

Figure 1.1 Live *Vibrio cholerae* imaged using different microscopy techniques: (a) brightfield, (b) phase-contrast, and (c) fluorescence. A transcription regulator in *V. cholerae* was fused with a fluorescent protein to provide fluorescence in (c). Scale bars: 1 µm.

The fluorescence microscope cannot provide spatial resolution below the diffraction limit, but the detection of fluorescing molecules below such limits is readily achieved with the advent of super-resolution methods. Therefore, it is possible to precisely localize macromolecules in space with high precision and to follow them in living cells to visualize molecular events and obtain dynamics. Fluorescence microscopy has advanced our understanding of biology and medicine[8], and has motivated the scientific community to explore how macromolecules function and come together to carry out biological processes of survival and adaptation in prokaryotes to eukaryotes[9-12].

1.2 Single-molecule imaging

In the mid-1980s, nanometer-scale detection was achieved for single electrons or ions confined in vacuum electromagnetic traps[13-15], scanning tunneling microscopy (STM)[16] and atomic force microscopy (AFM)[17]. Shortly after, single pentacene molecules were detected at liquid-helium temperatures[18,19]. Then single fluorescent dye molecules were detected at room temperature using near-field optical techniques and wide-field microscopy only a few years later[20,21]. As development in single-molecule imaging allowed for applications in cell biology, imaging experiments were first performed on mammalian cells[22]. Because mammalian cells are on the order of tens of microns compared to a few microns in bacteria, single-molecule detection was more readily done in these cells than in bacterial cells with green, blue, cyan, and yellow fluorescent proteins.

Single-molecule fluorescence (SMF) microscopy quickly became widely used in all areas of biology for many different applications, such as accessing chromatin substructures and organization[23-25], genome mapping[26,27], membrane transport[28], viral infection[29], and cell division[30,31]. With the sensitivity achieved from single-molecule measurements, it was possible to identify rare molecular events that were previously masked by ensemble averaging[32]. By circumventing the diffraction limit that restricted conventional light microscopy, SMF microscopy enabled the visualization of subcellular events *in vivo* with nanometer precision at millisecond time scales[22,33-35]. In mammalian cells, SMF microscopy has been applied to studies of macromolecular dynamics and interactions in and on the plasma membrane, revealing mechanisms of specialized membrane domains such as clathrin-coated pits, focal adhesions, synapses, signaling in immune cells, and others[22,36-38]. In bacterial cells, subcellular imaging SMF microscopy have contributed to the understanding of cytoskeletal organization, DNA

structure, and the central dogma of biology—replication, transcription and translation[39-41]—with nanometer-scale resolutions. Although conserved mechanisms in microbiology are still being elucidated in model bacterial systems like *Escherichia coli*[10], a wider range of bacterial species are now readily studied with SMF imaging[42-45]. The development of genetic tools in non-model bacteria has opened the field to visualize the inner workings of pathogens and the human gut microbes[46,47].

A fluorescently labeled biological sample typically contains a high density of fluorophore, and therefore make them difficult to resolve by the single-molecule localization approach. The resolution is limited by the diffraction of light passing through a lens that transforms the light emitted from a molecule into an Airy disk often more than 100 times its actual size[48]. Therefore, even light from an infinitesimally small emitter cannot be focused to a point, but rather expanded by the diffraction limit of light through this equation:

$$d = \frac{\lambda}{2NA} \qquad 1.1$$

where d is the smallest distance resolvable between two adjacent objects, λ is the wavelength of light, and NA is the numerical aperture of the objective lens. Even with the best available objectives (NA ~1.4 - 1.5), the diffraction-limited spot still has a diameter ~250 nm for an optical microscope.

However, if single emitters can be separated in space, the center positions of each emitter can be fit to a function to obtain nanometer-localization precision. The precision with which a molecule can be localized (Δx) depends on several factors: the size of the pixels in the detector (a), the background noise (b), the standard deviation (s) of the point-spread function, PSF, and the number of photons detected (N), as described by this equation[49]:

$$\Delta x = \sqrt{\frac{s^2 + \frac{a^2}{12}}{N} + \frac{8\pi s^4 b^2}{a^2 N^2}} \quad 1.2$$

Therefore, as long as background noise is minimized and the probes each give off many photons, it is possible to resolve single-molecules down to nanometer resolutions. In our two-dimensional optical set-up, we achieve ~50 nm resolutions along the *x*- and *y*-axes with fluorescent proteins.

SMF microscopy requires that the fluorophore being imaged be isolated in space from other emitters; it is difficult to distinguish individual molecules in a system with thousands of molecules. To accommodate this diffraction limit, single-molecule experiments require very low labeling densities to distinguish two molecules in space. In small cells like bacterial cells, a max of only a few fluorophores can be resolved at one time because the short axis of bacteria is only ~3-4 times the size of the diffraction limit. The discoveries of photoswitchable (PS)[50-52] and photoactivatable (PA)[53,54] fluorescent proteins (FPs) overcame this experimental constraint to allow higher localization precisions to be achieved in bacterial cells. By incorporating PA-FPs that switch from non-fluorescent to fluorescent states, Photoactivated Localization Microscopy (PALM)[22] and Fluorescence Photoactivation Localization Microscopy (FPALM)[55] separate FPs temporally in a diffraction-limited region because only a small subset of emitters are stochastically activated at one time, and then the experiment is repeated until all emitters are localized. Therefore, each individual FP can be localized with tens of nm precision by fitting the PSF to a 2D Gaussian function. PALM provides a high-density map of the distribution of protein in cells, but cytotoxicity can sometimes be the tradeoff[56]. To obtain lots of single-molecule localizations, imaging is typically done with high laser powers and long imaging durations. Photoactivation and photoswitching requires activation by 405-nm laser light, and this wavelength is enough to kill cells.

Since high spatial resolution can been attained with super-resolution methods, combining necessary optics with super-fast video-rate can provide insight into subcellular dynamics in relevant time scales[57]. A protein can be tracked for a reasonable amount of time (i.e., up to 30s) for as long as the sample does not drift over the acquisition period—usually up to a few minutes—and the molecule has not photobleached. A technique like PALM combined with single-particle tracking[58] can resolve the localizations and dynamics of individual molecules in live cells; acquiring a large dataset of single-molecule trajectories is needed to accurately determine molecular environments and detect heterogeneous diffusion within a single cell.

1.3 Fluorescence labeling methods

Almost all proteins have intrinsic fluorescence from their aromatic amino acid residues—tyrosine, phenylalanine, and tryptophan—but the photophysical properties (e.g., quantum yield and brightness) are not optimal for single-molecule work. Most bio-molecules, therefore, require selective attachment of extrinsic labels in order to be visualized by fluorescence microscopy. The choice of fluorophore labels and labeling schemes depends on whether an intracellular or extracellular protein of interest is under investigation. Small organic dyes and fluorescent proteins (FPs) are two classes of fluorophores commonly used in biology; these two fluorophores differ in their specificity, size, and stability[59]. Labeling with organic dyes requires conjugation to antibodies, enzymes, or chemical moieties, which each have their own advantages and disadvantages for cellular imaging. Antibody conjugation is both specific and quantitative *in vitro*[60,61] because the antigen can recognize a specific protein moiety, but antibodies are large (~150 kDa), polyvalent, less specific, and most importantly, not compatible with live-cell imaging. Enzyme-conjugation methods, such as the CLIP-tag[62] (20 kDa), SNAP-tag[63] (20 kDa), and HALO-tag[64] (33 kDa) technologies, are more efficient reactions than antibody conjugation

since a covalent interaction between an enzyme-substrate pair leads to greater specificity. However, a drawback of these enzymatic labeling methods is that they require the complete clearing of any free (unconjugated) dyes in the system to reduce background signals, which is not always attainable. Another labeling method, chemical moiety conjugation[65], eliminates the limitations on size by relying on side chain interactions (i.e., bonding to the ester group with primary amine of lysine chain); this labeling chemistry requires that specific side chains be exposed on the exterior of proteins. Due to the properties of organic dyes that make them ideal for high-resolution imaging, organic dye conjugation may be incomplete or nonspecific which is less than ideal for live-cell imaging[66,67]. FP labeling differ from organic-dye labeling methods described above in that FP labeling genetically fuses the FP gene to the target gene to produce a fusion gene that then gets translated into a single amino acid chain. By not relying on a chemical reaction for fluorophore attachment, FB labeling singularly labels all target proteins and ensures that there are no freely floating, unattached fluorophores[68]. The genetic encodability of FPs makes this labeling method the most suitable method for live-cell imaging.

Though no other labeling methods rival FP labeling in terms of specificity, there are drawbacks to using FPs as probes. Even the most optimized FPs suffer from less than ideal folding efficiencies (<100%) and slow maturation times (~30 mins)[54], which may limit their uses in some biological applications. Additionally, not every FP in the cell will fluoresce. Since FPs are not as bright as organic dyes, the presence of naturally fluorescent molecules in the cell may contribute to even lower signal-to-noise ratios. Autofluorescence in cells commonly comes from DNA (~380 nm), aromatic amino acid residues (~350-450 nm), NADPH (~450 nm), folic acid (~450 nm), retinol (~515 nm), and flavin (~540 nm). Despite having more optimal fluorescence properties, such as better quantum yields and brightness, organic dyes are not used as probes for

intracellular macromolecular labeling in bacteria, especially in Gram-negative bacteria, because these dyes do not readily diffuse into the bacterial cytosol[69]. The outer and inner cellular membranes in Gram-negative bacteria prevent dye permeation from diffusing into bacteria[70]. Despite the discovery of cell-penetrating peptides[71] (5-40 amino acids) for intracellular transport of larger molecules exist, this delivery system is not yet compatible in bacteria. In addition, the microinjection of organic dyes, which is commonly utilized in eukaryotes, is not feasible in bacteria because the microinjection needles themselves are on the same order of magnitude as the size of bacteria[72]. Despite these drawbacks, there are applications involving labeling with organic dyes in bacteria but these are generally restricted to fixed-cell studies and/or investigations of outer-membrane proteins in live bacterial cells. **Table 1.1** lists the optical properties and oligomeric states of the fluorophores used in this thesis.

Table 1.1 Optical properties and oligomeric states of fluorophores used in this study.

Fluorophore	Photo-Activation (nm)	Excitation maximum (nm)	Emission maximum (nm)	Quantum yield	Brightness (%)*	Oligomeric state
mCitrine[73]	N/A	516	529	0.76	174	monomer
PAmCherry[74]	405	564	595	0.22	77	monomer
PA-GFP[53]	405	504	517	0.79	132	monomer
CreiLOV[75]	N/A	450	495	0.51	85	monomer

*relative to eGFP brightness

1.4 Expression of fluorescent protein fusions in bacteria

FP labeling introduces foreign DNA into bacteria through chemical competence (heat-shock), mechanical disruption (electroporation), or natural transformation[76,77]. Once the fusion DNA is stabilized in bacteria, the protein is either expressed ectopically from a plasmid or endogenously from a location on the chromosome. An advantage to using ectopic expression to

produce protein fusions is the ability to overexpress low-copy number proteins; this is valuable in the case that less than half of FP-fused proteins are turned on due to the intrinsic nature of these FPs[54,78]. However, plasmid-expression may lead to overexpression which can induce artificial responses and possible toxicity[79]. Another disadvantage of ectopic expression from a plasmid is that these expression vectors are often leaky, and will result in protein production independent of induction. Though ectopic expressions may result in comparable expression levels to native expression levels, these levels will never be equivalent to native expression.

In order to maintain native expression levels, protein fusions are endogenously expressed from their native promoters on the bacterial chromosome. Creating cell strains with endogenous expression of protein fusions can be time consuming due to the selection and screening processes required to identify transformants[80], but it is the only method that guarantees native expression levels. For bacteria that easily take up and incorporate foreign and linear DNA fusions into their chromosomes by homologous recombination, labeling at the endogenous locus is not too difficult[81,82]. However, for non-model bacteria and some pathogens, the DNA fusion must first be cloned into a helper or a suicide vector before homologous recombination can proceed[80,83]. A major disadvantage for using additional vectors is that it is not always possible to ligate DNA fusions that are bigger than the vectors themselves, therefore, allelic exchange may not always be a feasible option. Though methods like recombineering[84] and the CRISPR/Cas system[85] make genetic editing possible for the insertion of bigger genes, these methods are not easily implemented. Since these latter methods rely on single-stranded DNA with very minimal homologous sequence requirements, these cloning methods are more readily adapted for bacteria without a natural competence system.

Regardless of the method used for genetic engineering, the location of the FP insertion in the target protein needs to be properly addressed to minimize perturbations to the native structure and function of the target protein. Most protein fusions typically fuse a FP to either the N- or C-terminus with or without a short flexible linker sequence. Sometimes, if a flexible region already exists at internal loops within the protein, protein fusions can be made there as well. A poorly placed label has the potential to completely disrupt protein-protein interactions and other relevant interactions in the cell. In many instances, where the size of the FP is comparable to the size of the protein target, proper experimental controls are needed to test for stability and validate function of the protein fusion.

Though FP labeling is commonly used for bacterial imaging, this method of labeling may introduce artifacts like mislocalization and dimerization because GFP and other non-optimized FPs are naturally tetrameric[73,86]. The natural tendencies of FPs to form quaternary structures can be minimized or eliminated through genetic manipulations, but these monomeric versions of FPs still exhibit some agglomeration even after years of optimization[87,88]. This oligomerization problem becomes a critical problem in experiments where multiple proteins are labeled. The native interactions and co-localizations of these protein fusions may be hindered by the agglomeration of these labels. Therefore, it is necessary to always carry out proper controls to determine that the labeled protein behaves like the unlabeled protein.

1.5 Cholera

Since its inception in 1817, eight pandemics of the cholera disease have been recorded with the most recent occurring in 1992[89-91]. In the United States, water-related spreading of this disease has been eliminated by modern water and sewage treatment systems. However, cholera remains a great public health concern in parts of Africa, Asia, and Latin America. This

gastrointestinal disease still afflicts more than 5 million people annually[92]. Cholera infections often result in life-threatening secretory diarrhea characterized by voluminous diarrhea, vomiting, hypovolemic shock and acidosis, but cholera is treatable if bacterial titer is detected early in the infection cycle. Cholera is not only epidemic but endemic to ~50 countries of poor sanitation, and thus treatment methods oral rehydration and antibiotics are often countered by the lack of clean water supplies[93,94].

Cholera is caused by a Gram-negative bacterium, *Vibrio cholerae*, and transmitted to humans by the ingestion of contaminated food and water sources. These bacteria are identified under the microscope by their curved rod shapes and a single polar flagellum. *V. cholerae* is classified as toxigenic or non-toxigenic based on their ability to produce the enterotoxin, cholera toxin (CTX), which creates imbalance of ions in the host to cause large amounts of water loss from the body[95]. Toxigenic strains of serogroups O1 and O139 have caused widespread epidemics around the world, but other serogroups exist and have caused milder, isolated outbreaks[96,97]. *V. cholerae* strains are classified by the agglutination in their O-group specific antiserum directed against the lipopolysaccharide component of their cell wall. Within O1, there are 2 biotypes, classical and El Tor, and each biotype has 2 distinct serotypes, Inaba and Ogawa. The clinical symptoms are indistinguishable, however, the El Tor biotype infections are typically associated with milder symptoms. Globally, most cholera outbreaks are caused by O1 El Tor biotype. Since 1986, an El Tor variant which has characteristics of both classical and El Tor biotypes emerged in Asia and was spread to Africa and the Caribbean, causing more severe episodes of cholera and higher death rates[96-98]. This thesis will focus on the *V. cholerae* O1 since O395 has been extensively characterized. The O1 serogroup was also responsible for seven of the last eight pandemics around the world, and therefore, identifying molecular events within this

serogroup may contribute to better understanding of the pathogenicity to reduce the severity of the outbreaks in future pandemics.

1.6 *V. cholerae* pathogenesis

During its lifetime, *V. cholerae* colonizes multiple environments where varying pH levels and temperatures are experienced[99]. Because various O1 and non-O1 *V. cholerae* have been isolated from diverse geographic areas around the world, this suggests that *V. cholerae* may have been formed in multiple aquatic microenvironments. *V. cholerae* are often associated with copepods or other zooplankton, shellfish, and aquatic plants[100]. To be infectious in humans, *V. cholerae* must pass through the acidic environment of the gut and colonize on the surface of the intestinal epithelial cells; this colonization requires the toxin co-regulated pilus (TCP)[93]. It is important to elucidate the mechanisms by which CTX and TCP make *V. cholerae* pathogenic in order to cure the disease, rather than to just to treat its symptoms.

As mentioned above, the two most important virulent factors critical for causing the cholera infection are CTX and TCP. CTX is a bipartite toxin with six subunits: one α subunit and five β subunits[101]. When localized inside the intestinal epithelial cells, the CTX-α subunit adenosine diphosphate (ADP) ribosylates G-proteins to constitutively activate cyclic adenosine monophosphate (AMP) production, which leads to the rapid secretion of chloride ions and water that causes severe diarrhea[102]. TCP, a type IV pilus, is responsible for microcolony formation, and acts as a receptor for the bacteriophage CTXϕ; this bacteriophage harbors the genes that encode CTX. CTXϕ is generally present as an integrated section of the genome—on each of the two chromosomes in O1 serotype and tandemly on the larger chromosome in El Tor biotype—rather than in a virion form[103]. Without TCP production, *V. cholerae* strains are not toxigenic and cause infections in humans. The gene expressions of CTX and TCP are the result of a

multiprotein regulatory cascade known as the ToxR regulon, coined after the discovery of ToxR, a key positive regulator of virulence[104].

The ToxR Regulon, a collection of regulatory elements composed of ToxS, ToxR, TcpP and TcpH, regulates CTX and TCP gene expression **(Figure 1.2)** through the activation of ToxT, a direct activator of the genes encoding CTX and TCP[105]. ToxT has two domains with distinct functions. The AraC/XylS family domain, C-terminal domain (CTD), of ToxT mediates DNA binding via two helix-turn-helix motifs. The CTD binds DNA as a dimer to two toxboxes, a 13-bp degenerate DNA sequence, organized as inverted repeats positioned at -44 to -67 relative to the +1 transcription start site of *toxT*. The N-terminal domain (NTD) of ToxT is a non-conserved region that shares no homology to any other proteins, but contains dimerization and regulatory elements that respond to positive effectors (i.e. bicarbonate) and negative effectors (i.e. bile and unsaturated fatty acids)[106]. Because the *toxT* gene is located in the *tcp* operon, ToxT can regulate its own gene expression by activating transcription of itself from the *tcp* promoter via an autoregulatory loop, independent of ToxR and TcpP. However, initial ToxT production absolutely requires the interaction of ToxR and TcpP[107].

ToxR and TcpP are bitopic membrane proteins that work in conjunction at the *toxT* operon in the cytoplasm to activate transcription of *toxT* via their NTDs; they share homology with the NTDs of the OmpR/PhoB family[108]. The functions of the periplasmic domains of these proteins are not known, but TcpP and ToxR are hypothesized to interact in their periplasm domains to activate *toxT* gene expression[109,110]. While *toxR* gene expression is constitutive, *tcpP* gene expression and degradation is mediated by quorum sensing via the AphA, AphB, HapR, and cAMP receptor proteins. Additionally, the membrane-bound effector proteins ToxS and TcpH bind to ToxR and TcpP, respectively, in a wild-type *V. cholerae* strain in the periplasm.

The exact mechanisms are yet to be elucidated, but it is hypothesized that the ToxS and TcpH effector proteins stabilize and/or enhance dimerization of their interacting counterparts[110,111].

The role of ToxR in *toxT* gene expression is less important than that of TcpP. ToxR alone cannot activate the *toxT* promoter, while overexpression of TcpP can activate this operon in the absence of ToxR[112]. Unlike TcpP, ToxR is not readily degraded by proteases in nonvirulent *in vitro* growth conditions[113,114]. On the other hand, ToxR activates OmpU and represses OmpT, two outer-membrane porin proteins in *V. cholerae* in a TcpP-independent manner[115]. ToxR binds to the *ompU* promoter to activate *ompU* gene expression, while ToxR binds to the *ompT* promoter to interfere with cAMP-receptor protein binding to stop *ompT* transcription activation[116]. Though the function of OmpU is found to protect the cells from bile, organic acids and antimicrobial peptides, the function of OmpT is not yet elucidated. The roles of ToxR in regulating OmpT/OmpU expression levels may be the reason for ToxR incorporation into the virulence regulatory network.

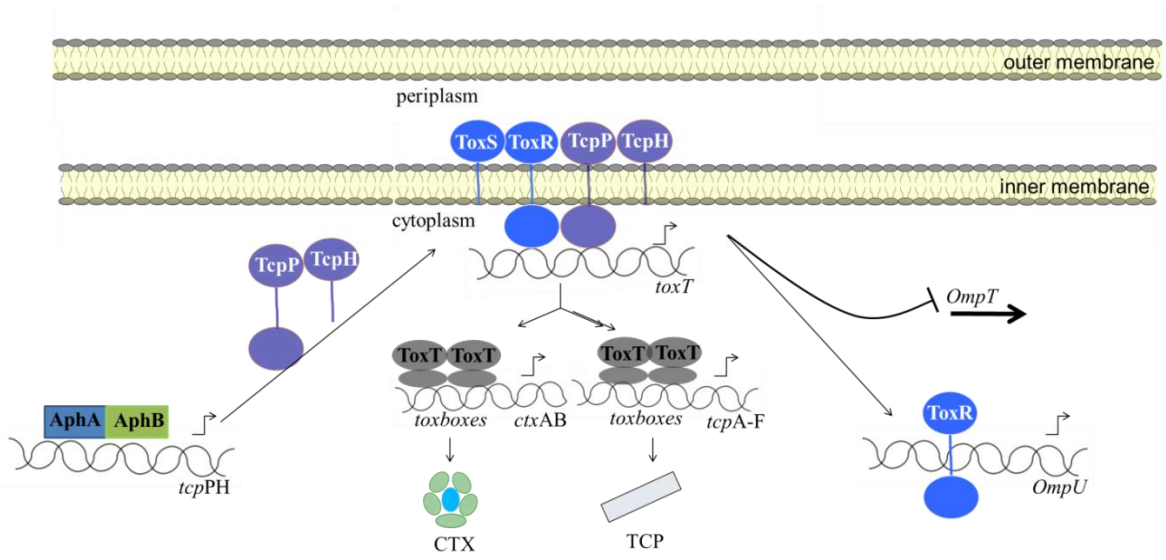

Figure 1.2. Model of the virulence cascade in *V. cholerae*. The pathway by which the ToxR Regulon (ToxS, ToxR, TcpP and TcpH) regulates gene expression of the major *V. cholerae* virulence factors CTX and TCP is tightly regulated by AphA and AphB. The expression of porins, OmpU and OmpT, is tightly regulated by ToxR.

It is known how *V. cholerae* causes infection in the human host, but the subcellular mechanism by which virulence gene production is turned on and off is not well characterized. It has been shown that TcpP, ToxR, and ToxT are proteolyzed *in vitro* under toxin-noninducing growth conditions[113,114]. Therefore, it is possible that late in the *V. cholerae* infection cycle, a termination mechanism exists that causes the bacteria to allocate its energy to maintain growth rather than to further colonize the host.

Though the elements in this toxin regulatory pathway have been identified, the mechanism by which membrane proteins can access DNA in the cell and recruit RNA polymerase has not been uncovered with standard genetic and biochemical approaches. So far single-molecule localization microscopy and tracking have added to a deeper understanding of the toxin regulatory pathway by elucidating a variation of the hand-hold model: a mechanism in which ToxR enhances TcpP diffusion along DNA by removing occluding nucleoid-associated proteins from the chromosome to facilitate TcpP diffusion, and ToxR also directly influences TcpP binding at the *toxT* promoter[47]. However, this mechanism was elucidated by tracking plasmid-expressed TcpP-PAmCherry that may or may not represent the "true" dynamics of TcpP. Furthermore, there remains to be a great deal of knowledge pertaining to the molecular-scale interactions happening within this regulon. Future experiments using these high-resolution imaging techniques will hopefully address the following questions: how often ToxR, TcpP, and other elements co-localize to form a stable complex; how sources of compaction and organization affect *toxT* transcription; and how locus freedom correlates with *toxT* transcription *in vivo*.

1.7 Biological mechanisms at the cellular membrane

Cellular membranes are essential components of life that act as barriers to separate the hostile extracellular environment from the cell interior, where all living reactions occur. Cellular membranes provide shape and structure, and allow cell motility to occur[117]. Bacteria can be classified into two categories based on the Gram-stain test: Gram-positive or Gram-negative[118]. Gram-positive bacteria take up the crystal violet stain, and then appear purple-colored under the microscope from the thick peptidoglycan layer in the bacterial cell wall. Gram-negative bacteria possess a cell envelope made of two membranes separated by a thin layer of peptidoglycan, and cause them to take up the counterstain (safranin or fuchsine) and appear red or pink. Because of their inner and outer membranes, Gram-negative bacteria transport macromolecules across the cell envelope using several types of secretion systems. In both Gram-positive and Gram-negative cell envelopes, the cellular membranes of bacteria allow for fundamental processes such as these: generating energy in the form of ion gradients; transporting ions, proteins, nucleic acids, nutrients and metabolites; and providing transduction systems to sense the surrounding environments[117,119]. Because the lipid portion of the outer membrane in Gram-negative bacteria is impermeable to charged molecules, porin channels in the outer membrane allow passive diffusion of molecules across the inner and outer membranes into the periplasm—the region between the cytoplasmic and outer membranes and the cytosol. The signals and substrates are available to be transported across the cytoplasmic membrane using transport and signaling proteins embedded in the periplasm[120,121].

An ability to adapt to changing environmental stresses and stimuli is essential for cell survival in all organisms. Bacteria sense environmental stimuli through cell surface receptors located on the periphery of the membrane, which in turn transduce the signals to intracellular

transcription factors to initiate gene expression in the cytoplasm. Although two-component signaling systems are found in all domains of life, they are most commonly found in bacteria, especially in Gram-negative bacteria[122]. This signaling system is achieved by the phosphorylation of a response regulator through a histidine kinase, which triggers a conformational change and leads to the activation or repression of target genes[123]. For most pathogens, sensing the host environment is crucial for inducing virulence in the host environment[124,125].

In bacteria, there is only one RNA Polymerase (RNAP) responsible for the transcription of all classes of RNA[126] compared to the multisubunit RNAPs in eukaryotes[126]. Since DNA and RNAP are localized in the bacterial cytoplasm, it has been generally assumed that transcription factors should be in close proximity to these transcription elements and have similar subcellular localizations. However, the initial discoveries of ToxR[127] and TcpP[128] in *V. cholerae* were quite surprising since these transcription regulators are membrane-localized. Though these two proteins do not contain any of the necessary elements of the prototypical two-component signaling system, ToxR and TcpP can still activate transcription. Because the membrane limits protein diffusion to two dimensions, whereas DNA is generally compact toward the center of the cell, it is still a mystery how membrane-bound transcription regulators bind specific regions on the DNA—like the helix-turn-helix motif in the cytosol. The discovery of these membrane-bound transcription activators in *V. cholerae* paved the way for the discovery of other membrane-bound transcription activators in other Gram-negative and Gram-positive bacteria[129].

Understanding the mechanism by which membrane-bound transcription activators like TcpP and ToxR induce gene expression can have a lot of impact in developing novel therapeutics to combat multidrug-resistant bacteria. Because bacterial membranes and

membrane-associated proteins and processes are the targets of natural antibiotics, they are also good drug targets for the development of novel synthetic antimicrobials. As mentioned previously, the membrane prevents passive penetration while the porins allow active transport of water-soluble compounds into the periplasmic space. Therefore, drug discovery must combat native efflux pumps that eject antibiotics and other foreign drugs into the extracellular space.

1.8 The human gut microbiome

The synergistic relationship between bacteria and humans begins at birth: when a newborn is immediately exposed to the microbial population in the surroundings[130,131]. As the baby matures through infancy and adulthood, the human digestive tract associated microbes—commonly referred to as the human gut microbiome—undergoes a succession of changes that are correlated with diet and numerous other external and internal host-related factors[132]. The human gut microbiome also contains archaea, viruses, and eukaryotic microbes, but here we only focus on anaerobic bacteria. The bacterial cells within the human gastrointestinal tract (GIT) outnumber the host cells by a factor of 10, and more than 100 times for the number of genes[133]. The human gut microbiome has recently emerged as a key factor in human health and diseases, especially in obesity, type 2 diabetes, cardiovascular disease, colorectal cancer, and inflammatory bowel diseases [133-137].

More than 50 bacterial phyla—mostly anaerobes—have been detected in the human gut to date through sequencing of the 16S rRNA-encoding genes[138]. *Bacteroidetes* and *Firmicutes* are the most dominant and conserved phyla in all individuals, representing up to 90% of the intestinal microbiota. Important variations in bacterial compositions are found between these individuals[139]; these variations depend on the selective pressures from the host for functions such

as in modulating diet, improving energy yields from food, regulating bile-acid metabolism, and regulating adipose tissue inflammation[140-142]. Because these gut microbes play important roles in human metabolism, nutrition, physiology, and immune function, new tools and methods outside of traditional microbiology methods are needed to uncover the complexity of this entangled networks of interactions[137,143].

Over the past several years, the European Metagenomics of the Human Intestinal Tract (MetaHIT) and the NIH-funded Human Microbiome Project accumulated copious amounts of microbial DNA sequences to understand the composition and the genetic potential of this complex ecosystem. By identifying the extensive non-redundant catalogue of the bacterial genes from the GIT, it is possible to distinguish bacterial functions that are housekeeping and those specifically for the gut[144]. All of this genetic information, along with metatranscriptomics, metaproteomics, metabolomics, are going to be useful as the field pushes toward understanding how structure and dynamics of different microbiota play a role in shaping human health and disease. Furthermore, studying human host/pathogen interactions can give us better understanding about commensalism, mutualism, and parasitism, but these experiments are not easily implemented and will require a lot of methods development.

In addition to using meta-omics data to determine the ecosystem inside the human gut microbiome, understanding how bacteria sustain life in a community at the cellular level may also be informative to identify the specific roles of each bacterial species in shaping the human microbiome. One direct tool that can be used to visualize the microbiome is single-molecule imaging[145]. This method can elucidate subcellular structure in bacteria, and can also elucidate key interactions involving proteins, RNA, and DNA. Though many single-molecule imaging experiments have been performed in live bacteria, these experiments mostly examine aerobic

bacteria in isolation[69,146]. One of the biggest challenges for examining anaerobes with fluorescence is identifying probes that can fluoresce without the use of oxygen as a cofactor — unlike GFP and its derivatives. Because of this oxygen limitation, imaging in anaerobes has been limited to studying proteins localized in the outer membrane where organic dye labeling is readily achieved. A recent advance in my lab elucidated the mechanism by which the abundant gut symbiont *Bacteroides thetaiotaomicron* (*B. theta*) recognizes and processes carbohydrates which humans cannot themselves digest, through the investigation of single *B. theta* cells grown in isolation[46]. Though this study was a good starting step toward visualizing the gut microbiome, it is necessary to take it a step further to image two bacterial species and then to image a community of bacteria. There is hope for nanoscale imaging of the microbiome in the future to impact our understanding of the coexistence of bacteria and the human host.

1.9 Dissertation objectives

While there are numerous applications of single-molecule imaging in bacteria, most focus on model systems like *E. coli*, *Bacillus subtilis*, or *Caulobacter crescentus*. The simplicity and ease with which these model bacterial systems can be propagated, manipulated, and studied in the laboratory has made this model organism ideal for understanding DNA replication, gene expression, and protein synthesis[10,147]. Though model bacterial systems have greatly facilitated fundamental experiments in both molecular biology and biochemistry, these simple organisms do not provide insight into infectious diseases caused by microbial pathogens. In this thesis, I address some of the challenges associated with protein fusion expressions in bacteria, and develop single-molecule fluorescence imaging methods to study non-model bacterial systems in isolated cultures and in a co-culture.

In Chapter 2, I use single-molecule tracking to probe the change in motion of protein fusions as a function of expression methods, growth conditions, and host systems. Single-particle tracking of proteins provides a very sensitive readout to address subcellular phenotypes that are invisible to averaging and bulk-scale biochemical assays. Overall, Chapter 2 highlights the need for relevant biological controls in fluorescence microscopy experiments to better understand bacterial behavior in the least perturbed manner. In Chapter 3, with the aim of advancing single-molecule imaging in pathogens, I explore the feasibility of simultaneously imaging and tracking two transcriptional activators, ToxR and TcpP, in live *V. cholerae* cells using two-color super-resolution imaging. I address some of the caveats with fluorescence labeling of ToxR and the simultaneous labeling of ToxR and TcpP—proteins that may be involved in the same complex[106]. My findings suggest that the location of fluorophore attachment in ToxR is crucial for maintaining its native function and stability. In addition, my results suggest that sterics induced by the simultaneous FP labeling of ToxR and TcpP hinder native interactions, and therefore reduce downstream virulence production. Overall, Chapter 3 presents the first approach to do simultaneous tracking of ToxR and TcpP in live *V. cholerae* cells.

With the aim of imaging subcellular behavior and intracellular interactions in a more complex system, I extend fluorescence imaging methods to another non-model bacterial system—a co-culture of anaerobes—in Chapter 4. By cloning different versions of flavin-based FPs into anaerobes, I assess the feasibility of using this novel class of FPs for imaging of *B. theta*. In addition to fluorescence, I use phase-contrast microscopy to distinguish the different bacterial species in a mixed-culture. The results in Chapter 4 provide the first experiments towards imaging a microbiome. Finally, in Chapter 5, I end my thesis by summarizing key findings and discussing how all of these results contribute to the single-molecule imaging field. I

also discuss ongoing methods developments for imaging live bacteria with increasing complexity and for enhancing the properties of fluorescence proteins to track biomolecules for longer periods of time.

1.10 References

1. Stephens, D. J.; Allan, V. J. Light Microscopy Techniques for Live Cell Imaging. *Science* **2003**, *300*, 82-86.

2. Lodish, H.; Berk, A.; Zipursky, S. L.; Matsudaira, P.; Baltimore, D.; Darnell, J. E. *Molecular Biology of the Cell;* W. H. Freeman and Co: New York, 2000.

3. Sadanandan, S. K.; Baltekin, O.; Magnusson, K. E. G.; Boucharin, A.; Ranefall, P.; Jalden, J.; Elf, J.; Wahlby, C. Segmentation and Track-Analysis in Time-Lapse Imaging of Bacteria. *Selected Topics in Signal Processing, IEEE Journal of* **2016**, *10*, 174-184.

4. Wolf, D. E. Fundamentals of Fluorescence and Fluorescence Microscopy. *Methods Cell Biol.* **2007**, *81*, 63-91.

5. Tsien, R. Y. The Green Fluorescent Protein. *Annu. Rev. Biochem.* **1998**, *67*, 509-544.

6. Andersson, H.; Baechi, T.; Hoechl, M.; Richter, C. Autofluorescence of Living Cells. *J. Microsc.* **1998**, *191*, 1-7.

7. Benson, R. C.; Meyer, R. A.; Zaruba, M. E.; McKhann, G. M. Cellular Autofluorescence – is it due to Flavins? *J. Histochem. Cytochem.* **1979**, *27*, 44-48.

8. Lichtman, J. W.; Conchello, J. A. Fluorescence Microscopy. *Nat. Methods* **2005**, *2*, 910-919.

9. Yao, Z.; Carballido-Lopez, R. Fluorescence Imaging for Bacterial Cell Biology: From Localization to Dynamics, from Ensembles to Single Molecules. *Annu. Rev. Microbiol.* **2014**, *68*, 459-476.

10. Stracy, M.; Uphoff, S.; Garza de Leon, F.; Kapanidis, A. N. In Vivo Single-Molecule Imaging of Bacterial DNA Replication, Transcription, and Repair. *FEBS Lett.* **2014**, *588*, 3585-3594.

11. Chen, B. C.; Legant, W. R.; Wang, K.; Shao, L.; Milkie, D. E.; Davidson, M. W.; Janetopoulos, C.; Wu, X. S.; Hammer, J. A.,3rd; Liu, Z.; English, B. P.; Mimori-Kiyosue, Y.; Romero, D. P.; Ritter, A. T.; Lippincott-Schwartz, J.; Fritz-Laylin, L.; Mullins, R. D.; Mitchell, D. M.; Bembenek, J. N.; Reymann, A. C.; Bohme, R.; Grill, S. W.; Wang, J. T.; Seydoux, G.; Tulu, U. S.; Kiehart, D. P.; Betzig, E. Lattice Light-Sheet Microscopy: Imaging Molecules to Embryos at High Spatiotemporal Resolution. *Science* **2014**, *346*, 1257998.

12. Ritter, J. G.; Veith, R.; Veenendaal, A.; Siebrasse, J. P.; Kubitscheck, U. Light Sheet Microscopy for Single Molecule Tracking in Living Tissue. *PloS One* **2010**, *5*, e11639.

13. Itano, W. M.; Bergquist, J. C.; Wineland, D. J. *Science* **1987**, *237*, 612.

14. Dehmelt, H. Experiments with an Isolated Subatomic Particle at Rest. *Rev.Mod.Phys.* **1990**, *62*, 525-530.

15. Diedrich, F.; Krause, J.; Rempe, G.; Scully, M. O.; Walther, H. *IEEE J.Quant.Elect.* **1988**, *24*, 1314.

16. Binnig, G.; Rohrer, H. *Rev.Mod.Phys.* **1987**, *59*, 615.

17. Binnig, G.; Quate, C. F.; Gerber, C. *Phys. Rev. Lett.* **1986**, *56*, 930.

18. Kador, L.; Horne, D. E.; Moerner, W. E. Optical Detection and Probing of Single Dopant Molecules of Pentacene in a P-Terphenyl Host Crystal by Means of Absorption Spectroscopy. *J. Phys. Chem.* **1990**, *94*, 1237-1248.

19. Orrit, M.; Bernard, J. Single Pentacene Molecules Detected by Fluorescence Excitation in a P-Terphenyl Crystal. *Phys. Rev. Lett.* **1990**, *65*, 2716-2719.

20. Betzig, E.; Chichester, R. J. Single Molecules Observed by Near-Field Scanning Optical Microscopy. *Science* **1993**, *262*, 1422-1425.

21. Shera, E. B.; Seitzinger, N. K.; Davis, L. M.; Keller, R. A.; Soper, S. A. Detection of Single Fluorescent Molecules. *Chem.Phys.Lett.* **1990**, *174*, 553-557.

22. Betzig, E.; Patterson, G. H.; Sougrat, R.; Lindwasser, O. W.; Olenych, S.; Bonifacino, J. S.; Davidson, M. W.; Lippincott-Schwartz, J.; Hess, H. F. Imaging Intracellular Fluorescent Proteins at Nanometer Resolution. *Science* **2006**, *313*, 1642-1645.

23. Flors, C. DNA and Chromatin Imaging with Super-Resolution Fluorescence Microscopy Based on Single-Molecule Localization. *Biopolymers* **2011**, *Current Issue*,.

24. Wang, W.; Li, G.; Chen, C.; Xie, X. S.; Zhuang, X. Chromosome Organization by a Nucleoid-Associated Protein in Live Bacteria. *Science* **2011**, *333*, 1445-1449.

25. Ma, H.; Naseri, A.; Reyes-Gutierrez, P.; Wolfe, S. A.; Zhang, S.; Pederson, T. Multicolor CRISPR Labeling of Chromosomal Loci in Human Cells. *Proc. Natl. Acad. Sci. U. S. A.* **2015**, *112*, 3002-3007.

26. Baday, M.; Cravens, A.; Hastie, A.; Kim, H.; Kudeki, D. E.; Kwok, P. Y.; Xiao, M.; Selvin, P. R. Multicolor Super-Resolution DNA Imaging for Genetic Analysis. *Nano Lett.* **2012**, *12*, 3861-3866.

27. Lubeck, E.; Cai, L. Single-Cell Systems Biology by Super-Resolution Imaging and Combinatorial Labeling. *Nat Meth.* **2012**, *9*, 743-748.

28. Wu, M.; Huang, B.; Graham, M.; Raimondi, A.; Heuser, J. E.; Zhuang, X.; De Camilli, P. Coupling between Clathrin-Dependent Endocytic Budding and F-BAR-Dependent Tubulation in a Cell-Free System. *Nat. Cell Biol.* **2010**, *12*, 902-908.

29. Chojnacki, J.; Staudt, T.; Glass, B.; Bingen, P.; Engelhardt, J.; Anders, M.; Schneider, J.; Muller, B.; Hell, S. W.; Krausslich, H. G. Maturation-Dependent HIV-1 Surface Protein Redistribution Revealed by Fluorescence Nanoscopy. *Science* **2012**, *338*, 524-528.

30. Mennella, V.; Keszthelyi, B.; McDonald, K. L.; Chhun, B.; Kan, F.; Rogers, G. C.; Huang, B.; Agard, D. A. Subdiffraction-Resolution Fluorescence Microscopy Reveals a Domain of the Centrosome Critical for Pericentriolar Material Organization. *Nat. Cell Biol.* **2012**, *14*, 1159-1168.

31. Lau, L.; Lee, Y. L.; Sahl, S. J.; Stearns, T.; Moerner, W. E. STED Microscopy with Optimized Labeling Density Reveals 9-Fold Arrangement of a Centriole Protein. *Biophys. J.* **2012**, *102*, 2926-2935.

32. Kapanidis, A. N.; Strick, T. Biology, One Molecule at a Time. *Trends Biochem. Sci.* **2009**, *34*, 234-243.

33. Moerner, W. E. Microscopy Beyond the Diffraction Limit using Actively Controlled Single Molecules. *J. Microsc.* **2012**, *246*, 213-220.

34. Nan, X.; Sims, P. A.; Xie, X. S. Organelle Tracking in a Living Cell with Microsecond Time Resolution and Nanometer Spatial Precision. *ChemPhysChem* **2008**, *9*, 707-712.

35. Liu, Z.; Lavis, L.; Betzig, E. Imaging Live-Cell Dynamics and Structure at the Single-Molecule Level. *Mol. Cell* **2015**, *58*, 644-659.

36. Kusumi, A.; Tsunoyama, T. A.; Hirosawa, K. M.; Kasai, R. S.; Fujiwara, T. K. Tracking Single Molecules at Work in Living Cells. *Nat Chem Biol* **2014**, *10*, 524-532.

37. Taylor, M. J.; Perrais, D.; Merrifield, C. J. A High Precision Survey of the Molecular Dynamics of Mammalian Clathrin-Mediated Endocytosis. *PLoS Biol.* **2011**, *9*, e1000604.

38. Frost, N. A.; Shroff, H.; Kong, H.; Betzig, E.; Blanpied, T. A. Single-Molecule Discrimination of Discrete Perisynaptic and Distributed Sites of Actin Filament Assembly within Dendritic Spines. *Neuron* **2010**, *67*, 86-99.

39. Xie, X. S.; Choi, P. J.; Li, G. W.; Lee, N. K.; Lia, G. Single-Molecule Approach to Molecular Biology in Living Bacterial Cells. *Annu. Rev. Biophys.* **2008**, *37*, 417-444.

40. Gahlmann, A.; Moerner, W. E. Exploring Bacterial Cell Biology with Single-Molecule Tracking and Super-Resolution Imaging. *Nat Rev Micro* **2014**, *12*, 9-22.

41. Fu, G.; Huang, T.; Buss, J.; Coltharp, C.; Hensel, Z.; Xiao, J. *in Vivo* Structure of the *E. Coli* FtsZ-Ring Revealed by Photoactivated Localization Microscopy (PALM). *PLoS ONE* **2010**, *5*, e12680.

42. Biteen, J. S.; Shapiro, L.; Moerner, W. E. Exploring Protein Superstructures and Dynamics in Live Bacterial Cells using Single-Molecule and Superresolution Imaging. *Method. Mol. Biol.* **2011**, *783*, 139-158.

43. Kim, S. Y.; Gitai, Z.; Kinkhabwala, A.; Shapiro, L.; Moerner, W. E. Single Molecules of the Bacterial Actin MreB Undergo Directed Treadmilling Motion in *Caulobacter Crescentus*. *Proc. Natl. Acad. Sci. USA* **2006**, *103*, 10929-10934.

44. Yao, Z.; Carballido-Lopez, R. Fluorescence Imaging for Bacterial Cell Biology: From Localization to Dynamics, from Ensembles to Single Molecules. *Annu. Rev. Microbiol.* **2014**, *68*, 459-476.

45. Liao, Y.; Li, Y.; Schroeder, J. W.; Simmons, L. A.; Biteen, J. S. Single-Molecule DNA Polymerase Dynamics at a Bacterial Replisome in Live Cells. *Biophys. J.* **2016**, *111*, 2562-2569.

46. Karunatilaka, K. S.; Cameron, E. A.; Martens, E. C.; Koropatkin, N. M.; Biteen, J. S. Superresolution Imaging Captures Carbohydrate Utilization Dynamics in Human Gut Symbionts. *mBio* **2014**, *5*, e02172-14.

47. Haas, B. L.; Matson, J. S.; DiRita, V. J.; Biteen, J. S. Single-Molecule Tracking in Live *Vibrio Cholerae* Reveals that ToxR Recruits the Membrane-Bound Virulence Regulator TcpP to the *toxT* Promoter. *Mol. Microbiol.* **2015**, *96*, 4-13.

48. Abbe, E. Contributions to the Theory of the Microscope and Microscopic Detection (Translated from German). *Arch. Mikroskop. Anat.* **1873**, *9*, 413-468.

49. Thompson, R. E.; Larson, D. R.; Webb, W. W. Precise Nanometer Localization Analysis for Individual Fluorescent Probes. *Biophys. J.* **2002**, *82*, 2775-2783.

50. Biteen, J. S.; Thompson, M. A.; Tselentis, N. K.; Shapiro, L.; Moerner, W. E. Superresolution Imaging in Live *Caulobacter Crescentus* Cells using Photoswitchable Enhanced Yellow Fluorescent Protein. *Proc. SPIE* **2009**, *7185*, 71850I.

51. Habuchi, S.; Ando, R.; Dedecker, P.; Verheijen, W.; Mizuno, H.; Miyawaki, A.; Hofkens, J. Reversible Single-Molecule Photoswitching in the GFP-Like Fluorescent Protein Dronpa. *Proc. Natl. Acad. Sci. U. S. A.* **2005**, *102*, 9511-9516.

52. Hofmann, M.; Eggeling, C.; Jakobs, S.; Hell, S. W. Breaking the Diffraction Barrier in Fluorescence Microscopy at Low Light Intensities by using Reversibly Photoswitchable Proteins. *Proc. Natl. Acad. Sci. U. S. A.* **2005**, *102*, 17565-17569.

53. Patterson, G. H.; Lippincott-Schwartz, J. A Photoactivatable GFP for Selective Photolabeling of Proteins and Cells. *Science* **2002**, *297*, 1873-1877.

54. Wang, S.; Moffitt, J. R.; Dempsey, G. T.; Xie, X. S.; Zhuang, X. Characterization and Development of Photoactivatable Fluorescent Proteins for Single-Molecule-Based Superresolution Imaging. *Proc. Natl. Acad. Sci. U. S. A.* **2014**, *111*, 8452-8457.

55. Hess, S. T.; Girirajan, T. P. K.; Mason, M. D. Ultra-High Resolution Imaging by Fluorescence Photoactivation Localization Microscopy. *Biophys. J.* **2006**, *91*, 4258-4272.

56. Waldchen, S.; Lehmann, J.; Klein, T.; van de Linde, S.; Sauer, M. Light-Induced Cell Damage in Live-Cell Super-Resolution Microscopy. *Sci. Rep.* **2015**, *5*, 15348.

57. Zhu, L.; Zhang, W.; Elnatan, D.; Huang, B. *Nat Meth* **2012**, *9*, 721-723.

58. Manley, S.; Gillette, J. M.; Patterson, G. H.; Shroff, H.; Hess, H. F.; Betzig, E.; Lippincott-Schwartz, J. High-Density Mapping of Single-Molecule Trajectories with Photoactivated Localization Microscopy. *Nat. Methods* **2008**, *5*, 155-157.

59. Dean, K. M.; Palmer, A. E. Advances in Fluorescence Labeling Strategies for Dynamic Cellular Imaging. *Nat. Chem. Biol.* **2014**, *10*, 512-523.

60. Coons, A. Immunological Properties of an Antibody Containing a Fluorescent Group. *P. Soc. Exp. Biol. Med.* **1941**, *47*, 200-202.

61. Platonova, E.; Winterflood, C. M.; Junemann, A.; Albrecht, D.; Faix, J.; Ewers, H. Single-Molecule Microscopy of Molecules Tagged with GFP Or RFP Derivatives in Mammalian Cells using Nanobody Binders. *Methods* **2015**, *88*, 89-97.

62. Gautier, A.; Juillerat, A.; Heinis, C.; Correa, I. R.,Jr; Kindermann, M.; Beaufils, F.; Johnsson, K. An Engineered Protein Tag for Multiprotein Labeling in Living Cells. *Chem. Biol.* **2008**, *15*, 128-136.

63. Keppler, A.; Gendreizig, S.; Gronemeyer, T.; Pick, H.; Vogel, H.; Johnsson, K. A General Method for the Covalent Labeling of Fusion Proteins with Small Molecules *in Vivo*. *Nat. Biotechnol.* **2003**, *21*, 86-89.

64. Los, G. V.; Darzins, A.; Karassina, N.; Zimprich, C.; Learish, R.; McDougall, M. G.; Encell, L. P.; Friedman-Ohana, R.; Wood, M.; Vidugiris, G.; Zimmerman, K.; Otto, P.; Klaubert, D. H.; Wood, K. V. HaloTag Interchangeable Labeling Technology for Cell Imaging and Protein Capture. *Cell Notes* **2005**, *11*, 2-6.

65. Tirat, A.; Freuler, F.; Stettler, T.; Mayr, L. M.; Leder, L. Evaluation of Two Novel Tag-Based Labelling Technologies for Site-Specific Modification of Proteins. *Int. J. Biol. Macromol.* **2006**, *39*, 66-76.

66. Bosch, P. J.; Correa, I. R.,Jr; Sonntag, M. H.; Ibach, J.; Brunsveld, L.; Kanger, J. S.; Subramaniam, V. Evaluation of Fluorophores to Label SNAP-Tag Fused Proteins for Multicolor Single-Molecule Tracking Microscopy in Live Cells. *Biophys. J.* **2014**, *107*, 803-814.

67. Zanetti-Domingues, L. C.; Tynan, C. J.; Rolfe, D. J.; Clarke, D. T.; Martin-Fernandez, M. Hydrophobic Fluorescent Probes Introduce Artifacts into Single Molecule Tracking Experiments due to Non-Specific Binding. *PLoS One* **2013**, *8*, e74200.

68. Snapp, E. Design and use of Fluorescent Fusion Proteins in Cell Biology. *Curr. Protoc. Cell. Biol.* **2005**, *Chapter 21*, Unit 21.4.

69. Tuson, H. H.; Biteen, J. S. Unveiling the Inner Workings of Live Bacteria using Super-Resolution Microscopy. *Anal. Chem.* **2015**, *87*, 42-63.

70. Demchick, P.; Koch, A. L. The Permeability of the Wall Fabric of Escherichia Coli and Bacillus Subtilis. *J. Bacteriol.* **1996**, *178*, 768-773.

71. Shen, Y.; Nagpal, P.; Hay, J. G.; Sauthoff, H. A Novel Cell-Penetrating Peptide to Facilitate Intercellular Transport of Fused Proteins. *J. Control. Release* **2014**, *188*, 44-52.

72. Goetz, M.; Bubert, A.; Wang, G.; Chico-Calero, I.; Vazquez-Boland, J. A.; Beck, M.; Slaghuis, J.; Szalay, A. A.; Goebel, W. Microinjection and Growth of Bacteria in the Cytosol of Mammalian Host Cells. *Proc. Natl. Acad. Sci. U. S. A.* **2001**, *98*, 12221-12226.

73. Shaner, N. C.; Steinbach, P. A.; Tsien, R. Y. A Guide to Choosing Fluorescent Proteins. *Nat. Methods* **2005**, *2*, 905-909.

74. Subach, F. V.; Patterson, G. H.; Manley, S.; Gillette, J. M.; Lippincott-Schwartz, J.; Verkhusha, V. V. Photoactivatable mCherry for High-Resolution Two-Color Fluorescence Microscopy. *Nat. Methods* **2009**, *6*, 153-159.

75. Lobo, L. A.; Smith, C. J.; Rocha, E. R. Flavin Mononucleotide (FMN)-Based Fluorescent Protein (FbFP) as Reporter for Gene Expression in the Anaerobe Bacteroides Fragilis. *FEMS Microbiol. Lett.* **2011**, *317*, 67-74.

76. Solomon, J. M.; Grossman, A. D. Who's Competent and when: Regulation of Natural Genetic Competence in Bacteria. *Trends Genet.* **1996**, *12*, 150-155.

77. Aune, T. E.; Aachmann, F. L. Methodologies to Increase the Transformation Efficiencies and the Range of Bacteria that can be Transformed. *Appl. Microbiol. Biotechnol.* **2010**, *85*, 1301-1313.

78. Tuson, H. H.; Aliaj, A.; Brandes, E. R.; Simmons, L. A.; Biteen, J. S. Addressing the Requirements of High Sensitivity Single-Molecule Imaging of Low-Copy Number Proteins in Bacteria. *ChemPhysChem* **2016**, *17*, 1435-1440.

79. Liu, H. S.; Jan, M. S.; Chou, C. K.; Chen, P. H.; Ke, N. J. Is Green Fluorescent Protein Toxic to the Living Cells? *Biochem. Biophys. Res. Commun.* **1999**, *260*, 712-717.

80. Ortiz-Martin, I.; Macho, A. P.; Lambersten, L.; Ramos, C.; Beuzon, C. R. Suicide Vectors for Antibiotic Marker Exchange and Rapid Generation of Multiple Knockout Mutants by Allelic Exchange in Gram-Negative Bacteria. *J. Microbiol. Methods* **2006**, *67*, 395-407.

81. Niaudet, B.; Janniere, L.; Ehrlich, S. D. Integration of Linear, Heterologous DNA Molecules into the Bacillus Subtilis Chromosome: Mechanism and use in Induction of Predictable Rearrangements. *J. Bacteriol.* **1985**, *163*, 111-120.

82. Juhas, M.; Ajioka, J. W. Lambda Red Recombinase-Mediated Integration of the High Molecular Weight DNA into the Escherichia Coli Chromosome. *Microb. Cell. Fact.* **2016**, *15*, 172.

83. Skorupski, K.; Taylor, R. K. Positive Selection Vectors for Allelic Exchange. *Gene* **1996**, *169*, 47-52.

84. Chang, S.; Stauffer, S.; Sharan, S. K. Using Recombineering to Generate Point Mutations: The Oligonucleotide-Based "Hit and Fix" Method. *Methods Mol. Biol.* **2012**, *852*, 111-120.

85. Sander, J. D.; Joung, J. K. CRISPR-Cas Systems for Editing, Regulating and Targeting Genomes. *Nat. Biotechnol.* **2014**, *32*, 347-355.

86. Baird, G. S.; Zacharias, D. A.; Tsien, R. Y. Biochemistry, Mutagenesis, and Oligomerization of DsRed, a Red Fluorescent Protein from Coral. *Proc. Natl. Acad. Sci. U. S. A.* **2000**, *97*, 11984-11989.

87. Campbell, R. E.; Tour, O.; Palmer, A. E.; Steinbach, P. A.; Baird, G. S.; Zacharias, D. A.; Tsien, R. Y. A Monomeric Red Fluorescent Protein. *Proc. Natl. Acad. Sci. U. S. A.* **2002**, *99*, 7877-7882.

88. Gurskaya, N. G.; Verkhusha, V. V.; Shcheglov, A. S.; Staroverov, D. B.; Chepurnykh, T. V.; Fradkov, A. F.; Lukyanov, S. A.; Lukyanov, K. A. Engineering of a Monomeric Green-to-Red Photoactivatable Fluorescent Protein Induced by Blue Light. *Nat. Biotechnol.* **2006**, *24*, 461-465.

89. Cravioto, A.; Lanata, C. F.; Lantagne, D. S.; Nair, G. B. Final Report of the Independent Panel of Experts on the Cholera Outbreak in Haiti. *http://www.un.org/News/dh/infocus/haiti/UN-cholera-report-final.pdf* 2014).

90. Sack, D. A.; Sack, R. B.; Chaignat, C. L. Getting Serious about Cholera. *N. Engl. J. Med.* **2006**, *355*, 649-651.

91. Charles, R. C.; Ryan, E. T. Cholera in the 21st Century. *Curr. Opin. Infect. Dis.* **2011**, *24*, 472-477.

92. Ali, M.; Nelson, A. R.; Lopez, A. L.; Sack, D. A. Updated Global Burden of Cholera in Endemic Countries. *PLoS Negl Trop. Dis.* **2015**, *9*, e0003832.

93. Finkelstein, R. A. Cholera, Vibrio cholerae O1 and O139, and Other Pathogenic Vibrios. In *Medical Microbiology;* Baron, S., Ed.; The University of Texas Medical Branch at Galveston: Galveston (TX), 1996; .

94. Guerrant, R. L.; Carneiro-Filho, B. A.; Dillingham, R. A. Cholera, Diarrhea, and Oral Rehydration Therapy: Triumph and Indictment. *Clin. Infect. Dis.* **2003**, *37*, 398-405.

95. Faruque, S. M.; Albert, M. J.; Mekalanos, J. J. Epidemiology, Genetics, and Ecology of Toxigenic Vibrio Cholerae. *Microbiol. Mol. Biol. Rev.* **1998**, *62*, 1301-1314.

96. Sharma, C.; Thungapathra, M.; Ghosh, A.; Mukhopadhyay, A. K.; Basu, A.; Mitra, R.; Basu, I.; Bhattacharya, S. K.; Shimada, T.; Ramamurthy, T.; Takeda, T.; Yamasaki, S.; Takeda, Y.; Nair, G. B. Molecular Analysis of Non-O1, Non-O139 Vibrio Cholerae Associated with an Unusual Upsurge in the Incidence of Cholera-Like Disease in Calcutta, India. *J. Clin. Microbiol.* **1998**, *36*, 756-763.

97. Saha, P. K.; Koley, H.; Mukhopadhyay, A. K.; Bhattacharya, S. K.; Nair, G. B.; Ramakrishnan, B. S.; Krishnan, S.; Takeda, T.; Takeda, Y. Nontoxigenic Vibrio Cholerae 01 Serotype Inaba Biotype El Tor Associated with a Cluster of Cases of Cholera in Southern India. *J. Clin. Microbiol.* **1996**, *34*, 1114-1117.

98. Na-Ubol, M.; Srimanote, P.; Chongsa-Nguan, M.; Indrawattana, N.; Sookrung, N.; Tapchaisri, P.; Yamazaki, S.; Bodhidatta, L.; Eampokalap, B.; Kurazono, H.; Hayashi, H.; Nair, G. B.; Takeda, Y.; Chaicumpa, W. Hybrid & El Tor Variant Biotypes of Vibrio Cholerae O1 in Thailand. *Indian J. Med. Res.* **2011**, *133*, 387-394.

99. Colwell, R. R. Global Climate and Infectious Disease: The Cholera Paradigm. *Science* **1996**, *274*, 2025-2031.

100. Lipp, E. K.; Huq, A.; Colwell, R. R. Effects of Global Climate on Infectious Disease: The Cholera Model. *Clin. Microbiol. Rev.* **2002**, *15*, 757-770.

101. Herrington, D. A.; Hall, R. H.; Losonsky, G.; Mekalanos, J. J.; Taylor, R. K.; Levine, M. M. Toxin, Toxin-Coregulated Pili, and the toxR Regulon are Essential for Vibrio Cholerae Pathogenesis in Humans. *J. Exp. Med.* **1988**, *168*, 1487-1492.

102. Sanchez, J.; Holmgren, J. Cholera Toxin - a Foe & a Friend. *Indian J. Med. Res.* **2011**, *133*, 153-163.

103. Boyd, E. F.; Moyer, K. E.; Shi, L.; Waldor, M. K. Infectious CTXPhi and the Vibrio Pathogenicity Island Prophage in Vibrio Mimicus: Evidence for Recent Horizontal Transfer between V. Mimicus and V. Cholerae. *Infect. Immun.* **2000**, *68*, 1507-1513.

104. Peterson, K. M.; Mekalanos, J. J. Characterization of the Vibrio Cholerae ToxR Regulon: Identification of Novel Genes Involved in Intestinal Colonization. *Infect. Immun.* **1988**, *56*, 2822-2829.

105. Matson, J. S.; Withey, J. H.; DiRita, V. J. Regulatory Networks Controlling *Vibrio Cholerae* Virulence Gene Expression. *Infect. Immun.* **2007**, *75*, 5542-5549.

106. Krukonis, E. S.; Yu, R. R.; DiRita, V. J. The *Vibrio Cholerae* ToxR/TcpP/ToxT Virulence Cascade: Distinct Roles for Two Membrane-Localized Transcriptional Activators on a Single Promoter. *Mol. Microbiol.* **2000**, *38*, 67-84.

107. Yu, R. R.; DiRita, V. J. Analysis of an Autoregulatory Loop Controlling ToxT Cholera Toxin, and Toxin-Coregulated Pilus Production in *Vibrio Cholerae*. *J. Bacteriol.* **1999**, *181*, 2584-2592.

108. Martinez-Hackert, E.; Stock, A. M. Structural Relationships in the OmpR Family of Winged-Helix Transcription Factors. *J. Mol. Biol.* **1997**, *269*, 301-312.

109. Hennecke, F.; Muller, A.; Meister, R.; Strelow, A.; Behrens, S. A ToxR-Based Two-Hybrid System for the Detection of Periplasmic and Cytoplasmic Protein-Protein Interactions in Escherichia Coli: Minimal Requirements for Specific DNA Binding and Transcriptional Activation. *Protein Eng. Des. Sel.* **2005**, *18*, 477-486.

110. DiRita, V. J.; Mekalanos, J. J. Periplasmic Interaction between Two Membrane Regulatory Proteins, ToxR and ToxS, Results in Signal Transduction and Transcriptional Activation. *Cell* **1991**, *11*, 29-37.

111. Beck, N. A.; Krukonis, E. S.; DiRita, V. J. TcpH Influences Virulence Gene Expression in Vibrio Cholerae by Inhibiting Degradation of the Transcription Activator TcpP. *J. Bacteriol.* **2004**, *186*, 8309-8316.

112. Goss, T. J.; Seaborn, C. P.; Gray, M. D.; Krukonis, E. S. Identification of the TcpP-Binding Site in the *toxT* Promoter of *Vibrio Cholerae* and the Role of ToxR in TcpP-Mediated Activation. *Infect. Immun.* **2010**, *78*, 4122-4133.

113. Matson, J. S.; DiRita, V. J. Degradation of the Membrane-Localized Virulence Activator TcpP by the YaeL Protease in Vibrio Cholerae. *Proc. Natl. Acad. Sci. U. S. A.* **2005**, *102*, 16403-16408.

114. Teoh, W. P.; Matson, J. S.; DiRita, V. J. Regulated Intramembrane Proteolysis of the Virulence Activator TcpP in Vibrio Cholerae is Initiated by the Tail-Specific Protease (Tsp). *Mol. Microbiol.* **2015**, *97*, 822-831.

115. Sperandio, V.; Girón, J. A.; Silveira, W. D.; Kaper, J. B. The OmpU Outer Membrane Protein, a Potential Adherence Factor of *Vibrio Cholerae*. *Infect. Immun.* **1995**, *63*, 4433-4438.

116. Provenzano, D.; Lauriano, C. M.; Klose, K. E. Characterization of the Role of the ToxR-Modulated Outer Membrane Porins OmpU and OmpT in Vibrio Cholerae Virulence. *J. Bacteriol.* **2001**, *183*, 3652-3662.

117. Silhavy, T. J.; Kahne, D.; Walker, S. The Bacterial Cell Envelope. *Cold Spring Harb Perspect. Biol.* **2010**, *2*, a000414.

118. Baker, H.; Bloom, W. L. Further Studies on the Gram Stain. *J. Bacteriol.* **1948**, *56*, 387-390.

119. Ruiz, N.; Kahne, D.; Silhavy, T. J. Advances in Understanding Bacterial Outer-Membrane Biogenesis. *Nat. Rev. Microbiol.* **2006**, *4*, 57-66.

120. Galdiero, S.; Falanga, A.; Cantisani, M.; Tarallo, R.; Della Pepa, M. E.; D'Oriano, V.; Galdiero, M. Microbe-Host Interactions: Structure and Role of Gram-Negative Bacterial Porins. *Curr. Protein Pept. Sci.* **2012**, *13*, 843-854.

121. Achouak, W.; Heulin, T.; Pages, J. M. Multiple Facets of Bacterial Porins. *FEMS Microbiol. Lett.* **2001**, *199*, 1-7.

122. Stock, A. M.; Robinson, V. L.; Goudreau, P. N. Two-Component Signal Transduction. *Annu. Rev. Biochem.* **2000**, *69*, 183-215.

123. Mascher, T.; Helmann, J. D.; Unden, G. Stimulus Perception in Bacterial Signal-Transducing Histidine Kinases. *Microbiol. Mol. Biol. Rev.* **2006**, *70*, 910-938.

124. Groisman, E. A.; Mouslim, C. Sensing by Bacterial Regulatory Systems in Host and Non-Host Environments. *Nat. Rev. Microbiol.* **2006**, *4*, 705-709.

125. Hughes, D. T.; Sperandio, V. Inter-Kingdom Signalling: Communication between Bacteria and their Hosts. *Nat. Rev. Microbiol.* **2008**, *6*, 111-120.

126. Werner, F.; Grohmann, D. Evolution of Multisubunit RNA Polymerases in the Three Domains of Life. *Nat. Rev. Microbiol.* **2011**, *9*, 85-98.

127. Miller, V. L.; Taylor, R. K.; Mekalanos, J. J. Cholera Toxin Transcriptional Activator ToxR is a Transmembrane DNA Binding Protein. *Cell* **1987**, *48*, 271-279.

128. Häse, C. C.; Mekalanos, J. J. TcpP Protein is a Positive Regulator of Virulence Gene Expression in *Vibrio Cholerae*. *Proc. Natl. Acad. Sci. U. S. A.* **1998**, *95*, 730-734.

129. Haas, B. L.; Matson, J. S.; Dirita, V. J.; Biteen, J. S. Imaging Live Cells at the Nanometer-Scale with Single-Molecule Microscopy: Obstacles and Achievements in Experimental Optimization for Microbiology. *Molecules* **2014**, *19*, 12116-12149.

130. Mueller, N. T.; Bakacs, E.; Combellick, J.; Grigoryan, Z.; Dominguez-Bello, M. G. The Infant Microbiome Development: Mom Matters. *Trends Mol. Med.* **2015**, *21*, 109-117.

131. Backhed, F.; Roswall, J.; Peng, Y.; Feng, Q.; Jia, H.; Kovatcheva-Datchary, P.; Li, Y.; Xia, Y.; Xie, H.; Zhong, H.; Khan, M. T.; Zhang, J.; Li, J.; Xiao, L.; Al-Aama, J.; Zhang, D.; Lee, Y. S.; Kotowska, D.; Colding, C.; Tremaroli, V.; Yin, Y.; Bergman, S.; Xu, X.; Madsen, L.; Kristiansen, K.; Dahlgren, J.; Wang, J. Dynamics and Stabilization of the Human Gut Microbiome during the First Year of Life. *Cell. Host Microbe* **2015**, *17*, 690-703.

132. D'Argenio, V.; Salvatore, F. The Role of the Gut Microbiome in the Healthy Adult Status. *Clin. Chim. Acta* **2015**, *451*, 97-102.

133. Bull, M. J.; Plummer, N. T. Part 1: The Human Gut Microbiome in Health and Disease. *Integr. Med. (Encinitas)* **2014**, *13*, 17-22.

134. Khanna, S.; Tosh, P. K. A Clinician's Primer on the Role of the Microbiome in Human Health and Disease. *Mayo Clin. Proc.* **2014**, *89*, 107-114.

135. David, L. A.; Maurice, C. F.; Carmody, R. N.; Gootenberg, D. B.; Button, J. E.; Wolfe, B. E.; Ling, A. V.; Devlin, A. S.; Varma, Y.; Fischbach, M. A.; Biddinger, S. B.; Dutton, R. J.; Turnbaugh, P. J. Diet Rapidly and Reproducibly Alters the Human Gut Microbiome. *Nature* **2014**, *505*, 559-563.

136. Koropatkin, N. M.; Cameron, E. A.; Martens, E. C. How Glycan Metabolism Shapes the Human Gut Microbiota. *Nat. Rev. Microbiol.* **2012**, *10*, 323-335.

137. Lynch, S. V.; Pedersen, O. The Human Intestinal Microbiome in Health and Disease. *N. Engl. J. Med.* **2016**, *375*, 2369-2379.

138. Schloss, P. D.; Handelsman, J. Status of the Microbial Census. *Microbiol. Mol. Biol. Rev.* **2004**, *68*, 686-691.

139. Blekhman, R.; Goodrich, J. K.; Huang, K.; Sun, Q.; Bukowski, R.; Bell, J. T.; Spector, T. D.; Keinan, A.; Ley, R. E.; Gevers, D.; Clark, A. G. Host Genetic Variation Impacts Microbiome Composition Across Human Body Sites. *Genome Biol.* **2015**, *16*, 191-015-0759-1.

140. Tremaroli, V.; Backhed, F. Functional Interactions between the Gut Microbiota and Host Metabolism. *Nature* **2012**, *489*, 242-249.

141. Swann, J. R.; Want, E. J.; Geier, F. M.; Spagou, K.; Wilson, I. D.; Sidaway, J. E.; Nicholson, J. K.; Holmes, E. Systemic Gut Microbial Modulation of Bile Acid Metabolism in Host Tissue Compartments. *Proc. Natl. Acad. Sci. U. S. A.* **2011**, *108 Suppl 1*, 4523-4530.

142. Osborn, O.; Olefsky, J. M. The Cellular and Signaling Networks Linking the Immune System and Metabolism in Disease. *Nat. Med.* **2012**, *18*, 363-374.

143. Biteen, J. S.; Blainey, P. C.; Cardon, Z. G.; Chun, M.; Church, G. M.; Dorrestein, P. C.; Fraser, S. E.; Gilbert, J. A.; Jansson, J. K.; Knight, R.; Miller, J. F.; Ozcan, A.; Prather, K. A.; Quake, S. R.; Ruby, E. G.; Silver, P. A.; Taha, S.; van, d. E.; Weiss, P. S.; Wong, G. C. L.; Wright, A. T.; Young, T. D. Tools for the Microbiome: Nano and Beyond. *ACS Nano* **2016**, *10*, 6-37.

144. Qin, J.; Li, R.; Raes, J.; Arumugam, M.; Burgdorf, K. S.; Manichanh, C.; Nielsen, T.; Pons, N.; Levenez, F.; Yamada, T.; Mende, D. R.; Li, J.; Xu, J.; Li, S.; Li, D.; Cao, J.; Wang, B.; Liang, H.; Zheng, H.; Xie, Y.; Tap, J.; Lepage, P.; Bertalan, M.; Batto, J. M.; Hansen, T.; Le Paslier, D.; Linneberg, A.; Nielsen, H. B.; Pelletier, E.; Renault, P.; Sicheritz-Ponten, T.; Turner, K.; Zhu, H.; Yu, C.; Li, S.; Jian, M.; Zhou, Y.; Li, Y.; Zhang, X.; Li, S.; Qin, N.; Yang, H.; Wang, J.; Brunak, S.; Dore, J.; Guarner, F.; Kristiansen, K.; Pedersen, O.; Parkhill, J.; Weissenbach, J.; MetaHIT Consortium; Bork, P.; Ehrlich, S. D.; Wang, J. A Human Gut Microbial Gene Catalogue Established by Metagenomic Sequencing. *Nature* **2010**, *464*, 59-65.

145. Lee, S. A.; Ponjavic, A.; Siv, C.; Lee, S. F.; Biteen, J. S. Nanoscopic Cellular Imaging: Confinement Broadens Understanding. *ACS Nano* **2016**, *10*, 8143-8153.

146. Smith, B. T.; Grossman, A. D.; Walker, G. C. *Mol. Cell* **2001**, *8*, 1197-1206.

147. Robinson, A.; van Oijen, A. M. Bacterial Replication, Transcription and Translation: Mechanistic Insights from Single-Molecule Biochemical Studies. *Nat. Rev. Microbiol.* **2013**, *11*, 303-315.

Chapter 2: Differences in Labeling, Expression Systems, and Hosts Produce Concealed Subcellular Phenotypes

The contents of this chapter will be included in the following reference:

Siv, C; DiRita, V.J.; and Biteen, J.S. Differences in labeling, expression systems, and hosts produce concealed subcellular phenotypes. *To be submitted June 2017.*

Author Contributions:

Experimental design: CS, VJD, and JSB; Data collection: CS;
Data analysis: CS, VJD, and JSB

Labeling and expressing fluorescent protein fusions *in vivo* has always presented a challenge for single-molecule fluorescence microscopy. In bacteria, where the cellular membrane restricts dye entry, fluorescent protein labels provide specificity and efficiency unmatched by other methods. Fluorescent protein fusions are either expressed ectopically from a plasmid or endogenously at the native chromosomal locus. Since fluorescent protein fusions do not generally perturb macroscopic cellular processes, changes in protein functionality and stability are often missed by traditional approaches. Here, I determine that single-molecule tracking of fluorescent protein fusions in living bacterial cells is a much more sensitive probe of labeling artifacts. I image the transcription regulator, TcpP, in live *Vibrio cholerae* and I demonstrate that endogenous and ectopic (plasmid-based) expression produce TcpP fusion proteins that move differently inside the cell. Though overexpression in the ectopic strain may lead to mislocalization and dimerization, which can slow protein diffusion, my data suggest that this overexpression artifact is minimal compared to the magnitude of the physiologically relevant motion changes associated with

expression methods, growth conditions, and host systems. I demonstrate the sensitivity of single-molecule imaging to elucidate subtle differences that are missed by static immunoblot detections, independent of protein expression levels. This study reveals the importance of key control experiments in single-molecule fluorescence experiments when trying to deduce the true mechanisms of proteins based on their motion in live cells.

2.1 Introduction

Though molecular biology, biochemistry, and genetics have extensively characterized genes and their associated biochemical processes, the application of fluorescent proteins (FPs) in live-cell fluorescence imaging has been invaluable to bridge the gap between genotype-phenotype relations and cellular function in cell biology and microbiology [1,2]. Because FPs can be genetically encoded to provide specificity, I can now elucidate molecular mechanisms with millisecond temporal resolution by directly visualizing subcellular localization and dynamic interactions of individual proteins in real time [3]. Beyond conventional imaging, single-molecule fluorescence (SMF) microscopy has transcended traditional ensemble measurements and enabled imaging at the nanometer scale to measure molecular-scale positioning and movement of essential and low-copy proteins in both model and pathogenic bacterial systems [4-7]. Such super-resolution imaging methods are particularly useful in microbiology, where the sizes of the organisms are on the same order of magnitude as the diffraction limit of light [8]. Despite these advances in fluorescence microscopy, efficiently expressing FPs without perturbing normal function *in vivo* still presents a challenge for fluorescence imaging. In live-cell experiments, the ability to use a FP fusion depends intimately on the scientific question; for instance whether an intracellular or extracellular protein is under investigation and whether or not the label hinders

functions due to steric hindrance within binding interfaces [9]. Even though routine characterizations of the functionality and stability of fusions to fluorescent proteins are performed, the fluorescence imaging community has not yet agreed on the best methods to express fusion proteins in cells. In this paper, I investigate the consequences of using common expression systems to study transcription regulation by a membrane-localized protein in live *Vibrio cholerae* cells.

In studies of protein mechanism within bacterial systems, fusion proteins can either be expressed at the native promoter on the chromosome or by an expression vector [10]. Though ectopic expression is often more convenient, endogenous chromosomal labeling ensures that the fusion protein is expressed at native levels. However, in systems where limited or underdeveloped genetic methods restrict the ability to alter genes on the chromosome, fusion proteins are nearly always expressed ectopically from a plasmid vector like the pBAD or pET series of plasmids [11]. These vectors can be tuned to some extent to control protein expression from inducible promoters, but such promoters are not subjected to the same gene regulation pathways as the native chromosomal promoters, and thus protein levels can differ significantly from wildtype levels [12]. In some cases, overexpression of this kind enables detection of low-copy number proteins, but, consequently, can also lead to artificial responses—such as mis-localization and/or dimerization—and toxicity [12,13]. Additionally, ectopic expression of a recombinant protein in a heterologous organism enables comparative studies of gene function across species to determine functional complementation or deleterious effects that changes phenotype morphologies. For instance, the very robust bacterium *Escherichia coli* has served as a prototype for understanding key pathways in other bacteria, including *V. cholerae* [14-16]. Yet, the physiological relevance of examining protein biophysics in a non-native host is also variable.

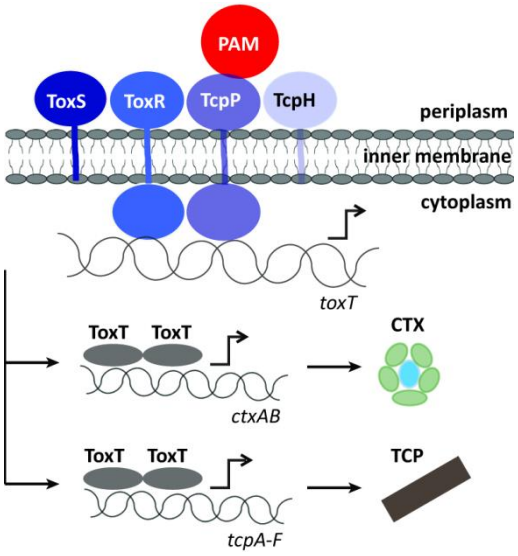

Figure 2.1 The ToxR Regulon regulates gene expression of the major *V. cholerae* virulence factors CTX and TCP through ToxT. This study compares the biophysical behaviors of the wildtype (wt) TcpP to that of a chimeric protein: TcpP fused to the photoactivatable fluorescent protein PAmCherry (PAM).

Directly measuring and understanding subcellular mechanisms of pathogenic microbes is extremely important for advancing knowledge of human health and disease. For instance, the human disease cholera remains a relevant health threat in many areas with poor sanitation, afflicting more than 5 million people annually [17]. The sudden loss of water and ions in infected patients is the result of *V. cholerae* expressing the principal virulence factors cholera toxin (CT) and toxin-co-regulated pilus (TCP) [18]. To control expression of these virulence factors, *V. cholerae* uses a complex transcription regulatory network that includes the bitopic membrane proteins TcpP and ToxR **(Figure 2.1)** [17,19]. These trans-membrane proteins collaborate to activate transcription of *toxT*, the primary direct transcriptional activator of *V. cholerae* virulence genes, via their cytoplasmic N-terminal domains [20]. TcpP and ToxR share homology with the activators of a large family of response regulators, the OmpR/PhoB family, which are common in prokaryotes [20-24]. To provide additional control, the less well characterized membrane-bound effector proteins ToxS and TcpH likely bind in the periplasm to ToxR and TcpP, respectively, to

stabilize the multiprotein transcription complex and activate genes associated with pathogenicity referred to as the ToxR regulon **(Figure 2.1)** [24,25]. During its lifetime, *V. cholerae* colonizes multiple environments—such as aquatic reservoirs, stool, and human host—demonstrating resilience to varying pH levels and temperatures [26]. And even just within the course of human infections, these bacterial cells must pass through the acidic gut environment and colonize the surface of intestinal epithelial cells to become virulent [27]. Variable protein expression profiles of key regulators in the ToxR regulon may play a significant role in the adaptability of *V. cholerae* to diverse growth condition and biofilm formation.

Overall, biophysical investigations can uncover important information about the transcription regulation of *V. cholerae* virulence by a cytoplasmic, DNA-binding transcription activator; molecular-scale experiments including single-molecule imaging will impact the understanding of *V. cholerae* infections as well as explain other subcellular processes in bacteria that share a similar regulatory system. However, to ensure that lab experiments can be extrapolated to real-world systems, key experimental parameters must be determined —in particular, for cellular imaging, even subtle differences between the behavior of a wildtype protein and its fluorescently-labeled fusion need to be assessed. In this report, I compare the expression and dynamics of fluorescently-labeled TcpP expressed endogenously from its native promoter on the chromosome and ectopically from an inducible expression vector in live *V. cholerae* cells, as well as in the non-native *E. coli* host, using single-particle tracking (SPT)[28]. Though the TcpP expression levels were controlled to be identical according to traditional colorimetric characterization [29], more efficient transfer and fluorescence immunodetection techniques uncover differences in protein expression levels *in vitro*, and high-sensitivity single-cell and single-molecule experiments uncover significant differences in protein motions in live

cells. Additionally, I compare single-molecule dynamics for varying growth conditions to understand how changes in the TcpP expression profile affect biophysical readouts. I show that plasmid-expression systems do not produce native levels of a TcpP fusion and cause an artifact in subcellular dynamics due to overexpression, but this overexpression artifact is minimal compared to the true dynamical changes caused by changing growth conditions. Overall, SPT elucidates the subtle underlying mechanisms missed by static immunoblot methods. In particular, I determined that TcpP slows down under the growth conditions that promote virulence protein activation and speeds up under toxin-noninducing conditions, suggesting complex formation between TcpP, other proteins, and the *toxT* promoter. Finally, I track ectopically expressed TcpP in *E. coli* and detect motion artifacts similar to those caused by ectopic expression in *V. cholerae*. Overall, these results define important parameters for future experiments by i) highlighting approaches that can lead to potential artifacts created by fluorescent labeling in cells and ii) validating mechanistic insights from protein dynamics.

2.2 Results and Discussion

2.2.1 Fluorescently labeled TcpP expressed by two different approaches has minimal effect on *V. cholerae* growth rate

TcpP localizes to the *V. cholerae* inner membrane, making its fluorescent labeling organic dyes a poor option as organic dyes do not readily pass through the cell membrane of this Gram-negative bacterium without mechanical perturbations [30,31]. Therefore, to study TcpP dynamics in live *V. cholerae*, I created a protein fusion with the photoactivatable mCherry (PAmCherry) fluorescent protein expressed at the TcpP C-terminus. I expressed TcpP-PAmCherry with two common approaches for fluorescent labeling of proteins in cells: (1)

ectopic expression from an inducible plasmid promoter and (2) endogenous expression from the native promoter on the chromosome. For ectopic expression of TcpP-PAmCherry, I genetically encoded *tcpP-pamcherry* in an arabinose-inducible vector (pBAD18) and electroporated the plasmid into an O395 *ΔtcpP V. cholerae* strain. For ectopic expression in this strain, pBAD18 was chosen to mimic native TcpP expression levels because it is a low-copy plasmid with only 10 – 12 copies per cell [11]. I previously used this ectopically-expressing strain ('ectopic strain'), along with other mutant strains containing *pBAD18:tcpP-pamcherry*, to uncover TcpP/ToxR/*toxT* interaction using single-molecule imaging [29]. Alternatively, to endogenously express this fluorescent fusion, I cloned the fusion gene into a suicide vector for allelic exchange into *V. cholerae* [32]; I denote this latter strain 'endogenous'. Both of these strains should express TcpP-PAmCherry under the growth conditions used in this study. **Table 2.1** lists the strains used in this study.

Table 2.1 Strains used in this study.

Strain	Description	Notation	Reference
CS1	O395 *Vibrio cholerae*	Wildtype	Lab stock
CS23	O395:*tcpP-pamcherry*	Endogenous	This study
RY1	O395 *ΔtcpP*		Yu and DiRita (1999)
JM707	O395 *ΔtcpP* pBAD18:*tcpP-pamcherry*	Ectopic	Haas et al. (2014)
CS120	*E. coli* pBAD18:*tcpP-pamcherry*	E-pBAD	This study
CS134	*E. coli* pMMB66EH:*tcpP-pamcherry*	E-pMMB	This study
CS138	O395 *ΔtcpP* pMMB66EH:*tcpP-pamcherry*	IPTG-ectopic	This study

Introducing protein fusions in bacteria may cause growth defects if their expression alters essential cellular processes or if expressing plasmids are a substantial metabolic burden to the cells. I characterized cell growth in the toxin-inducing conditions (LB pH 6.5/30 °C) that lead to

maximal expression of virulence factors, as well as in the toxin-noninducing conditions (LB pH 8.5/37 °C) that minimize virulence factor expression [33]. In the toxin-inducing conditions, both the ectopic and endogenous strains grow similarly to wildtype (wt) *V. cholerae*, irrespective of induction by arabinose **(Figure 2.2a)**. In contrast cultures grew more poorly after arabinose induction in the toxin-noninducing condition. Various bacterial species experience cell stresses at higher pH [34], which may affect lag periods, time of entry into the stationary phase, and final cell numbers and densities. However, *V. cholerae* should be adaptable to the toxin-noninducing alkaline pH conditions since these bacteria form habitats in marine and coastal environments where pH is basic [35,36]. Thus, the poor growth I observe indicates that the changes in protein expression under toxin-noninducing conditions may interfere with normal cellular processes.

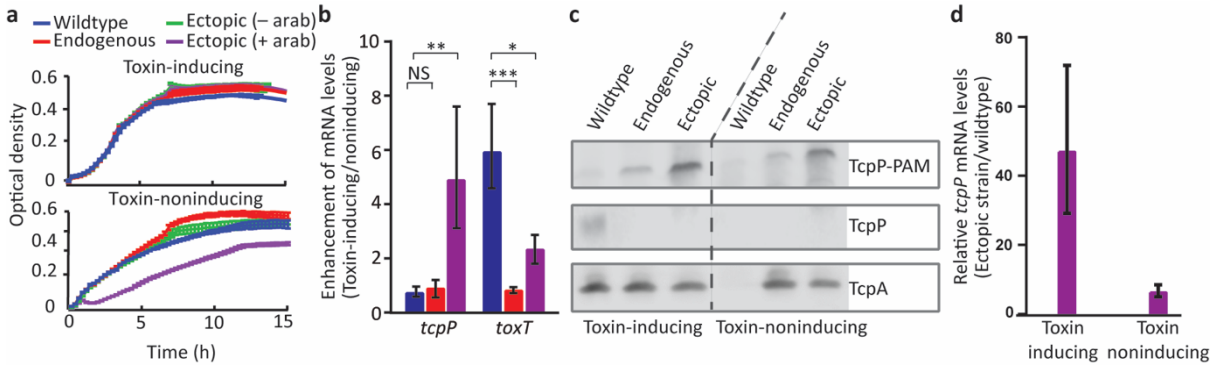

Figure 2.2 *In vitro* characterization of the O395 *V. cholerae* strains reveals differences in transcription and expression levels. O395 (wt), O395:*tcpP-pamcherry* (endogenous), and O395 *ΔtcpP* pBAD18:*tcpP-pamcherry* (ectopic) were grown either in toxin-inducing conditions (LB pH 6.5 30°C) to produce maximum virulence gene expression, or in toxin-noninducing conditions (LB pH 8.5/37 °C) to minimize virulence gene expression. Gene expression from pBAD18 was induced by arabinose. **(a)** Growth curves under toxin-inducing and toxin-noninducing conditions. **(b)** Enhancement of the transcript levels of *toxT* and *tcpP* due to toxin-inducing conditions (relative to toxin-noninducing conditions) for each strain. Blue: wt, red: endogenous, purple: ectopic (+arabinose). **(c)** TcpP or TcpP-PAmCherry (TcpP-PAM) and TcpA protein expression in all three strains probed by immunoblotting. **(d)** *tcpP* mRNA levels in the arabinose-induced ectopic strain relative to the wt strain.

2.2.2 Different TcpP-PAmCherry expression methods lead to different levels of transcription and downstream protein expression

To assess gene expression within the ToxR regulon in cells expressing TcpP-PAmCherry, I quantified the mRNA transcripts using reverse transcriptase quantitative polymerase chain reaction (RT-qPCR). Purified RNA was extracted from the three strains (ectopic, endogenous, and wt) after 4 h growth in toxin-inducing or toxin-noninducing conditions **(Figure 2.2b)**. In wt cells, *tcpP* transcript levels were independent of toxin-induction (i.e., *tcpP* transcript "enhancement" of 1), while transcription of *toxT* was enhanced by these conditions **(Figure 2.2b)**. As TcpP is the *toxT* transcription activator **(Figure 2.1)** I examined whether TcpP protein levels correlated to *toxT* transcription. I measured protein expression by immunoblotting with antibodies against TcpP. For the wt strain, I observed TcpP in toxin-inducing conditions, but not in toxin-noninducing conditions, where TcpP is rapidly degraded by regulated intramembrane proteolysis of TcpP **(Figure 2.2c)** [33,37].

RT-qPCR in the endogenous strain demonstrated that, as in wt, *tcpP* transcription is independent of toxin-inducing conditions **(Figure 2.2b)**. This result is not surprising because the endogenous strain transcription is driven by the same promoter as in wt, so I expected to observe a similar pattern of gene expression. However, unlike what I observed with the wt, I observed that for the endogenous strain TcpP-PAmCherry is detectable in both toxin-inducing and toxin-noninducing conditions **(Figure 2.2c)**. This difference between wt TcpP levels and endogenous strain TcpP-PAmCherry levels is consistent with the hypothesis that the fluorescent label at the TcpP C-terminus stabilizes the protein and inhibits regulated intramembrane proteolysis (RIP) of TcpP by Tsp and YaeL [37]. In keeping with this stabilizing effect of TcpP-PAmCherry, the total *toxT* transcription levels were increased in the endogenous relative to the wt in toxin-

noninducing conditions **(Figure 2.3)**. The sensitivity of downstream *toxT* transcription levels was also reduced in the endogenous relative to the wt **(Figure 2.2b)**, which further supports the hypothesis that TcpP-PAmCherry is more resistant than wt TcpP to RIP in toxin-noninducing conditions.

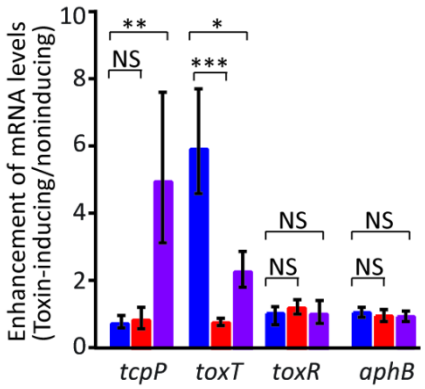

Figure 2.3 mRNA levels in the fusion strains relative to the wildtype (wt) strain. Red: endogenous, purple: ectopic (+arabinose). Bottom: zoom-in on the smaller relative values. Significance was calculated by a Student's *t*-test. NS, not significant; *, $P < 0.05$; **, $P < 0.001$; ****, $P < 0.0001$.

For the ectopic strain, 0.1% w/v arabinose was added to the growth medium at the start of induction. TcpP transcription in the ectopic strain is driven by an arabinose-inducible promoter, which likely does not respond the way the native *tcpP* promoter responds to growth signals, and indeed, I observed large increases in *tcpP* transcript levels in the ectopic strain relative to wt **(Figure 2.2d)**. This 10 – 50-fold increase indicates that this plasmid induction level was too high, even though the arabinose concentration is similar to what is commonly used for this plasmid in *V. cholerae.* Additionally, TcpP-PAmCherry expression in the ectopic strain is elevated **(Figure 2.2c)**. Taken together, it is clear that TcpP-PAmCherry is not expressed at native levels from the pBAD18 expression system. Therefore, arabinose induction here does not

yield native TcpP levels. As in the endogenous strain, TcpP-PAmCherry levels in the ectopic strains are insensitive to the difference between toxin-inducing and toxin-noninducing conditions **(Figure 2.2d)**. *tcpP* transcription in the ectopic strain seems to be enhanced in toxin-inducing conditions **(Figure 2.2b)**; this discrepancy must be related to the growth defect in toxin-noninducing conditions **(Figure 2.2a)** that negatively affects plasmid stability and maintenance.

Despite the elevated levels of *tcpP* mRNA and TcpP protein in the ectopic strain in toxin-inducing conditions, *toxT* transcripts are made in the ectopic and wt strains **(Figure 2.3)**. This implies that the TcpP-PAmCherry may not be as active as wildtype TcpP. Though *tcpP* mRNA levels are the same for the endogenous and wt strains, the *toxT* mRNA levels are not, which suggests that some regulation of the protein levels may be hidden by RT-qPCR results alone, and reveals that the TcpP concentration is not rate-limiting for *toxT* transcription. As a control, I measured the mRNA levels of *ToxR* (the co-transcriptional regulator of ToxT [38]) and *aphB* (an activator of the *tcpP* promoter [39]). These transcripts are independent of toxin induction in all strains **(Figure 2.4)**. Because downstream TcpA production is a direct readout of an active ToxR regulon, another measure of TcpP activity is to probe TcpA protein production. In all three strains, TcpA levels by immunoblot are equivalent irrespective of whether TcpP or TcpP-PAmCherry are being expressed **(Figure 2.2c)**, again confirming that functional TcpP-PAmCherry maintains its native function to activate *toxT* expression, and subsequent *tcpA* expression.

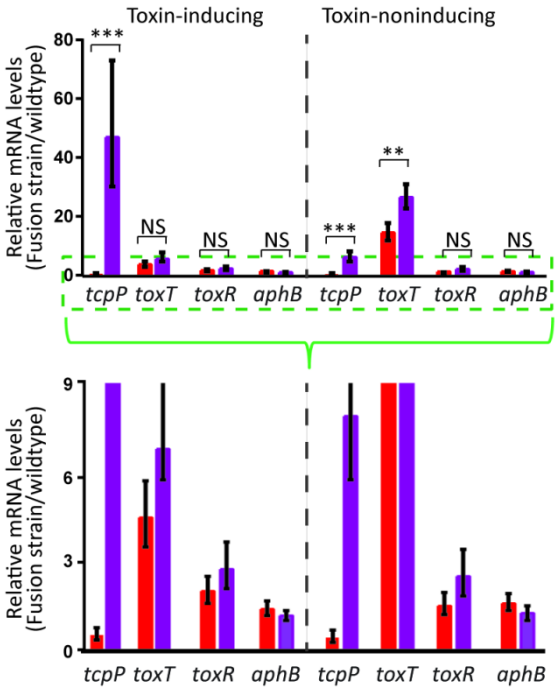

Figure 2.4 Transcript levels of *toxT*, *tcpP*, *toxR*, and *aphB* were determined for cultures grown as described in the text. **(c)** Enhancement of the transcript levels of *toxT* and *tcpP* due to toxin-inducing conditions (relative to toxin-noninducing conditions) for each strain. Blue: wt, red: endogenous, purple: ectopic (+arabinose). Significance was calculated by a Student's *t*-test. NS, not significant; *, $P < 0.05$; **, $P < 0.001$; ****, $P < 0.0001$.

2.2.3 Single-molecule tracking reveals altered TcpP-PAmCherry dynamics depending on the expression method

After verifying the TcpP-PAmCherry expression and activity, I tracked single molecules of this fusion protein in the endogenous **(Figure 2.5a)** and ectopic **(Figure 2.5d)** strains under toxin-inducing conditions with nanometer-scale resolution. I detected differences in the diffusive behavior, by comparing TcpP-PAmCherry trajectories in the endogenous **(Figure 2.5b)** and ectopic **(Figure 2.5e)** strains, TcpP-PAmCherry diffuses freely along the cell membrane in the endogenous strain, whereas it is sub-diffusive in the ectopic strain. The mean squared displacements (MSDs) of single-molecule tracks quantify the differences in the dynamics **(Figure 2.5b vs. e)**. One curve is plotted for each single-molecule track from the cells in (a) and

(d), respectively. By assuming that TcpP-PAmCherry exhibits homogeneous Brownian motion, I calculated the apparent diffusion coefficient, *D*, for each individual molecule from the slope of MSD vs. time lag, τ, according to MSD = $4D\tau$. The first five time steps in each trajectory, which correspond to the short-time linear region, were used to estimate the diffusion coefficient of each molecule, which was calculated for 4537 and 4097 single-molecule tracks in 195 endogenous and 202 ectopic cells, respectively. The average diffusion coefficient in the endogenous strain (D_{endo}: (46.2 ± 0.4) x10^{-3} $\mu m^2 s^{-1}$) is faster than the ectopic strain (D_{ecto}: (29.1 ± 0.3) x10^{-3} $\mu m^2 s^{-1}$ $\mu m^2 s^{-1}$). For comparison, the slopes that correspond to the average diffusion coefficient from all trajectories in the endogenous strain (red) and ectopic strain (purple) are both plotted in **Figure 2.5b and e**.

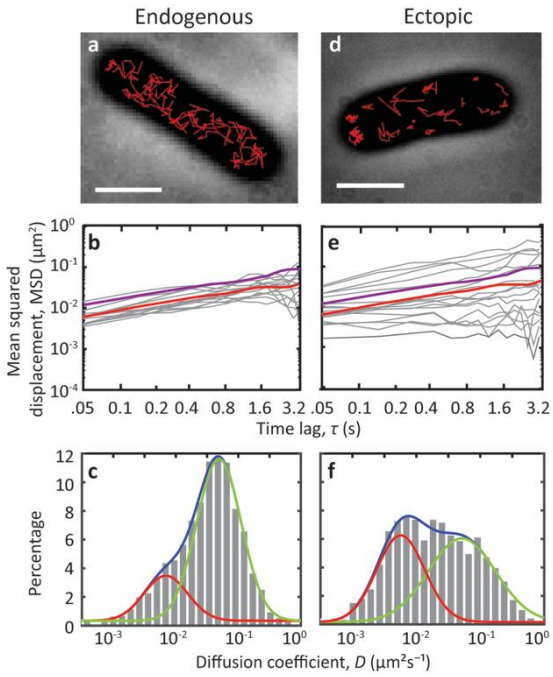

Figure 2.5 Single-molecule tracking of TcpP-PAmCherry in the endogenous and ectopic *V. cholerae* strains reveals differences in dynamics. **(a)** Single-molecule trajectories of endogenously expressed TcpP-PAmCherry on a phase-contrast image of a single bacterial cell. Scale bar: 1 μm. **(b)** Mean-squared displacement (MSD) versus time lag (τ) for the endogenous strain tracks. One curve is plotted for each single-molecule track in the cell in (a). The diffusion coefficient (D) is calculated from the slope of the first 5 time steps in each grey trajectory. The red curve is the average of all of the trajectories in this endogenous strain (D_{avg}: 0.046 $\mu m^2 s^{-1}$), the purple is the average for the ectopic strain (D_{avg}: 0.029 $\mu m^2 s^{-1}$). **(c)** Distribution of all 4537 calculated single-molecule diffusion coefficients from 195 cells. **(d)** Single-molecule trajectories of TcpP-PAmCherry in one ectopic strain *V. cholerae* cell overlaid on the phase-contrast image of that cell. Scale bar: 1 μm. (**e and f**) Corresponding analyses of the ectopic strains using 4097 calculated single-molecule diffusion coefficients from 195 cells. Movies were acquired with 40-ms integration time after a 4-h incubation in toxin-inducing conditions.

Furthermore, single-particle tracking allowed us to probe heterogeneous dynamics as shown by the distributions of D for the endogenous **(Figure 2.5c)** and ectopic **(Figure 2.5f)** strains. Using a two-term log-normal function, I fit these distributions of D to determine D_{slow} and D_{fast} in each strain. These fits reveal that TcpP-PAmCherry moves slower in the ectopic cells ($D_{slow,ecto}$: (6.2 ± 0.1) × 10^{-3} μm^2 s^{-1}) compared to the endogenous cells ($D_{slow,endo}$: (8.7 ± 0.4) × 10^{-3} μm^2 s^{-1}). However, these dynamics are reversed in the faster population: TcpP-

PAmCherry moves faster in the ectopic ($D_{fast,ecto}$: $(86.2 \pm 0.2) \times 10^{-3}$ μm^2 s^{-1}) than in the endogenous strain ($D_{fast,endo}$: $(52.6 \pm 0.2) \times 10^{-3}$ μm^2 s^{-1}). The diffusion rates calculated for TcpP-PAmCherry in these experiments are comparable to those of other membrane-bound proteins in other bacterial species [40]. Though the variance of *D* takes into account the day-to-day measurements, the broadness of the distribution of *D* values may also be a result from cell-to-cell heterogeneity. Because there are two identifiable subpopulations in these distributions, the results suggest that TcpP may be involved in transient or multiple modes of interaction in the cell irrespective of the source of expression.

By comparing the relative weights of slow and fast diffusers between the endogenous and the ectopic strains, I reveal subpopulations that are involved in different functions. Because the protein diffusion rate is related to the molecule size, I interpret the slow diffusion term to be the motion of a subpopulation that may be involved in complex formation and the fast diffusion term to be random motion. This slow subpopulation is present in the endogenous strain (26.5 ± 0.2%) at a lower same frequency than in the ectopic strain (62.8 ± 0.9%). Though this data suggests that TcpP-PAmCherry in the ectopic strain form more complexes than in the endogenous strain, these complexes may not all be related to the *toxT* transcription activation complex. Because there is only one *toxT* promoter that TcpP can act on at one time, the slow subpopulations in both strains should be similar. Therefore, by considering this diffusion data alongside the elevated mRNA and protein levels seen in the ectopic strain, I conclude that this subpopulation may be an artifact from overexpression or from plasmid expression itself for the ectopic strain. For instance, TcpP-PAmCherry agglomerates may interact with one another through dimerization and oligomerization because of the close proximity, thus resulting in higher occurrence of slow diffusers. This observation in my system is not surprising since photoactivatable FPs can exhibit

appreciable dimerization [41]. The results here provide precaution for plasmid expression of fusion proteins in cellular imaging: even though the TcpP-PAmCherry protein retains virulence function in the endogenous and ectopic strains **(Figure 2.2b and c)**, single-molecule trajectories demonstrate clear differences in the subcellular fusion protein motions.

2.2.4 Single-molecule trajectory analysis is a sensitive probe for elucidating subtle biophysical differences masked by bulk biochemical assays

V. cholerae colonizes various habitats and forms biofilm through quorum sensing [42,43]. To examine the effect of growth conditions—temperature, pH, and nutrient composition—on TcpP activity, I immunoblotted with antibodies against TcpP and TcpA to discern changes in protein levels. Though the toxin pathway can be completely turned off by increasing both the pH and temperature during growth, it is unclear about the intermediate stage when only one variable is changed. By comparing the change in temperature (conditions 1 vs. 2) and the change in pH (conditions 1 vs. 3) in **Figure 2.6a**, I detect no observable change for TcpP and TcpA expressions for both endogenous and ectopic strains. To examine the effect of nutrient composition on growth, I probed TcpP and TcpA in cells grown in M9 supplemented with NRES which should stimulate the highest level of toxin production [44]. Based on the protein levels observed between conditions 1 and 4, I do not detect observable changes going from toxin-inducing conditions to M9 supplemented with NRES. Based on the results in **Figure 2.6a**, immunoblot detection is not sensitive to probe changes in protein expression for changing growth conditions. Plasmid-expressed TcpP-PAmCherry is driven from a promoter unaffected by environmental stresses, and therefore I expected to observe these unchanged expression levels in the ectopic strain. On the other hand, since the endogenous strain should respond to

environmental stresses similarly to the wt strain, I conclude that environmental stresses regulate the protein degradation rates rather than the rates of protein expression. The TcpP-PAmCherry protein levels in changing growth conditions further support my hypothesis that TcpP-PAmCherry avoids RIP.

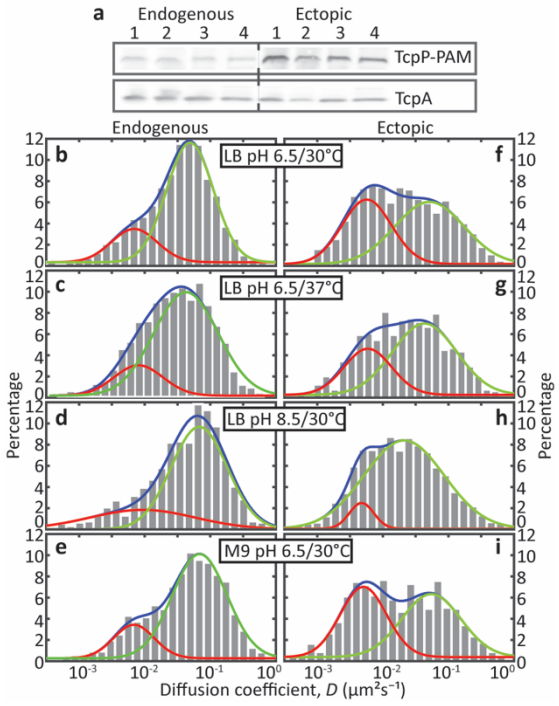

Figure 2.6 Changes in TcpP-PAmCherry dynamics as a function of growth pH and growth temperature for endogenous and ectopic expression of TcpP-PAmCherry in *V. cholerae* as detected by single-particle tracking. The *V. cholerae strains* were grown for 4 h in one of four conditions: (1) toxin-inducing (pH 6.5 LB at 30°C), (2) pH 6.5 LB at 37°C, (3) pH 8.5 LB at 30°C, and (4) pH 6.5 M9 (+NRES) at 30°C. **(a)** Immunoblot with antibodies against TcpP and TcpA for the wt, endogenous and ectopic *V. cholerae* strains. Western samples were normalized by OD_{600} before starting the assay. The diffusion coefficients of each single TcpP-PAmCherry molecule were calculated from individual trajectories as in Figure 2.5. Distributions of the diffusion coefficients calculated from all of the trajectories are shown for the endogenous strain **(b – d)** and the ectopic strain **(e – h)**. The distributions were fit to a two-term log-normal distribution. The red curve corresponds to the 'slow' diffusion term while the green curve corresponds to the 'fast' diffusion term.

Though immunoblotting is useful for measuring protein expression levels, I cannot extract kinetic details critical for determining mechanisms with this assay. Instead, I use single-particle tracking (SPT) to detect single-molecule dynamics in living *V. cholerae* cells to probe mechanism. Here, I cultured the endogenous and ectopic strains in four different conditions—toxin-inducing conditions (LB pH 6.5/37 ˚C), LB pH 6.5/37 °C, LB pH 8.5/30 °C, and M9 pH 6.5/30 °C—for 4 h before preparing the samples for imaging. As described above for **Figure 2.5**, TcpP-PAmCherry molecules were tracked in cells, and each single-molecule track was analyzed to find the diffusion coefficient, *D*. For each single-molecule track, the slope was used to calculate *D*, and the distribution of these *D* values is given in **Figure 2.6** for endogenous (b – e) and ectopic (f – i) cells grown in the same four conditions as in **Figure 2.6a**. **Table 2.2** indicates the number of tracks and cells used to generate the corresponding *D* values for the distributions of *D* in **Figure 2.6**. The difference in the shape of the distributions between endogenous and ectopic is very striking **(Figure 2.6b – e vs. Figure 2.6f – i)**; however, the changes within them are less obvious. Therefore, I fit these distributions in **Figure 2.6 (b – i)** with a two-term log-normal function to obtain D_{slow}, D_{fast}, and the relative weights of each diffusing term for the two strains under the four growth conditions. These calculated values are detailed in **Table 2.3**, and compared between strains and growth conditions in **Figure 2.7**.

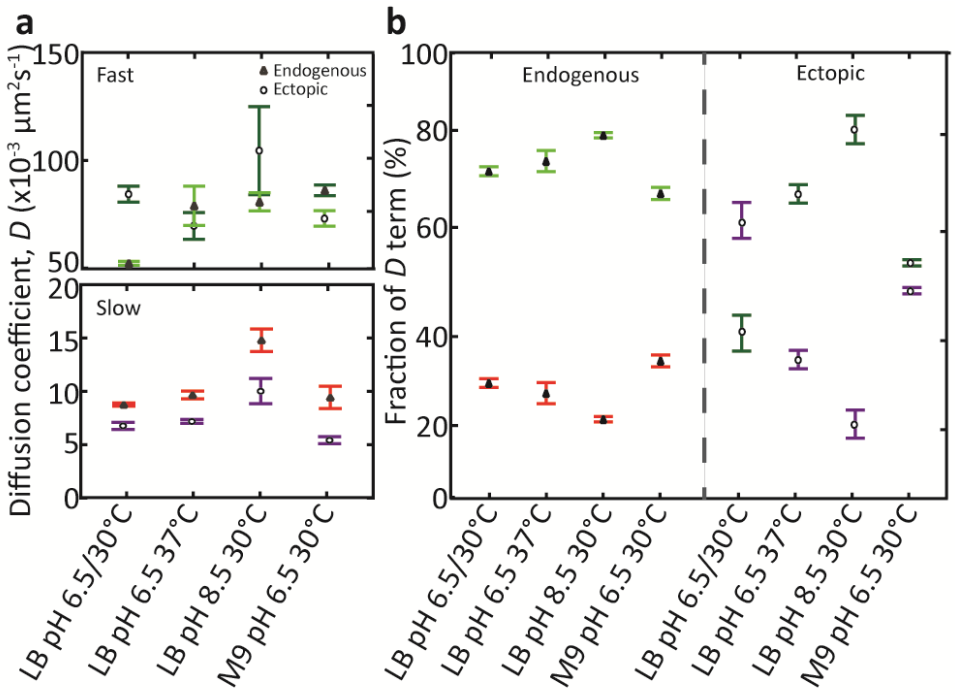

Figure 2.7 Diffusion coefficients and population weights of TcpP-PAmcherry as a function of pH and temperatures, calculated from the fits of diffusion coefficient distributions in Figure 2.6. For each strain in the four growth conditions: (a) Diffusion coefficients for the 'fast' and 'slow' populations, and (b) relative weights of the 'fast' and 'slow' populations.

Although imaging was done at room temperature for all growth conditions, I still detect changes in *D* **(Figure 2.7a)** and in population weights **(Figure 2.7b)**. Therefore, SPT reveals that TcpP-PAmCherry dynamics change with growth temperature, suggesting that growth temperature—and not imaging temperature—is the main contributor to the change in protein dynamics. A change in temperature does not change the D_{slow}, D_{fast}, or population weights in the endogenous strain **(Figure 2.7)**. However, altering pH changes motion significantly. D_{slow} increase **(Figure 2.7a, bottom panel)** while the population weights decrease **(Figure 2.7, left panel)** going from growth in toxin-inducing conditions to LB pH 8.5/30 °C. I attribute this shift to growth conditions that disfavor TcpP/ToxR/*toxT* promoter interactions when virulence factor production is reduced. For growth in M9 glycerol medium supplemented with NRES, the

distributions of *D* are similar for growth in toxin-inducing conditions and M9 **(Figure 2.6b vs. d)**. The slow term in endogenous is higher (34.4 ± 0.3% vs. 26.5 ± 0.2%) in M9 supplemented with NRES, which suggests that this slow term may be TcpP-PAmCherry involved in the *toxT* transcription activation complex. Similar trends for changes in dynamics are seen in the ectopic strain for the slow diffusing term **(Figure 2.7a, bottom panel)**. However, $D_{slow,ecto}$ is always slower for $D_{slow,endo}$ for all growth conditions. I also observed that population weight of the slow diffusing TcpP-PAmCherry in the ectopic strain is significantly more in toxin-inducing conditions and M9 supplemented with NRES **(Figure 2.7b)**. These results suggest that we may be capturing a complex formation in the ectopic strain, but these effects are enhanced by the dominant confined (slow) motion from non-native expression levels from plasmid induction. Based on the observation that TcpP-PAmCherry changes motion in different growth conditions, I speculate that the complex required for *toxT* transcription activation may be disassembled as growth temperatures and pH levels are increased in the environment which leads to downregulation of virulence proteins. I conclude that single-molecule imaging can sensitively visualize protein expression changes, as well as their associated kinetics, undetected by immunoblotting. TcpP-PAmCherry dynamics observed between the endogenous and ectopic strains **(Figure 2.7a, bottom panel)** indicate that motion is altered when fusion proteins are not natively expressed, exemplified by highly confined TcpP-PAmCherry population **(Figure 2.5d)** and a slowing down of D_{slow}, dynamic changes due to changing growth conditions can still be observed.

Table 2.2 Statistics for all strains in different growth conditions. Only trajectories lasting five frames or longer were included in the analysis.

Strain	Growth conditions	Cells	Trajectories
Endogenous	toxin-inducing (LB pH 6.5 30°C)	195	4537
	LB pH 6.5 37°C	208	2482
	LB pH 8.5 30°C	86	1604
	M9 pH 6.5 30°C	186	2732
Ectopic	toxin-inducing	202	4097
	LB pH 6.5 37°C	80	1387
	LB pH 8.5 30°C	131	3530
	M9 pH 6.5 30°C	82	1925
IPTG-ectopic	toxin-inducing (– IPTG)	67	874
	toxin-inducing (+IPTG)	93	1877
E-pBAD	toxin-inducing	199	2279
E-pMMB	toxin-inducing (+IPTG)	56	1042

Table 2.3 Statistics for 'slow' and 'fast' TcpP-PAmCherry for endogenous and ectopic strains in different growth conditions. D_{slow} and D_{fast} were calculated from fitting the distribution of all D (Figure 2.6) to a two-term log-normal distribution. The fractions were calculated from calculated from the areas below each log-normal distribution. Standard errors were generated through from day-to-day measurements.

Strain	Growth conditions	Slow fraction	Fast fraction	D_{slow} ($\times 10^{-3}$ μm^{2}s^{-1})	D_{fast} ($\times 10^{-3}$ μm^{2}s^{-1})
Endogenous	toxin-inducing	26.5 ± 0.2	73.5 ± 0.2	8.7 ± 0.4	52.6 ± 0.2
	LB pH 6.5 37°C	24.2 ± 0.5	75.6 ± 0.5	10 ± 0.1	80 ± 2
	LB pH 8.5 30°C	18.4 ± 0.1	81.6 ± 0.1	17 ± 0.3	81.4 ± 0.9
	M9 pH 6.5 30°C	34.4 ± 0.3	68.6 ± 0.3	9.7 ± 0.3	86.8 ± 0.5
Ectopic	toxin-inducing	62.8 ± 0.9	37.2 ± 0.9	6.2 ± 0.1	86.2 ± 0.2
	LB pH 6.5 37°C	31.2 ± 0.4	67.8 ± 0.4	6.7 ± 0.1	71 ± 1.0
	LB pH 8.5 30°C	16.6 ± 0.6	83.4 ± 0.6	10 ± 0.3	10^2 ± 4.0
	M9 pH 6.5 30°C	46.8 ± 0.1	53.2 ± 0.1	4.4 ± 0.1	74.8 ± 0.6

2.2.5 Expression of TcpP-PAmCherry from a plasmid expression system creates artificial protein dynamics independent of induction level

Figures 2.2 – 2.7 show that the ectopic strain containing pBAD18 can be induced with an arabinose concentration to turn on immunoblot-detectable expression of TcpP-PAmCherry. However, this induction level also results in the appearance of a very slow moving subpopulation during imaging **(Figure 2.5d and Figure 2.7a, bottom panel)**. To determine whether this subpopulation is created by elevated protein expression or attributed to the pBAD18 expression system itself, I cloned *tcpP-pamcherry* into another low-copy number expression vector, IPTG-inducible pMMB66EH [45], and transformed the new vector into O395 *ΔtcpP* for comparison. In **Figure 2.8a**, induction of pMMB66EH with 1 mM IPTG causes a growth defect in toxin-inducing conditions. Under toxin-noninducing conditions, this growth defect is further enhanced **(Figure 2.8b)**, consistent with the lag phase I observed after arabinose induction of pBAD18 in the same growth conditions **(Figure 2.2b)**. I characterized protein levels produced from the pMMB66EH vector by immunoblotting, and I observed that TcpP-PAmCherry is overexpressed with 1 mM IPTG induction in both toxin-inducing and noninducing conditions **(Figure 2.8c)**. Though IPTG-inducible promoters are known to be leaky, non-induction does not result in immunoblot-detectable TcpP or TcpA **(Figure 2.8c, condition 3)**. In addition, unlike the pBAD18-ectopic strain **(Figure 2.2d)**, when pMMB66EH vector is used, TcpP-PAmCherry expression is reduced by toxin-noninducing conditions for the ectopic strain, while the TcpA levels remain unchanged. The decreased TcpP-PAmCherry levels detected in the pMMB66EH-ectopic strain and the growth defect observed under toxin-noninducing conditions suggest that the pMMB66EH expression vector may be unstable at pH 8.5 such that imaging this construct at pH 8.5 may not elucidate native mechanisms.

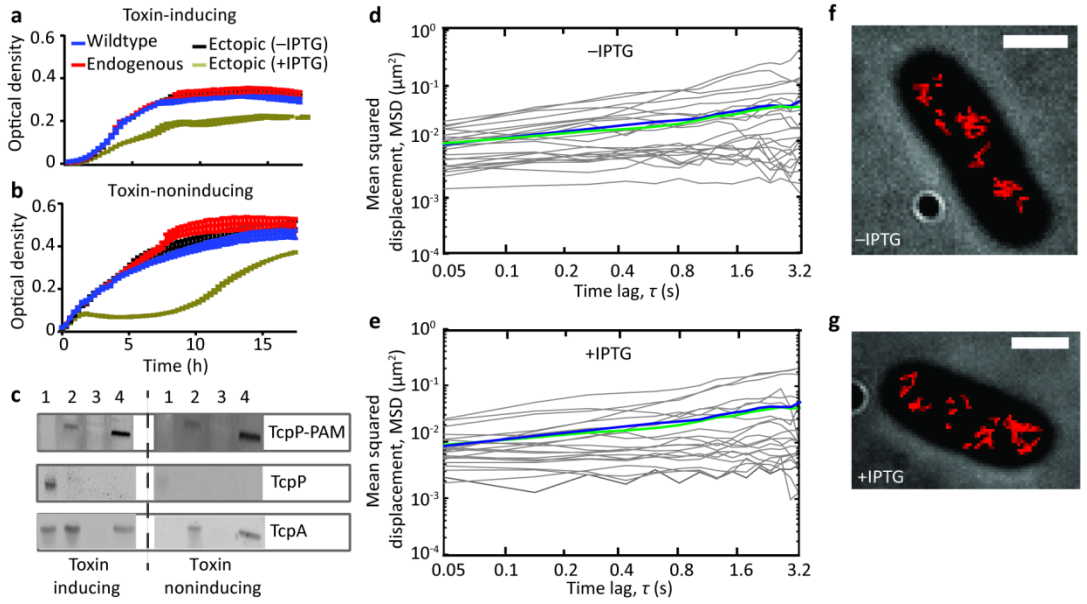

Figure 2.8 Characterization of ectopically expressed TcpP-PAmCherry from a second plasmid induced by IPTG. O395 (wt), O395:*tcpP-pamcherry* (endogenous), and O395 *ΔtcpP* pMMB66EH:*tcpP-pamcherry* (ectopic) were grown in **(a)** toxin-inducing, and **(b)** toxin-noninducing conditions. **(c)** Protein expression of TcpP and downstream TcpA detected by immunoblotting against TcpP and TcpA antibodies. The samples were run in toxin-inducing and repressing conditions in the order: (1) wt, (2) endogenous, (3) ectopic (– IPTG), (4) ectopic (+ IPTG). Mean square displacement curves for single-molecule trajectories of TcpP-PAmCherry expressed from **(d)** leaky IPTG promoter (–IPTG) and **(e)** 1 mM IPTG induction (+IPTG) in toxin-inducing condition. The diffusion coefficient (*D*) is calculated from the slope of the first 5 time steps in each grey trajectory. The green curve is the average of all of the trajectories in this –IPTG strain (D_{avg}: 0.049 $\mu m^2 s^{-1}$), the blue is the average for the +IPTG strain (D_{avg}: 0.039 $\mu m^2 s^{-1}$). Single-molecule trajectories of ectopically expressed TcpP-PAmCherry expressed from **(f)** leaky IPTG promoter (–IPTG) and **(g)** 1mM IPTG induction (+IPTG)leaky expression overlaid on a phase-contrast image of a single bacterial cell. Scale bars: 1 μm.

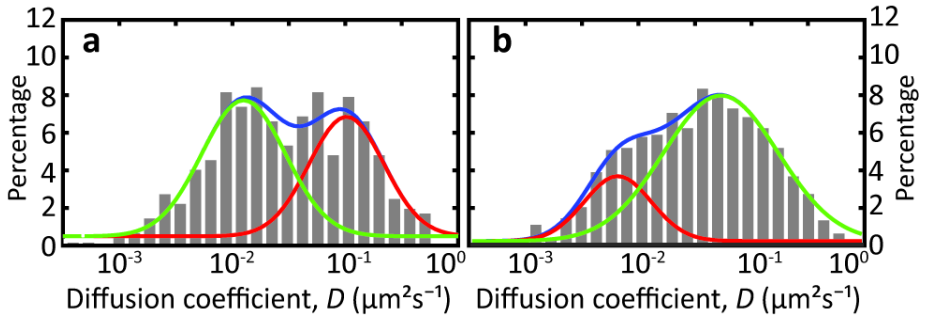

Figure 2.9 Dynamics of plasmid-expressed TcpP-PAmCherry from a second IPTG-induced plasmid. Distributions of calculated diffusion coefficients from single-molecule trajectories in the ectopic strain expressed from **(a)** leaky IPTG promoter (–IPTG) and **(b)** 1 mM IPTG induction (+IPTG) in toxin-inducing condition.

To understand how dynamics of a molecule may be altered by its expression system, I visualized and tracked individual TcpP-PAmCherry in the IPTG-ectopic strain under toxin-inducing conditions without IPTG and with IPTG induction. By calculating *D* for each track in **(Figure 2.8d)** and **(Figure 2.8e)** and plotting distributions in **Figure 2.9** for (a) for leaky expression and (b) 1 mM IPTG induction, respectively, I reveal that the slow diffusers move slower ($D_{\text{slow,+IPTG}}$: (7.2 ± 0.3) × 10^{-3} μm^2 s^{-1} vs. $D_{\text{slow,–IPTG}}$: (10.9 ± 0.4) × 10^{-3} μm^2 s^{-1}) when TcpP-PAmCherry protein levels are increased with IPTG induction. This similar trend for a change in dynamic for increased expression is also observed between the endogenous and pBAD18-expressed strains, which further supports that overexpression results in highly confined motion. For the fast diffusing subpopulation, TcpP-PAmCherry moves slower with IPTG induction ($D_{\text{fast,–IPTG}}$: (12.0 ± 0.4) × 10^{-2} μm^2 s^{-1} vs $D_{\text{fast, +IPTG}}$: (85.0 ± 0.6) × 10^{-2} μm^2 s^{-1}). By comparing D_{fast} for –IPTG and –IPTG growth conditions, I reveal a broader distribution for +IPTG **(Figure 2.9a vs. b, green curves)**. I speculate that this broadness may be attributed by the increased likelihood for TcpP-PAmCherry to bind transiently to other proteins due to high protein concentrations. My imaging, which can detect localizations with leaky **(Figure 2.8f)** and

IPTG-induced plasmid expression **(Figure 2.8g)**, reveals the sensitivity of single-molecule imaging to visualize the dynamics of low-copy numbers of TcpP-PAmCherry that are undetectable by immunoblotting **(Figure 2.8c, condition 3)**. The particle tracking results here further support the hypothesis that plasmid expression of a fluorescent protein fusion creates highly confined protein dynamics not seen in endogenous expression **(Figure 2.8f and g)**. It may be possible to extract dynamics that correspond to a virulence mechanism in *V. cholerae* from strains that utilize plasmid expression systems by tracking an unrelated chimera protein expressed in the same system, and discerning and subtracting dynamics that are induced by overexpression.

2.2.6 TcpP motion in a heterologous host is inconsistent with TcpP motion in *V. cholerae*

Allelic exchange in non-model bacterial systems are sometimes undeveloped or difficult, thus expression of protein fusions from plasmid expression systems are typically utilized. By investigating TcpP-PAmCherry expression and dynamics expressed from an endogenous locus and from plasmid expression systems, I uncover motion artifacts that must be addressed before I can deduce mechanisms from single-molecule dynamics. To understand if similar motion artifacts are present in another host, I measured single-molecule TcpP-PAmCherry dynamics in *E. coli*. I chose *E. coli* as a heterologous host because early discoveries of the *V. cholerae* proteins and mechanisms relevant for pathogenesis were first made in *E. coli* [46-48].

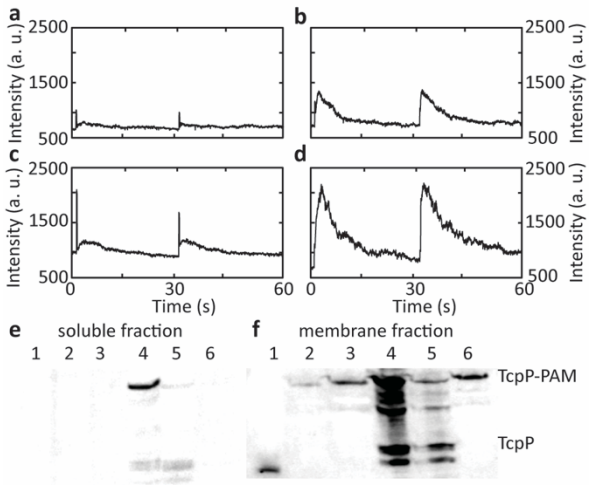

Figure 2.10 Fluorescence intensity of ectopically expressed TcpP-PAmCherry in *V. cholerae* and in a heterologous host. The fluorescence is measured in a single cell in which some of the photoactivatable PAmCherry is activated every 30s by a 405-nm laser. **(a)** *V. cholerae* (+arabinose), **(b)** *E. coli* (+arabinose), **(c)** *V. cholerae* (+IPTG), **(d)** *E. coli* (+IPTG). The fluorescence intensity is proportional to the number of photoactivated fusion protein copies. Fractionation of cells grown in toxin-inducing conditions, probed by immunoblotting with antibodies against TcpP determines where TcpP is localized in cell. (1) wt *V. cholerae*, (2) endogenous *V. cholerae*, (3) ectopic *V. cholerae* (+arabinose), (4) ectopic *V. cholerae* (–IPTG), (5) ectopic *V. cholerae* (+IPTG), (6) ectopic *E. coli* (+arabinose), (7) ectopic *E. coli* (–IPTG), and (8) ectopic *E. coli* (+IPTG). Equal amounts of total protein were loaded in each lane for **(e)** the soluble fraction and **(f)** the membrane fraction.

In *E. coli* containing either pBAD18:*tcpp-pamchery* or pMMB66EH:*tcpp-pamcherry*, I visualized and tracked individual plasmid-expressed TcpP-PAmCherry under toxin-inducing conditions as described above for *V. cholerae*. In *E. coli*, two types of motion were captured for arabinose-induced TcpP-PAmCherry. The slow-moving subpopulation is very similar to TcpP-PAmCherry observed in the ectopic *V. cholerae* strain, but I also detect a significant number of molecules that diffused too quickly to track. This fast TcpP-PAmCherry motion in the pBAD18-expression system was not detected for the pMMB66EH-expression system. To determine if this fast diffusing population is real and not just a result of elevated background fluorescence in *E. coli*, I plot the total fluorescence intensity in a single bacterial cell during a 1 min acquisition

(Figure 2.10a – d). The spikes in intensity correspond to the 200-ms 405-nm pulses meant to photoactivate PAmCherry. Because intensity increases after activation and decreases over time, this suggests that the fast motion I observed are TcpP-PAmCherry molecules—and not autofluorescence—that are activated, imaged, and bleached over time. Additionally, I extract relative protein copies from these traces by the fluorescence intensities after the activation pulses. Since the same 405-nm laser power is used for photoactivation, the higher intensities indicate that there are more TcpP-PAmCherry molecules in *E. coli* than in *V. cholerae* for pBAD18-expression system **(Figure 2.10b vs. a)**. The pMMB66EH expression system also leads to higher intensities in *E. coli* **(Figure 2.10d)** relative to *V. cholerae* **(Figure 2.10c)**. Overall, these differences in protein concentration for different hosts suggest different plasmid-expression system regulation or different plasmid copy numbers in different bacterial species. Therefore, I conclude that studying protein dynamics in a heterologous host may also result in artifacts.

Because its protein sequence targets TcpP to the *V. cholerae* inner membrane, and because membrane-bound fluorescent proteins generally move slow enough to be tracked in my 2D-imaging setup, the non-trackable, arabinose-induced TcpP-PAmCherry molecules in *E. coli* were unexpected. This fast motion is more consistent with molecules diffusing in the cytoplasm. Therefore, I separated soluble and insoluble fractions by ultracentrifugation, and I used immunoblotting to determine where TcpP-PAmCherry is localized in *E. coli*. I detected TcpP in the membrane of both the *E. coli* and *V. cholerae* strains **(Figure 2.10f)**. However, **Figure 2.10e** shows that whereas all TcpP-PAmCherry localizes to the *V. cholerae* membrane, TcpP-PAmCherry is also found in the soluble fraction of *E. coli* when expressed by arabinose induction of pBAD18, supporting the idea that the non-trackable subpopulation observed in the *E. coli* strain is cytosolic TcpP-PAmCherry. Based on the degradation bands in the

pBAD18:*tcpP-pamcherry E. coli* strain, these degraded molecules may also contribute to the non-trackable subpopulation. Since the diffusion rates experienced by most cytosolic proteins are faster than the limitations of SPT, this subpopulation is not captured by SPT. Based on the very fast TcpP-PAmCherry dynamics I obtained for *E. coli*, it is not evident that TcpP mechanisms in *V. cholerae* can be elucidated with pBAD18 expression in *E. coli*. However, because the pMMB66EH-expression system only leads to membrane-bound TcpP even in *E. coli* **(Figure 2.10, lane 8)**, this latter strain may still be useful for characterizing freely diffusing TcpP-PAmCherry in the periplasm of a Gram-negative bacterium. Future studies may characterize the motion of TcpP-PAmCherry in this heterologous host to establish a baseline to differentiate in *V. cholerae* between TcpP-PAmCherry actively engaging in transcription activation, and freely diffusing TcpP-PAmCherry in the *V. cholerae* periplasm.

2.3 Conclusions

Single-molecule protein tracking is invaluable for understanding subcellular biological interactions in living bacteria, but the consequences of labeling and expressing protein fusions *in vivo* may cause artifacts that are not obvious in bulk controls. In this study, I have measured the motion of a transcriptional regulator, TcpP, fused to the fluorescent protein PAmCherry in live bacterial cells, and have examined how the TcpP-PAmCherry motion changes based on expression. Though TcpP-PAmCherry expression in *V. cholerae* is stable and retains sufficient functional activity for downstream mRNA and protein expressions detectable in biochemical assays, single-molecule tracking reveals significant changes in physiologically relevant protein motion due to fusion protein expression and regulation. Plasmid expression of TcpP-PAmCherry from arabinose- and IPTG-inducible promoters causes overexpression, which leads in these SPT

studies to a slow-diffusing subpopulation that is not present under endogenous expression. Because TcpP-PAmCherry is not subjected to proteolysis like unlabeled TcpP, I probe similar downstream TcpA levels by immunoblot detection. However, tracking TcpP in *V. cholerae* cells at different growth conditions reveals the sensitivity at the single-molecule level to elucidate dynamical responses that are hidden in immunoblot detection. By comparing the distribution and average diffusion coefficients of TcpP-PAmCherry at different growth conditions, I found that TcpP moves faster under growth conditions that disfavor virulence production, possibly by destabilizing the ToxR regulon protein-DNA complex. Furthermore, by examining TcpP motion in a heterologous host like *E. coli*, my data suggests that it may not be relevant to directly translate findings in *E. coli* to findings in *V. cholerae*: I measure a significant amount of much faster TcpP-PAmCherry motion by SPT. Through cell fractionation, I found that this rapidly-diffusing subpopulation in *E. coli* corresponds to cytoplasmic TcpP. The data in this study suggests that single-molecule protein tracking has the capability to uncover mechanistic understandings above artifacts induced by labeling and incorrect protein expression levels, but experimental variables should be limited and controlled for in order to correlate protein dynamics with 'true' biological processes.

2.4 Materials and methods

2.4.1 Bacterial strains and culture conditions

The *Vibrio cholerae* classical strain O395 was used throughout this study. The *Escherichia coli* strain DH5α was used for cloning, and strain SM10λpir was used for conjugation of plasmid into *V. cholerae*. *V. cholerae* was cultured in two different media as indicated in the experiments: Luria-Bertani (LB) rich medium or M9 minimal medium

supplemented with 0.4% glycerol and an amino acid supplement (asparagine, arginine, glutamic acid and serine, 25 mM final concentration). Overnight cultures of *V. cholerae* were cultured in LB at neutral pH before subculturing 1:100 in toxin-inducing conditions (pH 6.5/30 °C, shaking) to activate full virulence gene expression or in toxin-repressing conditions (pH 8.5/37 °C, shaking) to turn off virulence gene expression [33]. Ectopic expression of TcpP-PAmCherry1 [49] from pBAD18 or from pMMB66EH was induced by the addition of L-arabinose to 0.1% final concentration and isopropyl-D-thiogalactopyranoside (Invitrogen) to 1 mM final concentration, respectively. *In vitro* and *in vivo* measurements were done on bacterial cells in mid-logarithmic phase, except for the growth curves for which the cells were grown until stationary phase was reached. The growth curves were performed on an Infinite 200 PRO (TECAN) in a 96-well plate with orbital shaking turned on and temperature set to either 30 °C or 37 °C, as indicated in the text. OD_{600} readings were taken at 20 min intervals for 23 h. Antibiotics for bacterial growth were used at the following concentrations: carbenicillin, 50 or 100 μg ml^{-1}; kanamycin, 50 μg ml^{-1}; and streptomycin, 100 μg ml^{-1}.

2.4.2 Plasmid and strain construction

Plasmids used in this study were the cloning vector pGEM-T Easy (Promega), the suicide vector pKAS32 [32], the arabinose-inducible expression vector pBAD18-Kan [50], and the isopropyl *β*-D-1-thiogalactopyranoside (IPTG)-inducible expression vector pMMB66EH [51]. The pMMB66EH:*tcpP-pamcherry* construct was constructed by amplifying the *tcpP-pamcherry* sequence from strain JM707 using primers CSP133 and CSP134 **(Table 2.4)**. For allelic exchange in *V. cholerae*, homologous recombination inserted the *pamcherry* gene sequence between the *tcpP* whole-gene sequence and 500 nt downstream of the *tcpP* stop codon. This

synthesized gene fragment (IDT) was used as a template to generate flanking restriction sites with primers CSP60 and CSP61 **(Table 2.4)**. The PCR products were ligated into pGEM-T Easy before moving into other backgrounds. The resulting plasmids were digested with EcoRI and XbaI and ligated into similarly digested pBAD18-Kan, digested with HindIII and XmaI and ligated into similarly digested pMMB66EH, or digested with Bglll and XbaI into similarly digested pKAS32 [32]. The resulting expression plasmids were confirmed by sequencing, and transformed into a *ΔtcpP V. cholerae* strain by electroporation. Plasmid DNA was introduced into *E. coli* by standard chemical or electroporation methods, and introduced into *V. cholerae* by electroporation or by conjugation through SM10*λ*pir [32]. Integration of the plasmid into the *V. cholerae* chromosome was selected for by plating on TCBS (thiosulfate-citrate-bile-sucrose) plates (Difco) containing 50 μg ml^{-1} ampicillin. The cointegrate was resolved by selection on LB plates containing 1 mg ml^{-1} streptomycin. PCR with primers flanking the deletion was used to determine recombination and loss of the wildtype allele.

Table 2.4 Primers used for cloning *tcpP-pamcherry*.

Primer	Sequence
CSP60	5'-GCAGATCTATGGGGTATGTCCGCGTGAT-3'
CSP61	5'-GCTCTAGACAACTGCGAACATTAGGGTA-3'
CSP133	5'-CCCGGGAGGAGGAAACGATGGGGTATGTCCG-3'
CSP134	5'-GCAAGCTTTTACTTGTACAGCTCGTCCATGCCGC-3'

2.4.3 Protein electrophoresis and immunodetection

Overnight cultures of *V. cholerae* were subcultured 1:100 in pH 6.5 or pH 8.5 LB and grown for 4 h at 30 °C or 37 °C. For ectopic expression, L-arabinose or IPTG was added to the

culture medium at the time of subculture for strains containing pBAD18 or pMMB66EH, respectively. One milliliter of midlogarithmic culture was pelleted by centrifugation and resuspended in 1× sample buffer. Proteins were separated by SDS/PAGE using 4 – 20% (weight/volume) Mini-PROTEAN pre-cast gels (Biorad), and loading volumes were adjusted to normalize the OD_{600}. Proteins were then transferred to a polyvinylidene difluoride (PVDF) membrane using the iBlot 2 Dry Blotting system (Invitrogen) and probed with rabbit anti-TcpP antibodies (generated by Rockland Immunochemicals), rabbit anti-TcpA antibodies (generated by Rockland Immunochemicals), or with mouse anti-RNA Polymerase β antibody (BioLegend). The blots were probed with IRDye 800CW goat anti-rabbit and IRDye 680RD goat anti-mouse, and imaged with the Odyssey CLx Imaging System (LICOR).

2.4.5 Reverse transcription polymerase chain reaction (qRT-PCR) analysis of mRNA expression

The bacterial strains were cultured in triplicate in each of the conditions listed above. 1-OD of cells from each sample was harvested, and RNA was extracted using TRIzol reagent (Life Technologies). RNA samples for qRT-PCR were DNase-treated with TURBO DNA Free Kit (Life Technologies), run on an agarose gel to check quality, and quantified by measuring the OD_{260}. The qRT-PCR experiments were performed using the QuantiTect SYBR green RT-PCR kit (Qiagen) according the manufacturer's manual. The qRT-PCR primers are shown in **Table 2.5**. Transcription levels were normalized to levels of *rpoB*, the transcript of the RNA polymerase β subunit, and fold change was calculated using the $2^{-\Delta\Delta CT}$ method [52]. Results are the averages for three biological replicates **(Table 2.6)**.

Table 2.5 Primers used for qRT-PCR analysis.

Target	Forward primer	Reverse primer
toxT	5'-TGGGCAGATATTTGTGGTGA-3'	5'-GAAACGCTAGCAAACCCAGA-3'
tcpP	5'-TGAGTGGGGGAAGATAAACG-3'	5'-TTGGATTGTTATCCCCGGTA-3'
rpoB	5'-GGCGGTGTTATCCAGTCAGT-3'	5'-CTGGTTCGAACGGGTGTACT-3'

Table 2.6 Raw data for qRT-PCR analysis with ΔΔCT method. These values were obtained from triplicate samples.

Strain	Growth condition	*toxT*	*tcpP*	*toxR*	*aphB*	*rpoB*	*recA*
Mean CT (threshold cycle)							
Wildtype	toxin-inducing	18.165	27.953	22.922	19.395	17.916	22.107
	toxin-noninducing	21.632	28.259	23.762	20.275	18.813	22.286
Endogenous	toxin-inducing	16.770	29.413	22.702	19.657	18.384	22.487
	toxin-noninducing	16.982	29.750	23.541	20.009	18.912	22.251
Ectopic	toxin-inducing	15.078	21.782	21.145	18.831	17.297	20.383
	toxin-noninducing	16.491	24.276	21.434	18.949	17.507	19.630
Standard deviation of CT (threshold cycle)							
Wildtype	toxin-inducing	0.303	0.320	0.225	0.049	0.054	0.580
	toxin-noninducing	0.163	0.169	0.296	0.148	0.132	0.294
Endogenous	toxin-inducing	0.162	0.378	0.226	0.205	0.085	0.343
	toxin-noninducing	0.061	0.327	0.042	0.172	0.035	0.369
Ectopic	toxin-inducing	0.210	0.534	0.303	0.136	0.128	0.455
	toxin-noninducing	0.180	0.304	0.292	0.095	0.115	0.347

2.4.6 Cell fractionation

Cell fractionation was carried out as previously described for *E. coli* [53] with a few modifications. Bacteria grown for 4 h in toxin-inducing conditions were harvested as described for protein electrophoresis. The pellet was washed twice with 10 mM Tris base (pH 7.5) before resuspension in 1/50 of the culture volume. After one freeze-thaw cycle at -80°C, cells were

sonicated with a microtip at 30% amplitude three times for 30s each time. Cell debris was pelleted by centrifugation (7,000 × g for 15 min at 4 °C in a tabletop centrifuge), and the supernatants were ultracentrifuged to form membrane pellets (100,000 ×g for 60 min at 4 °C with a Beckman 70 Ti rotor). The soluble fraction (supernatant) was collected, and the membrane fraction (pellet) was washed once in 10 mM Tris-HCl (pH 7.5). Protein concentrations were determined at 280 nm with a spectrophotometer. Equal concentrations of proteins were then analyzed by SDS-PAGE and immunoblot detection.

2.4.7 Super-resolution single-particle tracking in live bacterial cells

Bacterial cultures were grown in the same condition as described for immunodetection above. 4 h after subculturing the bacterial cultures into fresh media (with inducers added for the strains ectopically expressing TcpP-PAmCherry), 1 ml of midlogarithmic culture was pelleted by centrifugation and the pellet resuspended in 200-300 µl of growth medium. A 2.0-µl droplet of concentrated cells was then placed onto an agarose pad (2% agarose dissolved in M9 minimal media at pH 6.5 or 8.5, spread on a microscope slide, and cut into 1″ squares) and covered with a coverslip. M9 minimal media was used for making agarose pads to reduce background fluorescence.

All live bacterial cell imaging was done at room temperature using an Olympus IX71 inverted fluorescence microscope equipped with a 1.40 numerical aperture, 100× oil-immersion wide-field phase-contrast objective. PAmCherry fluorescence was activated in the cells using a 405-nm laser (Coherent Cube 405-100), and imaged using a 561-nm excitation laser (Coherent Sapphire 560-50) operating at 100 – 120 W/cm^2 and 30 – 60 W/cm^2, respectively. A 200-ms activation pulse was used to photo-activate 1 – 5 PAmCherry molecules per cell at a time. A

Photometrics Evolve EMCCD camera was used to capture a 256 × 256 pixel field of view at a speed of 40 frames per second, which corresponds to a 12.5 μm × 12.5 μm detection area. The movies collected were processed using custom MATLAB code previously written in the lab [54,55] to segment cells from phase-contrast images and to localize single TcpP-PAmCherry molecules on the scale of 50 nm according to the 95% confidence interval from fitting the emission to a 2D Gaussian function. Single-molecule tracks were constructed by connecting molecules that are localized within 350 nm in consecutive frames for a minimum of 5 frames. However, most track lengths are greater than 10 frames. The diffusion coefficient of each single-molecule trajectory was calculated from the mean squared displacement versus time lag. I used the squared displacements associated with the first five time lags to minimize errors associated with reduced statistics at higher time lags.

2.5 Acknowledgements

This work was supported by National Institutes of Health (NIAID) Grant R21-AI099497-02 to V.J.D and J.S.B. C.S. was supported by a University of Michigan Rackham Merit Fellowship. I would like to thank Andrew Perault and Jeremiah Johnson for help with strain constructions, Yi Liao for assistance with the single-molecule tracking and analysis code, and Wei Ping, Justin Lenhart, Josh Karslake, and Hannah Tuson for helpful comments.

2.6 References

1. Yao, Z.; Carballido-Lopez, R. Fluorescence Imaging for Bacterial Cell Biology: From Localization to Dynamics, from Ensembles to Single Molecules. *Annu. Rev. Microbiol.* **2014**, *68*, 459-476.

2. Day, R. N.; Schaufele, F. Fluorescent Protein Tools for Studying Protein Dynamics in Living Cells: A Review. *J. Biomed. Opt.* **2008**, *13*, 031202.

3. Tuson, H. H.; Biteen, J. S. Unveiling the Inner Workings of Live Bacteria using Super-Resolution Microscopy. *Anal. Chem.* **2015**, *87*, 42-63.

4. Lee, T. K.; Meng, K.; Shi, H.; Huang, K. C. Single-Molecule Imaging Reveals Modulation of Cell Wall Synthesis Dynamics in Live Bacterial Cells. *Nat. Commun.* **2016**, *7*, 13170.

5. Xie, X. S.; Choi, P. J.; Li, G. W.; Lee, N. K.; Lia, G. Single-Molecule Approach to Molecular Biology in Living Bacterial Cells. *Annu. Rev. Biophys.* **2008**, *37*, 417-444.

6. Yao, Z.; Carballido-Lopez, R. Fluorescence Imaging for Bacterial Cell Biology: From Localization to Dynamics, from Ensembles to Single Molecules. *Annu. Rev. Microbiol.* **2014**, *68*, 459-476.

7. Stracy, M.; Uphoff, S.; Garza de Leon, F.; Kapanidis, A. N. In Vivo Single-Molecule Imaging of Bacterial DNA Replication, Transcription, and Repair. *FEBS Lett.* **2014**, *588*, 3585-3594.

8. Haas, B. L.; Matson, J. S.; Dirita, V. J.; Biteen, J. S. Imaging Live Cells at the Nanometer-Scale with Single-Molecule Microscopy: Obstacles and Achievements in Experimental Optimization for Microbiology. *Molecules* **2014**, *19*, 12116-12149.

9. Dean, K. M.; Palmer, A. E. Advances in Fluorescence Labeling Strategies for Dynamic Cellular Imaging. *Nat. Chem. Biol.* **2014**, *10*, 512-523.

10. Gu, P.; Yang, F.; Su, T.; Wang, Q.; Liang, Q.; Qi, Q. A Rapid and Reliable Strategy for Chromosomal Integration of Gene(s) with Multiple Copies. *Sci. Rep.* **2015**, *5*, 9684.

11. Rosano, G. L.; Ceccarelli, E. A. Recombinant Protein Expression in Escherichia Coli: Advances and Challenges. *Front. Microbiol.* **2014**, *5*, 172.

12. del Solar, G.; Giraldo, R.; Ruiz-Echevarria, M. J.; Espinosa, M.; Diaz-Orejas, R. Replication and Control of Circular Bacterial Plasmids. *Microbiol. Mol. Biol. Rev.* **1998**, *62*, 434-464.

13. Kintaka, R.; Makanae, K.; Moriya, H. Cellular Growth Defects Triggered by an Overload of Protein Localization Processes. *Sci. Rep.* **2016**, *6*, 31774.

14. Reyes-Lamothe, R.; Sherratt, D. J.; Leake, M. C. Stoichiometry and Architecture of Active DNA Replication Machinery in Escherichia Coli. *Science* **2010**, *328*, 498-501.

15. DiRita, V. J.; Parsot, C.; Jander, G.; Mekalanos, J. J. Regulatory Cascade Controls Virulence in Vibrio Cholerae. *Proc. Natl. Acad. Sci. U. S. A.* **1991**, *88*, 5403-5407.

16. Brown, R. C.; Taylor, R. K. Organization of Tcp, Acf, and toxT Genes within a ToxT-Dependent Operon. *Mol. Microbiol.* **1995**, *16*, 425-439.

17. Matson, J. S.; Withey, J. H.; DiRita, V. J. Regulatory Networks Controlling *Vibrio Cholerae* Virulence Gene Expression. *Infect. Immun.* **2007**, *75*, 5542-5549.

18. Krukonis, E. S.; Yu, R. R.; DiRita, V. J. The *Vibrio Cholerae* ToxR/TcpP/ToxT Virulence Cascade: Distinct Roles for Two Membrane-Localized Transcriptional Activators on a Single Promoter. *Mol. Microbiol.* **2000**, *38*, 67-84.

19. Crawford, J. A.; Krukonis, E. S.; DiRita, V. J. Membrane Localization of the ToxR Winged-Helix Domain is Required for TcpP-Mediated Virulence Gene Activation in *Vibrio Cholerae*. *Mol. Microbiol.* **2003**, *47*, 1459-1473.

20. Goss, T. J.; Seaborn, C. P.; Gray, M. D.; Krukonis, E. S. Identification of the TcpP-Binding Site in the *toxT* Promoter of *Vibrio Cholerae* and the Role of ToxR in TcpP-Mediated Activation. *Infect. Immun.* **2010**, *78*, 4122-4133.

21. Martinez-Hackert, E.; Stock, A. M. Structural Relationships in the OmpR Family of Winged-Helix Transcription Factors. *J. Mol. Biol.* **1997**, *269*, 301-312.

22. Lin, Z.; Kumagai, K.; Baba, K.; Mekalanos, J. J.; Nishibuchi, M. *Vibrio Parahaemolyticus* has a Homolog of the *Vibrio Cholerae toxRS* Operon that Mediates Environmentally Induced Regulation of the Thermostable Direct Hemolysin Gene. *J. Bacteriol.* **1993**, *175*, 3844-3855.

23. Krukonis, E. S.; DiRita, V. J. DNA Binding and ToxR Responsiveness by the Wing Domain of TcpP, an Activator of Virulence Gene Expression in *Vibrio Cholerae*. *Mol. Cell* **2003**, *12*, 157-165.

24. Hase, C. C.; Mekalanos, J. J. TcpP Protein is a Positive Regulator of Virulence Gene Expression in Vibrio Cholerae. *Proc. Natl. Acad. Sci. U. S. A.* **1998**, *95*, 730-734.

25. Beck, N. A.; Krukonis, E. S.; DiRita, V. J. TcpH Influences Virulence Gene Expression in Vibrio Cholerae by Inhibiting Degradation of the Transcription Activator TcpP. *J. Bacteriol.* **2004**, *186*, 8309-8316.

26. Krukonis, E. S.; DiRita, V. J. From Motility to Virulence: Sensing and Responding to Environmental Signals in *Vibrio Cholerae*. *Curr. Opin. Microbiol.* **2003**, *6*, 186-190.

27. Herrington, D. A.; Hall, R. H.; Losonsky, G.; Mekalanos, J. J.; Taylor, R. K.; Levine, M. M. Toxin, Toxin-Coregulated Pili, and the toxR Regulon are Essential for Vibrio Cholerae Pathogenesis in Humans. *J. Exp. Med.* **1988**, *168*, 1487-1492.

28. Qian, H.; Sheetz, M. P.; Elson, E. L. *Biophys. J.* **1991**, *60*, 910-921.

29. Haas, B. L.; Matson, J. S.; DiRita, V. J.; Biteen, J. S. Single-Molecule Tracking in Live *Vibrio Cholerae* Reveals that ToxR Recruits the Membrane-Bound Virulence Regulator TcpP to the *toxT* Promoter. *Mol. Microbiol.* **2015**, *96*, 4-13.

30. Di Paolo, D.; Afanzar, O.; Armitage, J. P.; Berry, R. M. Single-Molecule Imaging of Electroporated Dye-Labelled CheY in Live Escherichia Coli. *Philos. Trans. R. Soc. Lond. B. Biol. Sci.* **2016**, *371*, 10.1098/rstb.2015.0492.

31. Crawford, R.; Torella, J.; Aigrain, L.; Plochowietz, A.; Gryte, K.; Uphoff, S.; Kapanidis, A. Long-Lived Intracellular Single-Molecule Fluorescence using Electroporated Molecules. *Biophys. J.* **2013**, *105*, 2439-2450.

32. Skorupski, K.; Taylor, R. K. Positive Selection Vectors for Allelic Exchange. *Gene* **1996**, *169*, 47-52.

33. Matson, J. S.; DiRita, V. J. Degradation of the Membrane-Localized Virulence Activator TcpP by the YaeL Protease in Vibrio Cholerae. *Proc. Natl. Acad. Sci. U. S. A.* **2005**, *102*, 16403-16408.

34. Padan, E.; Bibi, E.; Ito, M.; Krulwich, T. A. Alkaline pH Homeostasis in Bacteria: New Insights. *Biochim. Biophys. Acta* **2005**, *1717*, 67-88.

35. Faruque, S. M.; Albert, M. J.; Mekalanos, J. J. Epidemiology, Genetics, and Ecology of Toxigenic Vibrio Cholerae. *Microbiol. Mol. Biol. Rev.* **1998**, *62*, 1301-1314.

36. Mekalanos, J. J. The Evolution of *Vibrio cholerae* as a Pathogen. In *Epidemiological and Molecular Aspects on Cholera;* Ramamurthy, T., Bhattacharya, S. K., Eds.; Humana Press: 2010; pp 97-114.

37. Teoh, W. P.; Matson, J. S.; DiRita, V. J. Regulated Intramembrane Proteolysis of the Virulence Activator TcpP in Vibrio Cholerae is Initiated by the Tail-Specific Protease (Tsp). *Mol. Microbiol.* **2015**, *97*, 822-831.

38. Miller, V. L.; Taylor, R. K.; Mekalanos, J. J. Cholera Toxin Transcriptional Activator ToxR is a Transmembrane DNA Binding Protein. *Cell* **1987**, *48*, 271-279.

39. Kovacikova, G.; Skorupski, K. A Vibrio Cholerae LysR Homolog, AphB, Cooperates with AphA at the tcpPH Promoter to Activate Expression of the ToxR Virulence Cascade. *J. Bacteriol.* **1999**, *181*, 4250-4256.

40. Kumar, M.; Mommer, M. S.; Sourjik, V. Mobility of Cytoplasmic, Membrane, and DNA-Binding Proteins in *Escherichia Coli*. *Biophys. J.* **2010**, *98*, 552-559.

41. Wang, S.; Moffitt, J. R.; Dempsey, G. T.; Xie, X. S.; Zhuang, X. Characterization and Development of Photoactivatable Fluorescent Proteins for Single-Molecule-Based Superresolution Imaging. *Proc. Natl. Acad. Sci. U. S. A.* **2014**, *111*, 8452-8457.

42. Zhu, J.; Miller, M. B.; Vance, R. E.; Dziejman, M.; Bassler, B. L.; Mekalanos, J. J. Quorum-Sensing Regulators Control Virulence Gene Expression in Vibrio Cholerae. *Proc. Natl. Acad. Sci. U. S. A.* **2002**, *99*, 3129-3134.

43. Teschler, J. K.; Zamorano-Sanchez, D.; Utada, A. S.; Warner, C. J.; Wong, G. C.; Linington, R. G.; Yildiz, F. H. Living in the Matrix: Assembly and Control of Vibrio Cholerae Biofilms. *Nat. Rev. Microbiol.* **2015**, *13*, 255-268.

44. Callahan, L. T.,3rd; Ryder, R. C.; Richardson, S. H. Biochemistry of Vibrio Cholerae Virulence. II. Skin Permeability Factor-Cholera Enterotoxin Production in a Chemically Defined Medium. *Infect. Immun.* **1971**, *4*, 611-618.

45. Yu, R. R.; DiRita, V. J. Analysis of an Autoregulatory Loop Controlling ToxT Cholera Toxin, and Toxin-Coregulated Pilus Production in *Vibrio Cholerae*. *J. Bacteriol.* **1999**, *181*, 2584-2592.

46. Miller, V. L.; Mekalanos, J. J. Synthesis of Cholera Toxin is Positively Regulated at the Transcriptional Level by toxR. *Proc. Natl. Acad. Sci. U. S. A.* **1984**, *81*, 3471-3475.

47. Miller, V. L.; DiRita, V. J.; Mekalanos, J. J. Identification of toxS, a Regulatory Gene Whose Product Enhances toxR-Mediated Activation of the Cholera Toxin Promoter. *J. Bacteriol.* **1989**, *171*, 1288-1293.

48. Pearson, G. D.; Mekalanos, J. J. Molecular Cloning of Vibrio Cholerae Enterotoxin Genes in Escherichia Coli K-12. *Proc. Natl. Acad. Sci. U. S. A.* **1982**, *79*, 2976-2980.

49. Subach, F. V.; Patterson, G. H.; Manley, S.; Gillette, J. M.; Lippincott-Schwartz, J.; Verkhusha, V. V. Photoactivatable mCherry for High-Resolution Two-Color Fluorescence Microscopy. *Nat. Methods* **2009**, *6*, 153-159.

50. Guzman, L. M.; Belin, D.; Carson, M. J.; Beckwith, J. Tight Regulation, Modulation, and High-Level Expression by Vectors Containing the Arabinose PBAD Promoter. *J. Bacteriol.* **1995**, *177*, 4121-4130.

51. Anthouard, R.; DiRita, V. J. Small-Molecule Inhibitors of toxT Expression in Vibrio Cholerae. *MBio* **2013**, *4*, 10.1128/mBio.00403-13.

52. Schmittgen, T. D.; Livak, K. J. Analyzing Real-Time PCR Data by the Comparative C(T) Method. *Nat. Protoc.* **2008**, *3*, 1101-1108.

53. Sandrini, S. M.; Haigh, R.; Freestone, P. P. Fractionation by Ultracentrifugation of Gram Negative Cytoplasmic and Membrane Proteins. *Bio-protocol* **2014**, *4(21)*, e1287.

54. Liao, Y.; Schroeder, J. W.; Gao, B.; Simmons, L. A.; Biteen, J. S. Single-Molecule Motions and Interactions in Live Cells Reveal Target Search Dynamics in Mismatch Repair. *Proc. Natl. Acad. Sci. U. S. A.* **2015**, *112*, E6898-E6906.

55. Liao, Y.; Li, Y.; Schroeder, J. W.; Simmons, L. A.; Biteen, J. S. Single-Molecule DNA Polymerase Dynamics at a Bacterial Replisome in Live Cells. *Biophys. J.* **2016**, *111*, 2562-2569.

Chapter 3: Two-Color Super-Resolution Imaging and Tracking in Live *Vibrio cholerae*

The work presented in this chapter was a collaboration between the following authors: Chanrith Siv, Andrew I. Perault, Victor J. DiRita, and Julie S. Biteen

Author contributions:
Experimental design: CS, VJD and JSB; Data collection: CS, AIP, VJD and JSB;
Data Analysis: CS, VJD and JSB

Cholera is a threat to public health, afflicting more than 5 million people annually[1]. Here, I used single-molecule fluorescence imaging and single-particle tracking to localize and track two transcription regulators in the virulence pathway of this cholera disease in live *Vibrio cholerae* cells, the bacteria responsible for producing the cholera toxin. In *V. cholerae*, virulence gene expression is under control of an unusual set of membrane proteins. From biochemical and genetic data, it has been hypothesized that a membrane complex composed of two activators, ToxR and TcpP, binds the *toxT* promoter, recruits RNA polymerase, and activates *toxT* gene expression leading to activation of the ToxT-controlled virulence genes. However, the biophysical mechanism and sequence of events for the binding of transcription elements to the *toxT* promoter have yet to be fully elucidated. In this chapter, I created fusions of the membrane-bound transcription activators TcpP and ToxR to orthogonal fluorescent proteins and assessed the suitability of the labeling and expression methods for two-color single-molecule fluorescence

imaging. The results indicate that simultaneous fluorophore labeling of ToxR and TcpP at the endogenous locus does not lead to downstream virulence production, whereas ectopic expression of these protein fusions does activate virulence. In addition, I detected the localization patterns and subcellular dynamics of plasmid-expressed ToxR and TcpP to access information about the processes happening inside live cells. The developments and demonstrations in this chapter indicate that two-color imaging of membrane-bound transcription activators is possible in live *V. cholerae* cells, and that this approach may be applied to understand the regulatory behavior of ToxR and TcpP in the transcriptional activation of the *toxT* gene and the subsequent activation of downstream virulence genes.

3.1 Introduction

Cholera is a waterborne disease caused by an infection of the intestine with the bacterium *Vibrio cholerae*[2]. An estimated 3-5 million cases and over 100,000 deaths occur each year around the world, especially in developing countries where proper sanitation and waste handling procedures are not regulated[3]. Cholera, when detected within the first few hours of infection, is typically treated with oral rehydration therapy to restore fluids to the patient and to allow the immune system to clear the infection[4]. Antibiotics can also be administered to reduce the severity of vomiting and diarrhea and to shorten illness duration by 50%, but patients are still at risk of severe dehydration caused by the secretion of cholera toxin (CTX) by the bacterium[5]. Because this disease remains a threat to human health, ongoing research strives to identify other treatment modalities based on the underlying mechanisms of CTX regulation.

In the Gram-negative pathogen *V. cholerae*, virulence gene expression is under the control of an unusual set of membrane proteins. Here, a membrane complex composed of two activators, ToxR and TcpP, binds the *toxT* promoter, recruits RNA polymerase, and activates

toxT gene expression **(Figure 3.1A)**. This signaling event leads to the activation of ToxT-controlled virulence genes[6]. Though both TcpP and ToxR have binding sites on the *toxT* promoter, TcpP directly activates *toxT* transcription while ToxR plays an accessory role. The mechanism of ToxR is unclear, but ToxR is hypothesized to enhance DNA-binding and/or facilitates transcription activation of TcpP[7,8]. Expression of CTX in *V. cholerae* is the result of this multiprotein transcription regulatory cascade—the ToxR regulon. The biophysical details of this complex, such as the co-localization of these transcription activators in cells and the associated protein-protein and protein-DNA interactions, have yet to be fully elucidated.

Fluorescence microscopy, which uses probes that are excited and emit in the visible wavelength range, remains the preferred method for live bacterial cell imaging despite the limited resolution[9,10]. With the advent of super-resolution methods, this trade-off between spatial and temporal resolution can be mitigated. One of the ways to circumvent the diffraction limit of light, which bounds the resolution of optical microscopy to ~250 nm, is through Photoactivated Localization Microscopy (PALM)[11]. This method achieves resolutions more than an order of magnitude better than the diffraction limit through imaging single fluorescent proteins one at a time. By combining PALM and single particle tracking (SPT)[12], dynamic interactions occurring on the scale of tens of nanometers can be visualized and investigated.

In this study, I constructed protein fusions of the membrane-bound transcription activators TcpP and ToxR with an orthogonal pair of fluorescent proteins (FPs), and examined the dynamics and localization patterns of single ToxR-mCitrine and TcpP-PAmCherry molecules under growth conditions that activate the virulence pathway. In particular, I determined that ToxR-mCitrine and TcpP-PAmCherry do not localize to a particular region of the cell but rather diffuse throughout the cell. In addition, I characterized the heterogeneous motion of these

fluorescent fusions to understand their regulatory behavior in the transcriptional activation of the *toxT* gene and the subsequent activation of downstream virulence genes. The data get us closer to establishing a model for the formation of the ToxR/TcpP/*toxT* protein-DNA complex important in the production of downstream cholera toxin.

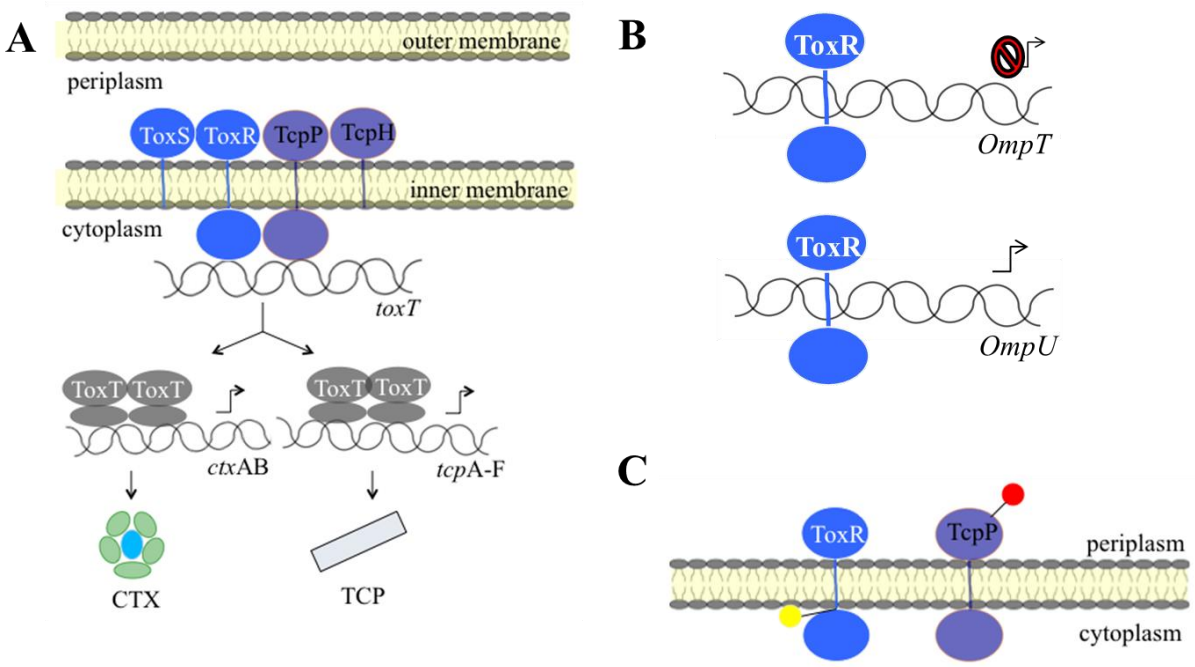

Figure 3.1 (A) Virulence signaling cascade in *V. cholerae*. Adapted from Matson et al.[13] **(B)** The ToxR pathway independent of TcpP and ToxT. **(C)** FP labeling locations in ToxR and TcpP. The green FP, *mCitrine,* is genetically encoded in a linker region of *toxR* in the middle of the gene while the red FP, *pamcherry*, is genetically encoded at the C-terminus of *tcpP*.

3.2 Results

3.2.1 Simultaneous endogenous fluorescence labeling of ToxR and TcpP downregulates transcription activation

Ectopic expression of proteins fusions is often used when genetic manipulations of bacterial chromosomes have yet to be developed. There are many different types of expression plasmids available for use in different bacterial species[14], and therefore many interesting proteins

have been fused to FPs and expressed from plasmids for live bacterial cell imaging. However, plasmid-expressed protein expression levels may not lead to native expression levels. Moreover, incorrect protein expression may result in irrelevant protein dynamics in cells that masks the relevant dynamics, making inferences to biological processes more difficult. To eliminate the possibility of non-native expressions, I expressed ToxR and TcpP protein fusions from their native loci on the bacterial chromosome. I used two orthogonal photoactivatable FPs as labels: PAGFP and PAmCherry for ToxR and TcpP, respectively.

O395 *V. cholerae* is not naturally competent; therefore, I used a suicide vector to facilitate homologous recombination of DNA fusions into the bacteria[15] **(Figure 3.2A)**. After filter mating and five successive rounds of antibiotic selections, final constructs containing the fusions were verified by PCR and sequencing. I created three different bacterial strains using this approach: O395:*toxR-pagfp*, O395:*tcpP-pamcherry*, and O395:*toxR-pagfp:tcpP-pamcherry*. For ToxR-PAGFP, I attached the FP to ToxR at two different locations: at an internal linker region in the cytoplasm and at the C-terminus of the protein. From immunoblot detection against ToxR antibody, I detected a stable ToxR-internal fusion **(Figure 3.2B, lane 2)** and an unstable ToxR C-terminal fusion **(Figure 3.2B, lane 3)**. This Western also show that ~50% of the PAGFP on the ToxR C-terminal fusion was cleaved; a band appears where the wildtype-copy of ToxR also appears in the wildtype strain. Furthermore, immunoblot detection against TcpA show that the ToxR-internal fusion is functionally active and causes downstream TcpA production. For TcpP-PAmCherry, I attached the FP to the C-terminal fusion for TcpP since this protein fusion had been found to be functional in another study[16]. By immunoblot detection against the TcpP antibody, I detected a band that corresponds to a stable TcpP-PAmCherry fusion **(Figure 3.2C, top panel)**. Though degradation bands also appear on this blot, TcpP-PAmCherry was the

dominant species detected. Assessment of TcpP-PAmCherry function by immunoblot detection against TcpA antibody reveals functional activity that cause downstream TcpA production **(Figure 3.2C, bottom panel)**. From these immunoblots, I provide evidence for the endogenous expressions of FP fusions to ToxR and TcpP in *V. cholerae*, and that these protein fusions only minimally perturb native protein functions.

To directly probe interactions of ToxR and TcpP, I constructed a double-color mutant strain that expressed ToxR-PAGFP and TcpP-PAmCherry from their endogenous loci. The Western shows that in the double-color strain, TcpP-PAmCherry was not expressed **(Figure 3.2D, lane 3)**. Though DNA sequencing verified that both *toxR-pagfp* and *tcpP-pamcherry* genes were successfully recombined at their native loci on the bacterial chromosome, it is unclear about the mechanisms causing this result. These two genes are located on different promoters, and therefore should be regulated independently. Nevertheless, these results here, which demonstrate a case where protein fusions cannot be expressed from their endogenous promoters, describe a situation in which ectopic expression of proteins fusions may be the best option to probe existing interactions of ToxR and TcpP.

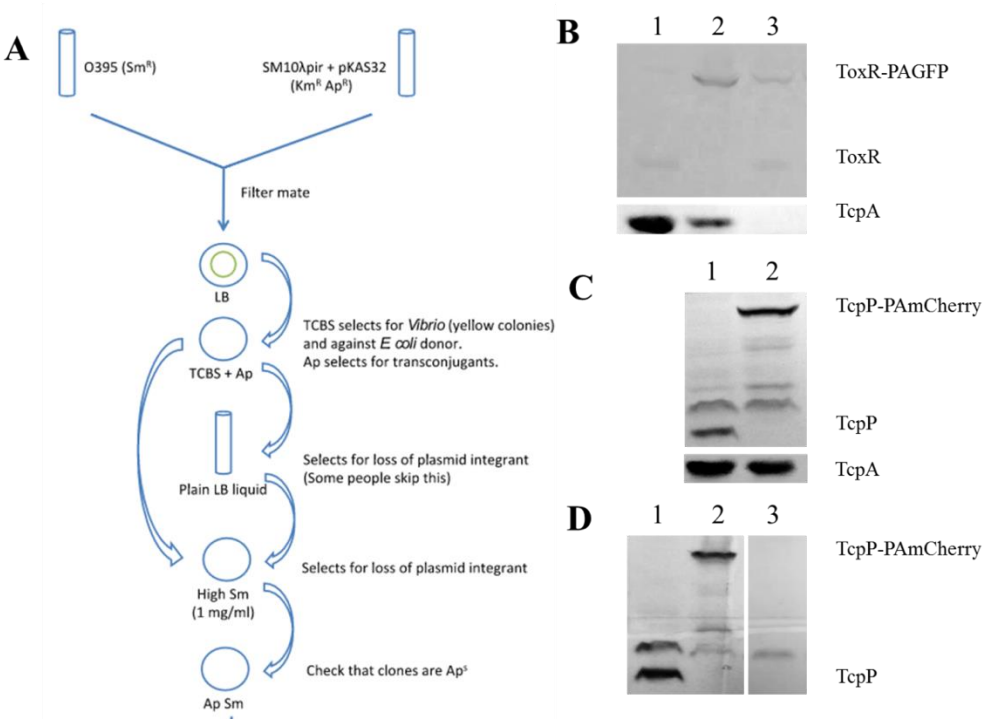

Figure 3.2 Endogenous expressions of ToxR and TcpP protein fusions in *V. cholerae.* **(A)** Allelic exchange in *V. cholerae* using the pKAS32 suicide vector[15]. **(B)** Endogenous expression of ToxR-PAGFP in O395 leads to a stable fusion when the FP is attached to an internal linker in the cytoplasm (lane 2) compared to the C-terminus of ToxR (lane 3). **(C)** Endogenous expression of TcpP-PAmCherry in O395 strain produces a stable fusion where the dominant species is full-length TcpP-PAmCherry (lane 2). **(D)** O395*:toxR-pagfp,tcpp-pamcherry* strain does not produce TcpP-PAmCherry (lane 3) as it did for the O395*:tcpp-pamcherry* strain (lane 2). Lane 1 in (B-D) is wildtype O395.

3.2.2 Ectopic expressions of ToxR and TcpP protein fusions in the two-color *V. cholerae* strain

To examine ToxR and TcpP protein fusion expressions in a *V. cholerae* O395 *ΔtoxRΔtcpP* double-mutant strain ("two-color"), I compared ToxR and TcpP protein levels produced by the two-color strain to protein levels in the wildtype and the O395 *ΔtcpP* pBAD18:*tcpP-pamcherry* ("one-color") strains. Because PAGFP was not detectable under standard single-molecule imaging conditions (λ excitation = 488 nm, appropriate filters, laser power = 30 – 100 W/cm^2), I used monomeric Citrine instead to label ToxR at the internal linker.

Since mCitrine is not photoactivatable, I did some initial photobleaching prior to data collection to obtain a sparse subset of molecules. Immunoblot detection samples were prepped from bacterial cultures that were grown in toxin-inducing conditions for 4 h. Immunoblotting against ToxR serum demonstrated that the ToxR-mCitrine fusion was intact and stable **(Figure 3.3A, lane 3)**. Though leaky expression from the IPTG-inducible promoter resulted in some expression of ToxR-mCitrine **(Figure 3.3A, lane 2)**, protein expression level was low compared to the expression of ToxR in the wildtype strain **(Figure 3.3A, lane 1)**. Contrastingly, IPTG induction resulted in elevated ToxR-mCitrine levels compared to the wildtype strain **(Figure 3.3A, lane 3 vs. 1)**. By immunoblotting against TcpP serum, I detected TcpP-PAmCherry when arabinose (arab) was added to the single (0395:*ΔtcpP)* and double mutant *V. cholerae* strains **(Figure 3.3B, lanes 3 and 5)**. Because lower molecular-weight bands were detected in the samples expressing TcpP-PAmCherry **(Figure 3.3B, lanes 3 and 5)**, I speculate that this FP fusion is degraded to some extent. Though unlabeled TcpP can undergo intramembrane proteolysis degradation under toxin-noninducing conditions *in vitro* to produce a truncated form of TcpP called TcpP*, this species was not present for the strains expressing TcpP-PAmCherry. However, there was some degradation of TcpP-PAmCherry as shown by the appearance of low molecular weight species, the dominant product of arabinose induction was still TcpP-PAmCherry **(Figure 3.3B, lanes 3 and 5)**. Taken together, the results from these Westerns confirm ectopic expression of ToxR-mCitrine and TcpP-PAmCherry in the two-color strain.

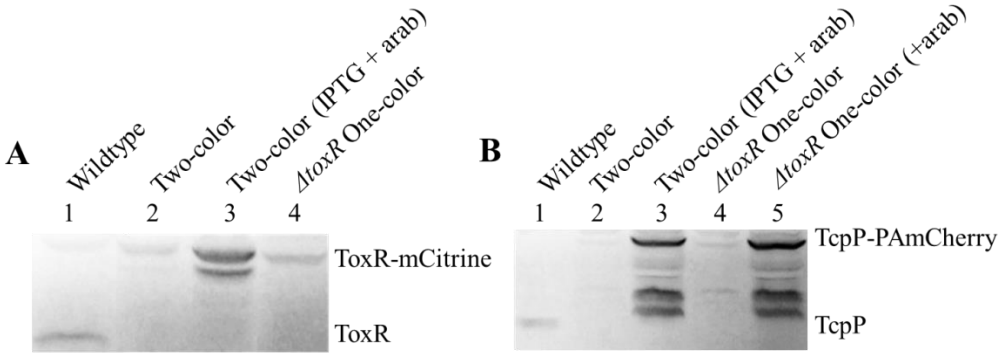

Figure 3.3 Immunoblots against **(A)** ToxR and **(B)** TcpP antibody. These bacterial strains were grown in toxin-inducing conditions. IPTG was used to induce ToxR-mCitrine expression while arabinose (arab) was added to induce TcpP-PAmCherry expression.

3.2.3 The two-color *V. cholerae* strain maintains a functional ToxR regulon

To assay the functionality of ToxR-mCitrine and TcpP-PAmCherry fusions in the ToxR regulon, I performed immunoblot detection against the toxin co-regulated pilus A (TcpA) **(Figure 3.3)**. TcpA is a functional readout for the ToxR regulon since its expression is intrinsically tied to ToxR and TcpP protein expression **(Figure 3.1A)**. TcpA was not produced in the absence of a functional ToxR and/or TcpP. TcpA was produced when arabinose was added to the one-color and two-color *V. cholerae* strains **(Figure 3.4, lanes 5, 6, and 8)**. Despite some ToxR-mCitrine and TcpP-PAmCherry production as a result of leaky expression from the plasmids **(Figure 3.3A, lane 2; 3.3B, lane 2)**, TcpA protein was not produced **(Figure 3.4, lane 3)**. Furthermore, I observed decreased TcpA production in the two-color strain after inductions with both IPTG and arabinose **(Figure 3.4, lane 6 vs. lane 5),** compared to arabinose induction alone **(Figure 3.4, lane 5)**. This decreased TcpA expression in the two-color strain **(Figure 3.4, lanes 5 and 6)** compared to the wildtype strain **(Figure 3.4, lane 2)** suggests that steric hindrance or other disruption mechanisms minimize the interactions of TcpP and ToxR to activate downstream virulence proteins. For both the one- and two-color strains, TcpA proteins

levels were lower compared to the wildtype strain **(Figure 3.4, lanes 5, 6 and 8 vs. lane 2)**; this result suggests that ToxR and TcpP protein fusions may be less active in either binding to or enhancing the *toxT* promoter. Furthermore, this data indicates that some optimal protein concentrations of ToxR and TcpP are needed to fully activate the ToxR regulon. Additionally, TcpA was produced when arabinose was added to the one-color *V. cholerae* strain **(Figure 3.4, lane 8)**, which agrees well with previous reports that overexpression of TcpP results in the activation of virulence proteins[17-19]. Contrastingly, by comparing TcpA production when either IPTG or arabinose was added **(Figure 3.4, lane 4 vs 5)**, I detected that IPTG alone produces lower levels of TcpA than arabinose alone, thus indicating that TcpP has a more critical role in the ToxR regulon[7,20].

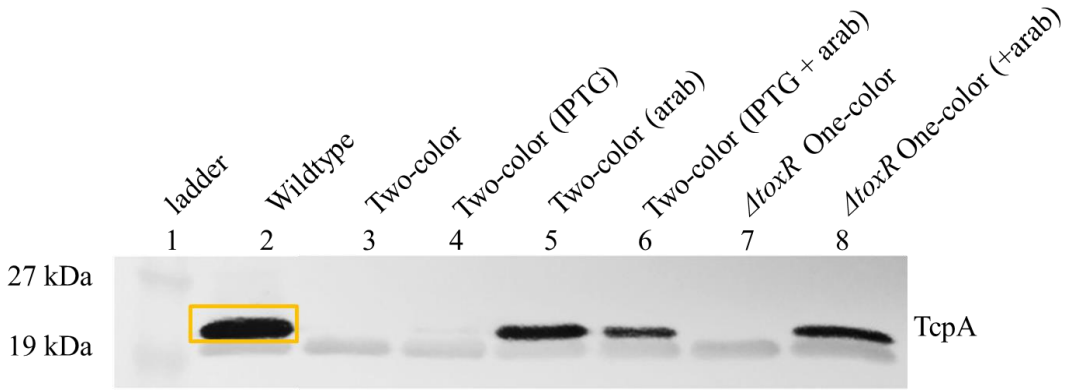

Figure 3.4 Immunoblot of *toxT*-regulated toxin coregulated pilus protein TcpA, a downstream virulence product of the ToxR regulon. The yellow box corresponds to the band corresponding to the TcpA protein.

To determine the functional activities of ToxR and TcpP protein fusions in the one-color and two-color strains, I performed an enzyme-linked immunosorbent assay (ELISA) to detect for CTX. Samples were harvested from cells that were induced with arabinose and IPTG for 4 h. CTX protein levels were lower in the induced cells expressing the protein fusions compared to the wildtype cells **(Figure 3.5)**, which suggests that these protein fusions may not be as efficient

as unlabeled ToxR and TcpP to activate *toxT* transcription and downstream CTX production. The results from the ELISA assay agree well with the Western results **(Figure 3.4)** to support the conclusion that ToxR and TcpP proteins fusions are less active in the virulence pathway to activate cholera toxin gene expression; this observation may be the result of steric hindrance that minimizes the favorable interactions of ToxR and TcpP.

A caveat to consider when assessing the implications of these results is that ectopic expressions of these ToxR and TcpP protein fusions may not be comparable to native expression levels. Overexpression of these proteins may cause proteins to dimerize or oligomerize, and thus block RNA polymerases from accessing the DNA promoters more readily to stimulate transcription. Because I detected CTX in both the one-color and two-color strains, this result suggests that the ToxR and TcpP functions are not so perturbed by FP labeling that functions are completely lost.

Taking the TcpA Western and CTX ELISA results together, the levels of TcpA and CTX detected from these strains in the absence and presence of inducers suggest that ToxR-mCitrine and TcpP-PAmCherry fusions maintain a functional—though perhaps weakened—ToxR regulon capable of activating the *toxT* promoter to trigger downstream production of TcpA.

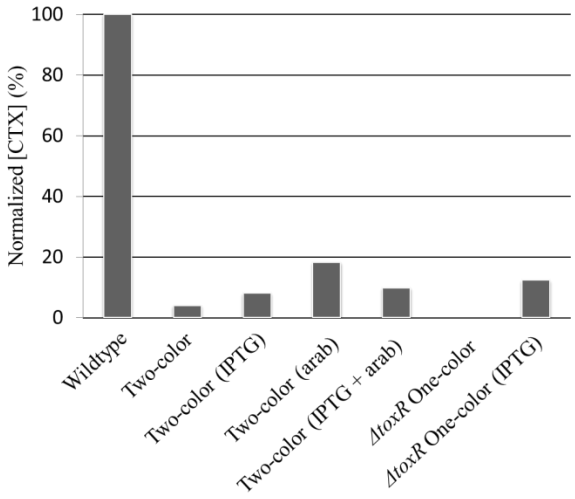

Figure 3.5 Cholera toxin ELISA of the *V. cholerae* strains used in this study with and without the addition of inducers. CTX levels from the one and two-color strains were normalized to the CTX levels in the wildtype strain.

3.2.4 ToxR-mCitrine regulates porin production independent of TcpP

The transmembrane transcriptional activators ToxR and TcpP modulate expression of *V. cholerae* virulence factors by controlling *toxT*. However, in a pathway independent of TcpP and ToxT, ToxR also activates and represses transcription of genes encoding two outer-membrane porins OmpU and OmpT **(Figure 3.1B)**. These outer membrane proteins are transcriptionally regulated by ToxR: ToxR activates *ompU* transcription but represses *ompT* transcription. To understand if ToxR-mCitrine retains function in this orthogonal pathway, I measured OmpU and OmpT protein expressions. To perform this assay, cell lysates from cultures grown in toxin-inducing conditions for 4 h were separated by a SDS-PAGE gel. Coomassie blue makes highly-expressed proteins visible on a gel, which includes the OmpU and OmpT proteins. I detected OmpU in a wildtype strain **(Figure 3.6, lane 2)** and in *V. cholerae* strains where ToxR was produced **(Figure 3.6, lanes 4 and 6)**. In the two-color strain where ToxR expression was controlled with IPTG induction, I detected OmpU when IPTG was added **(Figure 3.6, lanes 4**

and 6) and OmpT when IPTG was not added **(Figure 3.6, lanes 3 and 5)**. For the *ΔtoxR* one-color strain, there was no OmpU production independent of IPTG induction **(Figure 3.6, lanes 6-8)**. These observations for OmpU and OmpT protein expressions suggest that ToxR-mCitrine in the two-color strain is active, and ToxR-mCitrine expression is correlated with the regulation of porins in cells. Since ToxR regulates porin production by targeting the DNA promoter in a similar way as in the TcpP pathway, this result suggests that the location of ToxR labeling does not hinder its ability to access DNA promoters in the toxin regulation pathway.

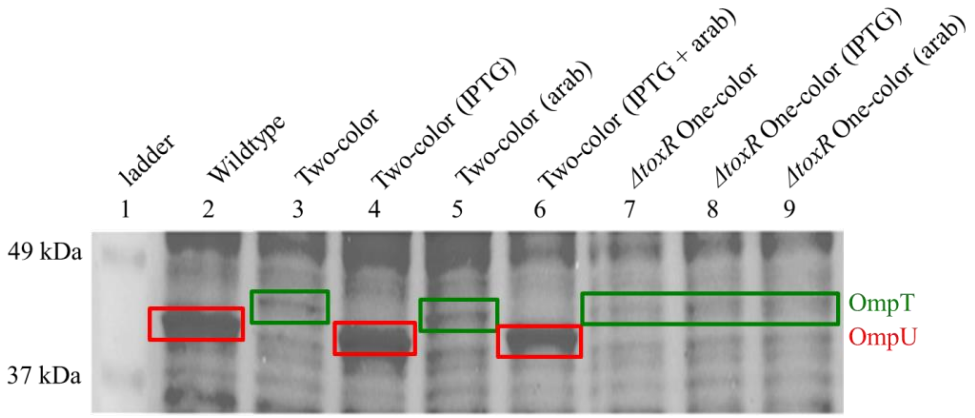

Figure 3.6 Coomassie stain of cell lysates grown with and without arabinose and IPTG inducers. ToxR regulates porin production in *V. cholerae* through OmpU and OmpT expression. High ToxR expression results in OmpU production while low ToxR expression results in OmpT production. Red boxes correspond to the OmpU protein bands while green boxes correspond to the OmpT protein bands.

3.2.5 Live-cell single-molecule imaging reveals localizations of ToxR and TcpP in cells

Since I have already verified that ToxR-mCitrine and TcpP-PAmCherry were expressed and active in the two-color strain, I determined next where these proteins are localized within live *V. cholerae* cells. To determine localizations, the two-color strain was grown in toxin-inducing conditions in minimal media with IPTG and arabinose for 4 h before the cells were imaged on the microscope. The emission from each channel was collected separately using an image splitter (Optosplit II, Cairn Research). Because mCitrine is not photoactivatable—all

copies of ToxR-mCitrine fluoresce at one time—this precludes single-molecule imaging. Therefore, to separate ToxR-mCitrine molecules spatially, I bleached a small region of the sample window with the 488-nm excitation laser for ~2-4 min; this allowed for single molecules to be detected. One disadvantage from this bleaching method is that I may be missing information from all ToxR-mCitrine copies in the cell. Though there is only one *toxT* promoter where ToxR binds in the cell, localizations from all ToxR-mCitrine copies may reveal mechanistic insight into *toxT* transcription activation, possibly through the positioning of ToxR throughout the cell. In contrast, to visualize TcpP-PAmCherry, a photobleaching step was not necessary. Instead, 200 ms pulses of 405-nm laser light stochastically activated a few copies of the photoactivatable PAmCherry, and allowed for the imaging of low protein densities.

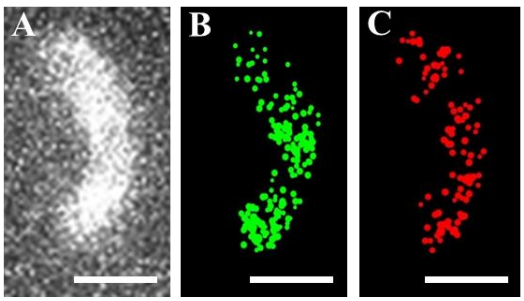

Figure 3.7 Imaging live *V. cholerae* cells with high resolution. **(A)** Diffraction limited image of ToxR-mCitrine. Resolution can be improved by creating super-resolution reconstructions of **(B)** ToxR-mCitrine and **(C)** TcpP-PAmCherry in live *V. cholerae* cells. Scale bars: 1 µm.

From the movies, I determined the center positions of the punctate spots by fitting the emission profile of each emitter to a 2D Gaussian, a computationally preferable approximation for the real Airy function[21], to determine the coordinates for a super-resolution reconstruction of ToxR-mCitrine **(Figure 3.7B)** and TcpP-PAmCherry **(Figure 3.7C)** in one bacterial cell. I only used the first 500 imaging frames for these PALM reconstructions to show the localizations of

these two protein fusions. These density maps show that ToxR-mCitrine and TcpP-PAmCherry did not localize to a particular area—for instance to the poles of the cell—but rather diffused about the whole cell **(Figure 3.7B and C)**. These localization patterns negate a potential consequence of labeling that causes protein fusions to be mislocalized at the poles due to aggregation[22]. Future work would need to illuminate just the membrane of the cells—like an evanescent field in total internal reflection microscopy—in order to access information regarding co-localization of ToxR and TcpP, possibly with x,y, and z information.

3.2.6 Single-molecule trajectory analysis reveals dynamics in transcription regulation

I explored the dynamics of these membrane bound transcription activators by using a tracking algorithm to follow the motion of single molecules in cells. From each trajectory, a mean-squared displacement (MSD) can be determined for every time lag (τ), where τ is an integer multiple of the imaging frame time, or 40 ms. **Figure 3.8B** shows the MSD curves from individual tracks plotted for each protein (blue: ToxR-mCitrine, red: TcpP-PAmCherry). A diffusion coefficient, *D*, can be extracted from the slope of each curve in the plot. However, this method of calculating *D* is only quantitative for homogenous motion and not easily interpreted. By observing their localization patterns, I predict that ToxR and TcpP undergo multiple modes of motion because ToxR and TcpP may not always be involved in activating *toxT* transcription at all times. By using the MSD plot **(Figure 3.8B)** to extract average motion, I am precluding interpretations that explain the behaviors of these proteins as they freely diffuse in the cell, interact with each other, and/or interact in large complexes in a single trajectory.

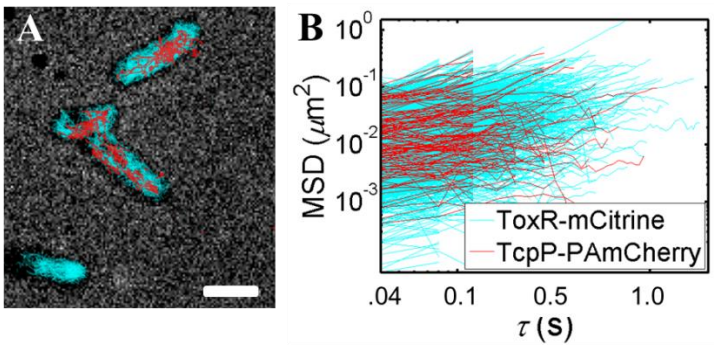

Figure 3.8 Single-molecule protein tracking in live cells. (A) All trajectories from all molecules were overlaid on a phase-contrast image of induced live *V. cholerae* cells (blue: ToxR-mCitrine, red: TcpP-PAmCherry). Scale bar: 1 μm. **(B)** Mean-squared displacement curves were plotted from each individual trajectory in (A).

Dynamic information pertaining to molecules that explored various motions throughout their trajectories was analyzed by cumulative probability distribution (CPD)[23,24]. Rather than using individual tracks from each individual molecule, the CPD gives the probability that the squared step-size is less than some given radius. A fit of the CPD to a model that groups the motions into three terms—fast, medium and immobile—indicates that a fit with three terms is a good estimate (based on the residuals) to explain the motions of ToxR-mCitrine **(Figure 3.9A)** and TcpP-PAmCherry **(Figure 3.9B)**. From these curves, I calculated the *D* values and populations of each motion **(Table 3.1)** from **Equation 3.3**. Therefore, each *D* and its corresponding weight indicate the probability that a molecule experiences that type of motion. I observed that the fast TcpP-PAmCherry population diffused faster than the fastest ToxR-mCitrine. However, by comparing the diffusion coefficients of the medium population of ToxR-mCitrine and TcpP-PAmCherry, I uncover very similar *D* values. Moreover, the medium population sizes of these two proteins were also very similar to *D*s of membrane-mobility fusions. Therefore, I speculate that this medium population may correspond to ToxR and TcpP interactions with one another in the ToxR regulon. The *D* values obtained in these experiments

for this two-color strain are very similar to membrane bound proteins observed in other biological systems, which suggests that the tracking algorithm is capturing relevant dynamics for membrane-localized proteins.

Table 3.1: Using a 3-term diffusion model (Eq. 3.3) to fit to CPD (Fig. 8). Diffusion coefficients and relative populations were extracted from CPD vs. τ curve.

	Mobile (fast)	**Mobile (medium)**	**Immobile**
ToxR	0.164 ± 0.009 μm^2/s (29.1 ± 0.8 %)	0.027 ± 0.005 μm^2/s (44.6 ± 0.5 %)	(26.3 ± 0.6 %)
TcpP	0.325 ± 0.004 μm^2/s (23.6 ± 0.5 %)	0.031 ± 0.003 μm^2/s (41.4 ± 0.4 %)	(35.0 ± 0.6 %)

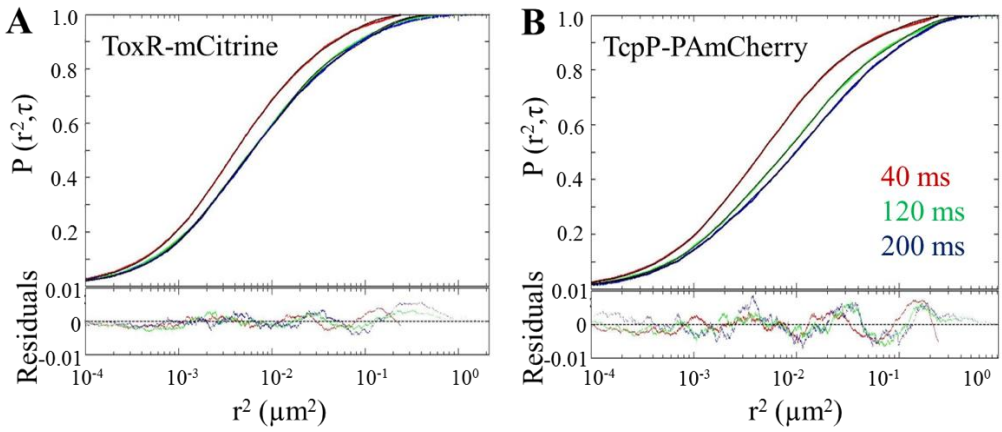

Figure 3.9 Cumulative probability distributions (red, blue, and green correspond to τ = 40, 120, and 200, respectively), fits to Eq. 3.3 (black), and residuals (lower) for **(A)** ToxR-mCitrine and **(B)** TcpP-PAmCherry. Time lags are indicated in the legend, and fit parameters can be found in Table 1.

3.3 Discussion

The mechanisms by which the ToxR regulon regulates CTX expression have been elucidated by various groups based on molecular biology, biochemistry and genetic experiments[6,18,19,25-27], but direct visualization of these events *in vivo* has yet to reported. Single-molecule imaging has been very valuable to elucidate mechanisms in model bacteria[28]—*Caulobacter crescentus, Escherichia coli* and *Bacillus subtilis*—but there are few examples of the application of this technique to study pathogenic bacteria[16]. A complication that often arises when imaging pathogens is the lack of methods development in the manipulation of their genomes. Since fluorescence imaging relies heavily on the ability to fluorescently label macromolecules in living cells, it is critical that cloning strategies are developed for these pathogens to allow for imaging-based studies.

In this study, I used single-molecule imaging to study a pair of transcription regulators in pathogenic *V. cholerae*. I provide evidence for the expression of stable fluorescent fusion proteins in live cells and the retention of their native functions through *in vitro* experiments. Though fluorescence labeling of ToxR and TcpP doubled the proteins sizes, the results from immunoblot detection and Coomassie-stained protein gel data suggest that the activity was only slightly altered, such that expression of downstream genes were still produced at slightly dimished levels. Therefore, I conclude that the added bulkiness from the fluorescence labeling does not cause major steric hindrance that would, otherwise, block essential interactions from occurring. Because the two-color strain still produced both CTX and TcpA, I provide further support for the useful application of this strain in fluorescence imaging to study the ToxR regulon.

Single-molecule imaging offers high spatial resolution and temporal resolution, and has the ability to capture relevant interactions *in vivo*. Single-particle tracking of these proteins in live cells provides a glimpse into the possible protein-protein and protein-DNA interactions of the ToxR regulon. The *D* values I obtained for ToxR and TcpP suggest that these proteins are localized in the membrane rather than in the cytoplasm, which is consistent with published biochemical work characterizing ToxR and TcpP in the membrane fractions of cell separation experiments[29]. With imaging acquisition at 40 ms integration time, I may be capturing ToxR and TcpP molecules that are interacting with themselves to form dimers, interacting with each other, and/or interacting with the chromosome. The slowing down of these proteins may be due to transient interactions with other membrane-associated proteins. Furthermore, the CPD of the squared displacements for ToxR and TcpP show a significant overlap in *D* values. These similarities suggest a relation between these two proteins, and may provide the first direct evidence of ToxR and TcpP interactions in live *V. cholerae* cells.

Several models for the mechanism of ToxR–TcpP–*toxT* interaction have been proposed by Goss et al[20]. In the 'hand-holding' model, TcpP and ToxR interact directly while bound to the *toxT* promoter. This mechanism is quite different from the 'catch and release' model, where ToxR releases TcpP upon DNA binding. Another interesting model is the 'promoter alteration' model, in which the displacement of H-NS by ToxR bends or unwinds the DNA promoter to permit TcpP to locate and bind to the *toxT* promoter. Finally, the 'membrane recruitment' model is a mechanism in which ToxR brings the *toxT* promoter closer to the inner membrane where both ToxR and TcpP have easier access to binding at the promoter. Based on the dynamics and the localizations of ToxR and TcpP previously characterized in this chapter, the data support the 'catch and release' model. Because ToxR and TcpP moved with similar diffusion coefficients in

the "medium population" and with different *D* values in the other populations, these measurements support a model where ToxR and TcpP interact transiently and then move away from each other. Since ToxR and TcpP did not always perfectly localize in the same locations in the cell, this eliminates the possibility for the more permanent hand-holding mechanism. In order to comment on the models involving the promoter, future work will involve the construction and imaging of strains where the *toxT* promoter is altered or completely removed.

3.4 Conclusions

The ToxR Regulon, an inner-membrane-bound complex, regulates CTX and TCP gene expression through ToxT. Four transcriptional regulators in the ToxR Regulon primarily regulate the gene expression of *toxT*. In this chapter, I used single-molecule imaging to directly visualize two of these activators, ToxR and TcpP, in live *V. cholerae* cells. Previous reports have suggested that these two transcription regulators work in conjunction at the *toxT* operon to activate transcription of *toxT* via their N-terminal domains in the cytoplasm[30,31]. Because the data show that ToxR and TcpP diffused similarly in *V. cholerae* cells, I propose a mechanism where ToxR and TcpP transiently interact with each other to participate in transcription activation. Despite the increase in spatial resolution, I am unable pinpoint exactly where this interaction may be occurring in the cell. Nevertheless, I speculate that this interaction happens in the periplasm, where external stimuli can trigger cellular responses to turn on and off virulence gene production[32]. The functions of the periplasmic domains of ToxR and TcpP have yet to be determined, but it is hypothesized that TcpP and ToxR interact in the periplasm during *toxT* transcription due to their adjacent DNA-binding regions[7,18,33]. Future work involving site-directed mutagenesis of ToxR and TcpP may reveal these critical interacting domains.

Recently, Haas et al. proposed a variation of the 'hand-holding model', in which H-NS protein blocks the *toxT* promoter until ToxR can remove these proteins, and then binds the *toxT* promoter[16]. By following the motion of TcpP-PAmCherry in mutant strains, the authors proposed a hypothesis in which ToxR recruits TcpP to the exposed *toxT* promoter to activate *toxT* transcription. This unusual membrane-bound transcription mechanism of the ToxR regulon is not only relevant in *V. cholerae*, but can be found in several other organisms. Investigating the specific roles of bitopic membrane-bound transcription activators in the *V. cholerae* virulence pathway will have general implications for similar mechanisms in other bacteria. This study highlights a new perspective on membrane-bound transcription factors elucidated by single-molecule imaging of pathogens.

3.5 Materials and Methods

3.5.1 Cell Growth and Sample Preparation

V. cholerae strains expressing TcpP-PAmCherry and ToxR-mCitrine fusions were first grown on LB growth medium (10 g bactotryptone, 5 g yeast extract, and 5 g NaCl diluted to 1 L water; Fisher) and agarose (LB Agar; Fisher) containing appropriate antibiotics (kanamycin: 50 μg/mL, ampicillin or carbenicillin: 100 μg/mL, and streptomycin: 50 μg/mL) at 37°C for ~ 16 - 18 h. A single colony was picked before growing in LB growth medium and antibiotics for another ~ 16 - 18 h. The overnight cultures were diluted 1:25 into M9 minimal medium (200 mL M9 salts, 2 mL 1 M $MgSO_4$, 20 mL 20 % v/v glycerol, and 100 μL $CaCl_2$ diluted to 1L; Fisher), an amino acid mixture NRES (L- asparagine, L-(+)-arginine, L-glutamic acid and L-serine to a final concentration of 25 mM), and appropriate antibiotics, and grown overnight at 30 °C with shaking. The cultures were diluted 1:25 for a second time in M9, NRES, and

antibiotics, and grown at 30 °C for ~ 16 h. To activate the virulence pathway, cells were diluted 1:10 in M9, NRES, and antibiotics, and induced with L-(+)-arabinose (0.1 % v/v final concentration) and Isopropyl β-D-1-thiogalactopyranoside (IPTG, 0.1 mM final concentration). The cultures were grown at 30 °C for ~ 4 h. A 1 mL aliquot of cells was concentrated in a centrifuge (Eppendorf 5430 R) for 30 s at 25 °C and 17500 rpm. The supernatant was removed, and the pellet was washed with M9 two more times. Finally, the pellet was resuspended in 500 µL of M9 before a 2 µL aliquot was placed on a 2% agarose pad and inverted onto a larger cover slip (35 X 50 mm). A second smaller cover slip (22 X 22 mm) was placed on top of the agarose pad.

3.5.2 Detection of proteins by Western

Cultures of *V. cholerae* were grown under toxin-inducing conditions for 4 h with arabinose and IPTG, 0.1 % v/v and 0.1 mM final concentrations, respectively. Toxin-inducing conditions correspond to growth conditions in LB pH 6.5 at 30 °C in which maximal downstream toxin proteins are produced. OD_{600} equivalents of whole-cell lysates were prepared in SDS-PAGE sample buffer before the samples were electrophoresed on a 15% polyacrylamide gel with a 5% stacking gel, transferred to nitrocellulose, and blocked with 5% dried nonfat milk in Tris-buffered saline containing 0.1% Tween 20 (TBS-T) for 2 h at room temperature. Next, the blot was incubated overnight at 4°C with TcpP, ToxR, or TcpA polyclonal antisera. The TcpA antibody was used at 1:10,000 dilution, the ToxR antibody at 1:1,000 dilution, and the TcpP antibody at 1:500 dilution. All antibody dilutions were made in 5% milk–TBS-T. The blot was then washed 3 × 15 min in TBS-T and incubated for 1 h at room temperature with goat anti-rabbit IgG linked to alkaline phosphatase diluted 1:1000 in 5% milk–TBS-T. The blot was then

washed 3 × 15 min with TBS-T. The chromogenic substrates for alkaline phosphatase, nitroblue tetrazolium chloride (NBT) and 5-bromo-4-chloro-3-indolylphosphate p-toluidine salt (BCIP) were added to develop the blot.

3.5.4 Detection of Cholera Toxin by ELISA (enzyme-linked immunosorbent assay)

Cultures of *V. cholerae* were grown under toxin-inducing conditions for 4 h with arabinose and IPTG, 0.1 % v/v and 0.1 mM final concentrations, respectively. An equal volume of the supernatants from each culture was added to 96-well plates coated with the cholera toxin receptor, GM1. After a 2 h incubation at RT, the plates were washed three times with wash solution composed of phosphate-buffered-saline (PBS; pH 7.4), 0.2% BSA, and 0.05% Tween 20. CTX antisera was added to each well and allowed to incubate for 2 h at RT. The plates were washed three times with wash solution before goat anti-rabbit antibodies linked to alkaline phosphatase were added. After a 2 h incubation at RT, the plates were washed again for three times with the wash solution. P-nitrophenyl phosphate was then added, and absorptions were taken at 420 nm. These values were converted to CTX concentration by normalizing the A_{420} value to the absorption value generated by a known concentration of CTX present on the 96-well plate. CTX expression values were normalized to the OD_{600}.

3.5.5 Strain Construction

A ToxR-mCitrine chimera protein was created by overlap extension polymerase chain reaction (OE-PCR). *toxR* was PCR amplified with a HindIII restriction site from wildtype O395, while *mcitrine* was PCR amplified with a XmaI restriction site from a plasmid purchased from Addgene. The ligation of *toxR* to *mcitrine* was done at a stable linker region near the inner

membrane in the cytoplasm. The stop codon on *mcitrine* was removed to allow for continuous transcription and translation of the fluorescent protein. Gel electrophoresis and DNA sequencing verified the DNA fusion sequence. *toxR* was ligated into an isopropyl β-D-1-thiogalactopyranoside (IPTG)-inducible plasmid, pMMB66EH, at HindIII and XmaI restriction sites using DNA ligase. The ligated product was gel purified and electroporated into O395 *ΔtoxR ΔtcpP* that already had TcpP-PAmCherry on an arabinose-inducible plasmid, pBAD18-Kan. The colonies were screened by PCR with primers flanking the ends of TcpP-PAmCherry and ToxR-mCitrine. This two-color strain was verified by sequencing.

3.5.6 Microscopy and imaging parameters

mCitrine (excitation: 516 nm, emission: 529 nm) is compatible to use alongside PAmCherry (excitation: 564 nm, emission: 595 nm) for two-color imaging with the optical setup in my lab. In the setup, each laser beam was passed through an excitation filter (Semrock) and then a quarter-wave plate (Tower optical) to become circularly polarized. Adjustable mirrors and a periscope (CVI Melles Griot) directed the beams into a standard widefield inverted epifluorescence microscope (Olympus IX71) with a 100x 1.40 N.A. oil-immersion objective. The laser beam was focused at the back aperture of the objective using a lens (Semrock) at the back of the microscope. The emission and excitation light from the different lasers were separated using a dual band pass filter (Figure 3.10). The emitted light was then passed through a beam splitter before reaching an electron-multiplying charge-coupled device (EMCCD) detector (Photometrics Evolve) that was connected to a computer. Fluorescence of mCitrine in the cells was excited with 488-nm fluorescence excitation laser (Coherent Sapphire 488–50) at 7 W/cm^2, and imaged until all molecules were photobleached. Then, fluorescence of PAmCherry in the

cells was activated using a 405-nm laser (Coherent Cube 405-100) at 200 ms pulses at 35–110 W/cm^2, co-aligned with the 561-nm fluorescence excitation laser (Coherent Sapphire 560-50) at 120 W/cm^2, and imaged for an additional 2 mins. Acquisitions at 40 ms integration time lasted for a total of 4-5 min for each movie per each 256 x 256 pixel region. 10-15 movies were collected from each sample before a new sample was made.

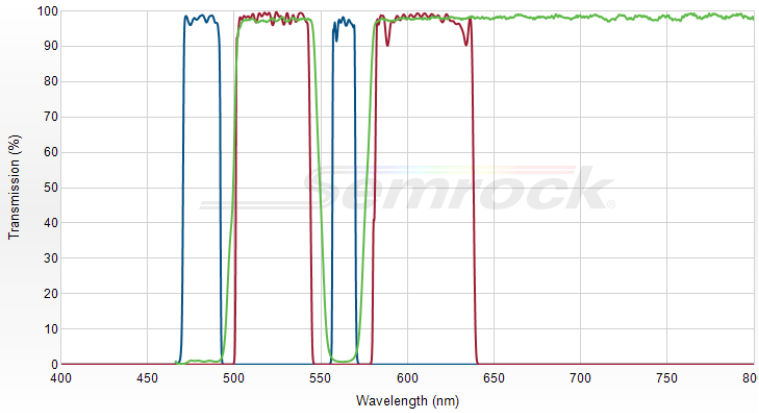

Figure 3.10 This dual band pass filter is optimized for laser excitation utilizing a 488-nm laser source for mCitrine and a 561-nm laser source for PAmCherry. This set provides high brightness, low crosstalk, and a good signal-to-noise ratio (https://searchlight.semrock.com/).

3.5.7 Image processing and data analysis

Phase-contrast images of *V. cholerae* were segmented using a custom MATLAB script before analysis can be done within the cell boundaries. Single molecules were localized in the cells, and single-molecule trajectories were created based on a nearest-neighbor algorithm. From each trajectory, the mean-squared displacement (MSD or $\langle r^2 \rangle$) was determined for every time lag (τ), where τ is an integer multiple of the imaging frame time, 40 ms. For Brownian motion, the diffusion coefficient, D, is proportional to the slope of MSD versus τ, as given by the following equation:

$$\langle r^2(\tau) \rangle = 2nD\tau \quad \textbf{(3.1)}$$

where *n* denotes the imaging dimension[34]. In my experimental setup, $n = 2$ because I did not capture motion in the z-direction. However, this method of calculating *D* is an oversimplification which may not take into account the heterogeneity along a single trajectory.

To describe heterogeneous motion, I analyzed diffusion based on the cumulative probability distribution (CPD) of squared step sizes[23]. Rather than obtaining one data point for each τ value, I get a distribution of values for each τ. For homogenous two-dimensional Brownian motion, the CPD of squared displacements for a given τ is described by:

$$P(r^2, \tau) = 1 - \exp\left(\frac{-r^2}{\langle r^2 + \sigma^2 \rangle}\right) \quad \textbf{(3.2)}$$

where σ is the localization accuracy. To accommodate heterogeneous motion involving multiple diffusion coefficients, additional populations were incorporated by additional exponential terms in the expression. The three-term model for the CPD of squared displacements for a given τ is therefore described by:

$$P(r^2, \tau) = 1 - \alpha \cdot exp\left(\frac{-r^2}{\langle r_\alpha^2 + \sigma^2 \rangle}\right) - \beta \cdot exp\left(\frac{-r^2}{\langle r_\beta^2 + \sigma^2 \rangle}\right) - \gamma \cdot exp\left(\frac{-r^2}{\sigma^2}\right) \quad \textbf{(3.3)}$$

where α and β describe the population weights of the two mobile terms, and $\gamma = 1 - (\alpha + \beta)$ describes the population weight of the immobile term ($\langle r^2 \rangle = 0$).

3.6 Acknowledgements

This work was supported in part by a Burroughs Wellcome Fund Career Award at the Scientific Interface to Julie Biteen and by National Institutes of Health (NIAID) Grant R21-AI099497-02 to Victor DiRita and Julie Biteen. I was partially supported by a University of Michigan Rackham Merit Fellowship. I thank Andrew Perault and Dr. Jeremiah Johnson for help with the strain constructions, Dr. Yi Liao for single-molecule tracking algorithms, and Dr. Wei Ping, Dr. Justin Lenhart, and Dr. Hannah Tuson for helpful comments.

3.7 References

1. AnonymousCholera Vaccines: WHO Position Paper. *Wkly. Epidemiol. Rec.* **2010**, *85*, 117-128.

2. Faruque, S. M.; Albert, M. J.; Mekalanos, J. J. Epidemiology, Genetics, and Ecology of Toxigenic Vibrio Cholerae. *Microbiol. Mol. Biol. Rev.* **1998**, *62*, 1301-1314.

3. Sack, D. A.; Sack, R. B.; Chaignat, C. L. Getting Serious about Cholera. *N. Engl. J. Med.* **2006**, *355*, 649-651.

4. Guerrant, R. L.; Carneiro-Filho, B. A.; Dillingham, R. A. Cholera, Diarrhea, and Oral Rehydration Therapy: Triumph and Indictment. *Clin. Infect. Dis.* **2003**, *37*, 398-405.

5. Sanchez, J.; Holmgren, J. Cholera Toxin - a Foe & a Friend. *Indian J. Med. Res.* **2011**, *133*, 153-163.

6. DiRita, V. J.; Parsot, C.; Jander, G.; Mekalanos, J. J. Regulatory Cascade Controls Virulence in Vibrio Cholerae. *Proc. Natl. Acad. Sci. U. S. A.* **1991**, *88*, 5403-5407.

7. Krukonis, E. S.; DiRita, V. J. DNA Binding and ToxR Responsiveness by the Wing Domain of TcpP, an Activator of Virulence Gene Expression in *Vibrio Cholerae*. *Mol. Cell* **2003**, *12*, 157-165.

8. Goss, T. J.; Morgan, S. J.; French, E. L.; Krukonis, E. S. ToxR Recognizes a Direct Repeat Element in the *toxT*, *ompU*, *ompT*, and *ctxA* Promoters of *Vibrio Cholerae* to Regulate Transcription. *Infect. Immun.* **2013**, *81*, 884-895.

9. Tuson, H. H.; Biteen, J. S. Unveiling the Inner Workings of Live Bacteria using Super-Resolution Microscopy. *Anal. Chem.* **2015**, *87*, 42-63.

10. Haas, B. L.; Matson, J. S.; Dirita, V. J.; Biteen, J. S. Imaging Live Cells at the Nanometer-Scale with Single-Molecule Microscopy: Obstacles and Achievements in Experimental Optimization for Microbiology. *Molecules* **2014**, *19*, 12116-12149.

11. Betzig, E.; Patterson, G. H.; Sougrat, R.; Lindwasser, O. W.; Olenych, S.; Bonifacino, J. S.; Davidson, M. W.; Lippincott-Schwartz, J.; Hess, H. F. Imaging Intracellular Fluorescent Proteins at Nanometer Resolution. *Science* **2006**, *313*, 1642-1645.

12. Qian, H.; Sheetz, M. P.; Elson, E. L. *Biophys. J.* **1991**, *60*, 910-921.

13. Matson, J. S.; Withey, J. H.; DiRita, V. J. Regulatory Networks Controlling *Vibrio Cholerae* Virulence Gene Expression. *Infect. Immun.* **2007**, *75*, 5542-5549.

14. del Solar, G.; Giraldo, R.; Ruiz-Echevarria, M. J.; Espinosa, M.; Diaz-Orejas, R. Replication and Control of Circular Bacterial Plasmids. *Microbiol. Mol. Biol. Rev.* **1998**, *62*, 434-464.

15. Skorupski, K.; Taylor, R. K. Positive Selection Vectors for Allelic Exchange. *Gene* **1996**, *169*, 47-52.

16. Haas, B. L.; Matson, J. S.; DiRita, V. J.; Biteen, J. S. Single-Molecule Tracking in Live *Vibrio Cholerae* Reveals that ToxR Recruits the Membrane-Bound Virulence Regulator TcpP to the *toxT* Promoter. *Mol. Microbiol.* **2015**, *96*, 4-13.

17. Häse, C. C.; Mekalanos, J. J. TcpP Protein is a Positive Regulator of Virulence Gene Expression in *Vibrio Cholerae*. *Proc. Natl. Acad. Sci. U. S. A.* **1998**, *95*, 730-734.

18. Higgins, D. E.; DiRita, V. J. Transcriptional Control of *toxT* a Regulatory Gene in the ToxR Regulon of *Vibrio Cholerae*. *Mol. Microbiol.* **1994**, *14*, 17-29.

19. Murley, Y. M.; Carroll, P. A.; Skorupski, K.; Taylor, R. K.; Calderwood, S. B. Differential Transcription of the *tcpPH* Operon Confers Biotype-Specific Control of the *Vibrio Cholerae* ToxR Virulence Regulon. *Infect. Immun.* **1999**, *67*, 5117-5123.

20. Goss, T. J.; Seaborn, C. P.; Gray, M. D.; Krukonis, E. S. Identification of the TcpP-Binding Site in the *toxT* Promoter of *Vibrio Cholerae* and the Role of ToxR in TcpP-Mediated Activation. *Infect. Immun.* **2010**, *78*, 4122-4133.

21. Thompson, R. E.; Larson, D. R.; Webb, W. W. Precise Nanometer Localization Analysis for Individual Fluorescent Probes. *Biophys. J.* **2002**, *82*, 2775-2783.

22. Landgraf, D.; Okumus, B.; Chien, P.; Baker, T. A.; Paulsson, J. Segregation of Molecules at Cell Division Reveals Native Protein Localization. *Nature Methods* **2012**, *9*, 480-482.

23. Schütz, G. J.; Schindler, H.; Schmidt, T. Single-Molecule Microscopy on Model Membranes Reveals Anomalous Diffusion. *Biophys. J.* **1997**, *73*, 1073-1080.

24. Liao, Y.; Yang, S. K.; Koh, K.; Matzger, A. J.; Biteen, J. S. Heterogeneous Single-Molecule Diffusion in One-, Two-, and Three-Dimensional Microporous Coordination Polymers: Directional, Trapped, and Immobile Guests. *Nano Lett.* **2012**, *12*, 3080-3085.

25. Peterson, K. M.; Mekalanos, J. J. Characterization of the Vibrio Cholerae ToxR Regulon: Identification of Novel Genes Involved in Intestinal Colonization. *Infect. Immun.* **1988**, *56*, 2822-2829.

26. Beck, N. A.; Krukonis, E. S.; DiRita, V. J. TcpH Influences Virulence Gene Expression in *Vibrio Cholerae* by Inhibiting Degradation of the Transcription Activator TcpP. *J. Bacteriol.* **2004**, *186*, 8309-8316.

27. Krukonis, E. S.; Yu, R. R.; DiRita, V. J. The *Vibrio Cholerae* ToxR/TcpP/ToxT Virulence Cascade: Distinct Roles for Two Membrane-Localized Transcriptional Activators on a Single Promoter. *Mol. Microbiol.* **2000**, *38*, 67-84.

28. Xie, X. S.; Choi, P. J.; Li, G. W.; Lee, N. K.; Lia, G. Single-Molecule Approach to Molecular Biology in Living Bacterial Cells. *Annu. Rev. Biophys.* **2008**, *37*, 417-444.

29. Crawford, J. A.; Krukonis, E. S.; DiRita, V. J. Membrane Localization of the ToxR Winged-Helix Domain is Required for TcpP-Mediated Virulence Gene Activation in *Vibrio Cholerae*. *Mol. Microbiol.* **2003**, *47*, 1459-1473.

30. Pfau, J. D.; Taylor, R. K. Mutations in toxR and toxS that Separate Transcriptional Activation from DNA Binding at the Cholera Toxin Gene Promoter. *J. Bacteriol.* **1998**, *180*, 4724-4733.

31. Hennecke, F.; Muller, A.; Meister, R.; Strelow, A.; Behrens, S. A ToxR-Based Two-Hybrid System for the Detection of Periplasmic and Cytoplasmic Protein-Protein Interactions in Escherichia Coli: Minimal Requirements for Specific DNA Binding and Transcriptional Activation. *Protein Eng. Des. Sel.* **2005**, *18*, 477-486.

32. Skorupski, K.; Taylor, R. K. Control of the ToxR Virulence Regulon in Vibrio Cholerae by Environmental Stimuli. *Mol. Microbiol.* **1997**, *25*, 1003-1009.

33. Miller, V. L.; Taylor, R. K.; Mekalanos, J. J. Cholera Toxin Transcriptional Activator ToxR is a Transmembrane DNA Binding Protein. *Cell* **1987**, *48*, 271-279.

34. Anderson, C. M.; Georgiou, G. N.; Morrison, I. E.; Stevenson, G. V.; Cherry, R. J. Tracking of Cell Surface Receptors by Fluorescence Digital Imaging Microscopy using a Charge-Coupled Device Camera. Low-Density Lipoprotein and Influenza Virus Receptor Mobility at 4 Degrees C. *J. Cell Sci.* **1992**, *101*, 415-425.

Chapter 4: Toward *In-vivo* Imaging of the Gut Microbiome

The work presented in this chapter is an ongoing collaboration between the following authors: Chanrith Siv, Hannah Chia, Shannon Wetzler, Matt Foley, Nicole Koropatkin, and Julie Biteen

Author Contributions:

Experimental design: CS, HC, SW, MF, NK and JB; Data collection: CS, HC, SW; Data analysis: CS, HC, SW

The human gut microbiome influences human development, diseases, immunity, and health. For decades, scientists have only studied pathogens to understand ways to eliminate them from our systems. However, recent newfound awareness about how the microbiome is essential for human life has led to an explosion in human microbiome research. In this chapter, I developed and applied imaging modalities to probe cell-cell interactions in anaerobic co-cultures. With the aim to address questions pertaining to resource sharing in a communal environment, I looked at commensal growth of *Bacteroides* and *Ruminococcus* bacterial species. I also assessed several means of introducing fluorescence into an aerobic imaging environment. The results presented in this chapter provide a new methodology for studying the interactions happening inside the gut.

4.1 Introduction

The human gastrointestinal tract harbors nearly 100 trillion microbes that are collectively known as the gut microbiota[1]. This microbial community is established shortly after birth and evolves throughout the life of the individual[2]. The gut microbiota has a profound effect in both health and disease[3-5]. The health benefits of maintaining a healthy gut microbiota include the

modulation of immune development[1,6], inhibition of pathogen colonization[7], and bidirectional communication between the gut and brain that triggers peristalsis and mucin production, and immune functions[8,9]. However, abnormalities in the microbiota composition—a dysbiotic state—can lead to irritable bowel syndrome and inflammatory bowel disease[10-12], colon cancer[13,14], antibiotic-associated colitis[15], and systemic metabolic diseases like type 2 diabetes[16] and obesity[17]. A heterogeneous etiology of metabolic and gastrointestinal diseases has been associated with the compositions of microbes, especially due to an increase in potentially harmful bacteria. In this chapter, I extend the capabilities of live bacterial cell imaging to understand this community, specifically the gut microbes responsible for metabolizing carbohydrates not readily digested by human enzymes.

A Gram-negative anaerobic microbe, *Bacteroides thetaiotaomicron* is a major endosymbiont of the human intestinal tract[18]. This bacterium brings in and hydrolyzes non-digestible polysaccharides found in complex material produced by plants, animals, fungi and bacteria, such as the following: amylose, amylopectin, glycogen, and maltooligosaccharides[19]. The starch utilization system (Sus) of *B. theta* consists of cell-associated enzymes that are responsible for hydrolyzing the polysaccharides into smaller fragments, which are then digestible by the human host[20-23]. Because large substrates cannot easily pass the bacterial cell membrane, this Sus complex is stationed at the outer membrane where it uses different Sus proteins to bind, cleave, and translocate these substrates[22]. Despite the difficulties of studying membrane proteins, recent efforts in structural biology[23] and single-molecule fluorescence imaging[24] have uncovered structural insights into this large complex and the sequential dynamic characteristics of the Sus proteins in the presence of different substrates, respectively. Though not all interactions and

stoichiometry have been fully elucidated, protein structure determinations predict a model for starch catabolism by *B. theta* Sus as shown in **Figure 4.1**.

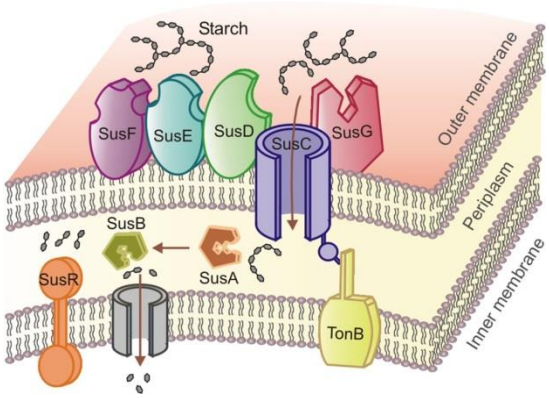

Figure 4.1 Model for starch catabolism by the *B. thetaiotaomicron* Sus, which consists of eight proteins (SusABCDEFG) that promote starch binding, degradation, and translocation. This figure was reprinted from Karunatilaka et al., *mBio* 2014[24].

Starch is a polymeric carbohydrate composed of glucose units joined by glycosidic bonds, which range in the degree of branching, chain lengths connecting branch points, and degree of polymerization. The microbiota has the capacity to degrade many starch macrostructures through a glycoside hydrolase family 13[25]. *B. theta* digests many forms of starch, but this bacterium cannot digest resistant starches (RS)[26]. RS are classified into four types (RS1 through RS4) based on their structure and degree of resistance to enzymatic degradation **(Table 4.1)**. Since *B. theta* cannot degrade all starches, the gut microbiota harbors other species that operate to establish an intricate synergy between the member cells that sustain community living[27]. *Ruminococcus bromii* is the keystone species for the degradation of resistant starch in the human colon[28]. Recent evidence from co-cultures of *R. bromii* with *B. theta* and other amylolytic bacteria suggests that *R. bromii* stimulates RS utilization so that other bacterial species can grow in the same medium [29]. *R. bromii* is a primary degrader of RS; the byproducts

from RS can be further utilized by other gut microbes[29]. Because RS fermentation confer health benefits, such as reducing insulin resistance[30], reversing infectious diarrhea[31], and preventing colorectal cancer[32], there is an active area of research that evaluates the utility of RS as a prebiotic[33]. However, previous research in this field have all been done *in vitro*, thus in this chapter I use cellular imaging to understand these community interactions.

Table 4.1 Classification of resistant starches and food sources.

Type of Resistant Starch	Description	Examples
RS1	Physically inaccessible, non-digestible matrix	Whole or partly milled grains and seeds
RS2	Tightly packed, ungelatinized starch granules	Raw potato starch, green bananas, high-amylose cornstarch
RS3	Retrograded starch (i.e., non-granular starch-derived materials)	Cooked and cooled potato, bread and pudding
RS4	Chemically modified starch	Etherized, esterified or cross-bonded starches (processed foods)

Since most bacteria do not live in isolation on petri dishes, bacterial cell imaging from monocultures alone may not provide the complete details of the biological processes happening inside them. This study demonstrates the use of imaging techniques on a mixed community of bacterial species. Single-cell superresolution imaging and tracking is used to study localizations and dynamics of proteins inside one cell at a time to understand cellular processes specific to that cell, but has yet to be applied to understand mechanisms that respond to interspecies or intraspecies interactions. Moving away from experiments at the single-cell level, I determined the conditions under which *B. theta* and *R. bromii* can grow in a commensal fashion and visualize the growth of these two bacterial species under the microscope. Under the co-culture

conditions used in this study, the results indicate that *B. theta* cannot digest the RS carbohydrates (corn and potato starches) on its own; rather, in the absence of carbon sources that *B. theta* can catabolize, *B. theta* uses the RS breakdown products supplied by *R. bromii* as its carbohydrate source. These investigations also reveal that growth of a monolayer of a bacterial co-culture can be established on a coverslip.

In addition, I address the challenges involved in performing fluorescence imaging in an anaerobic environment. Fluorescence imaging is typically done at the benchtop. Thus, the absence of oxygen when growing and imaging live anaerobic microbes severely limits the types of fluorophores that can be used for labeling in these studies. For instance, fluorescent proteins, which offer multiple advantages for live-cell imaging, require oxygen for the chromophore to mature. Therefore, I instead labeled bacteria with alternative fluorescent proteins that use a flavin cofactor instead of oxygen[34]. Here, I present preliminary data on imaging a microbiome, and discuss the challenges in developing a technique to probe the unique roles of bacterial species in a mixed community.

4.2 Results and Discussion

4.2.1 Live-cell imaging of gut microbes

Cellular imaging provides a non-invasive, minimally perturbative means to examine live cells. Because cellular imaging is typically done on a benchtop in an open environment, this experimental setup precludes visualizing anaerobic bacteria. There are very few microscopy studies of living anaerobic bacteria due to this limitation, but work in my lab has extended cellular imaging to live cells of the obligate anaerobe *B. theta*[24], one of the many human gut microbes found in humans that are sensitive to the presence of oxygen. Here, I further extend

live-cell imaging using the experimental setup I have developed in the lab to examine another anaerobe, *R. bromii*.

B. theta becomes dormant when exposed to oxygen, but resumes growth and division within 30 min to 1 h once bacterial cells are brought back into the anaerobic chamber to equilibrate[35]. Therefore, this characteristic of *B. theta* makes preparing these bacterial cells on coverslips for imaging at the bench possible, as long as any manipulations in air are followed by an incubation time in the anaerobic chamber. However, *R. bromii* is more sensitive to oxygen and thus cannot be prepared in a similar fashion. To mitigate these challenges, I developed a different approach to prepare cells for imaging. As shown in **Figure 4.2a**, I sandwiched bacterial cells in media between an agarose pad and a coverslip, and sealed all sides of the coverslip with epoxy. The preparations of these slides were done inside the anaerobic chamber. The addition of epoxy ensured that no atmospheric exchange can occur when the slides leave the anaerobic chamber. This preparation method has enabled us to visualize live *R. bromii* under the microscope. To continue growth on a coverslip, the sample was maintained at different temperatures outside of the anaerobic chamber. *R. bromii* grew at room temperature but not as efficiently as in 37 °C. However, *R. bromii* can be imaged for many days with this sample preparation method **(Figure 4.2b)**. Because bacterial cells initially expand radially—primarily in plane—before a 3D architecture is established[36], this creates a single layer of bacteria that can be imaged without a confocal or light-sheet microscope setup. Though I have not imaged bacterial cells beyond 72 h, in theory the bacteria can continue to grow and divide as long as nutrients are not depleted.

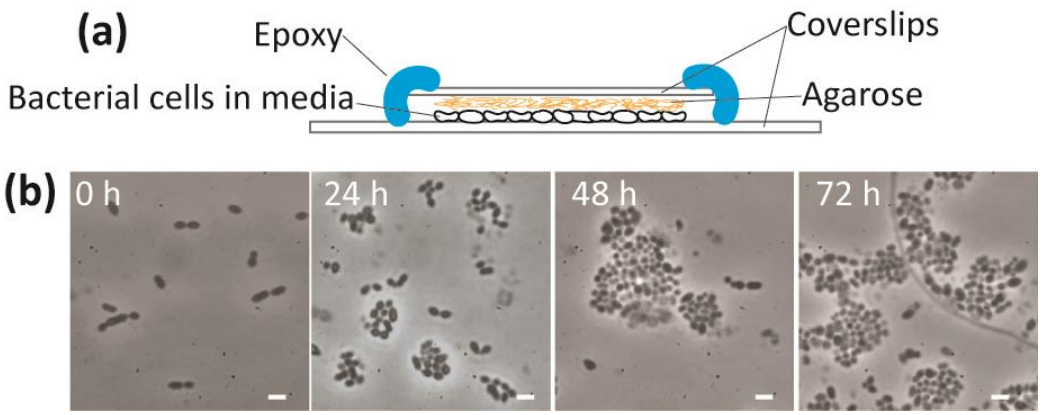

Figure 4.2 Imaging live anaerobic bacterial cells on a conventional benchtop microscope. **(a)** Sample preparation for imaging anaerobes in oxygen-exposing environment. Bacterial cells (~1-2 µm in length) are not drawn to scale relative to the microscope coverslips (22 mm and 50 mm in lengths for top and bottom, respectively). Using this setup, **(b)** *R. bromii* sustained growth on a coverslip over multiple days. Scale bars: 1 µm.

4.2.2 Growth of co-cultures in spent media

After developing a method to image *R. bromii*, I investigated optimal growth conditions to study mixed bacterial species. Since the release of energy from RS in the human colon depends on the presence of specialist primary degraders, like *R. bromii*, within the microbial community[29], I explored how different starches in the media affect *B. theta* growth. In particular, I used corn and potato starches in this study; these starches cannot be used as carbon sources for growing *B. theta* alone. I hypothesized that if cross-feeding is present, *B. theta* may be able to grow in a media containing RS by utilizing the metabolic byproducts of *R. bromii*.

To test this concept, I grew *R. bromii* in Ruminococcus (Rum) media with either corn starch or potato starch for up to 3 days, ensuring that abundant amounts of metabolic byproducts were maintained in the media. The *R. bromii* cultures were filtered through a 0.22 µm filter under a vacuum to obtain spent Rum media that was free of bacterial cells and RS. I measured the growth of *B. theta*, *R. bromii*, and a co-culture of the two anaerobes in different media

conditions for 6 days (**Figure 4.3**). In minimal media that was free of sugar, there was no bacterial growth. When maltose and glucose were added to the minimal media, there was growth in the monoculture of *B. theta* and in the co-culture, but not in the monoculture of *R. bromii*. As expected, these results support that *R. bromii* cannot utilize these simple sugar sources. I detected similar trends for growth in Rum media alone and in Rum with glucose. Based on my hypothesis of cross-feeding, *B. theta* should grow in the spent Rum media. Indeed, the results from the bottom two growth curves in **Figure 4.3** show that *B. theta* can grow in spent Rum.

However, several growth behaviors appeared on these growth curves that could not be explained. For instance, there was a drop-off for all conditions in the growth curves starting at ~100 h, perhaps as the nutrient source was depleted. And yet, in several other conditions (Rum + glucose, Rum + maltose), the co-culture sustained prolonged growth for a significant time after the *B. theta* monoculture OD dropped to zero. Overall, since *R. bromii* takes three times as long to reach similar steady-state levels as *B. theta*, it is possible that *R. bromii* densities were too low to be detected, and thus this method of detecting growth of co-cultures needs to be optimized.

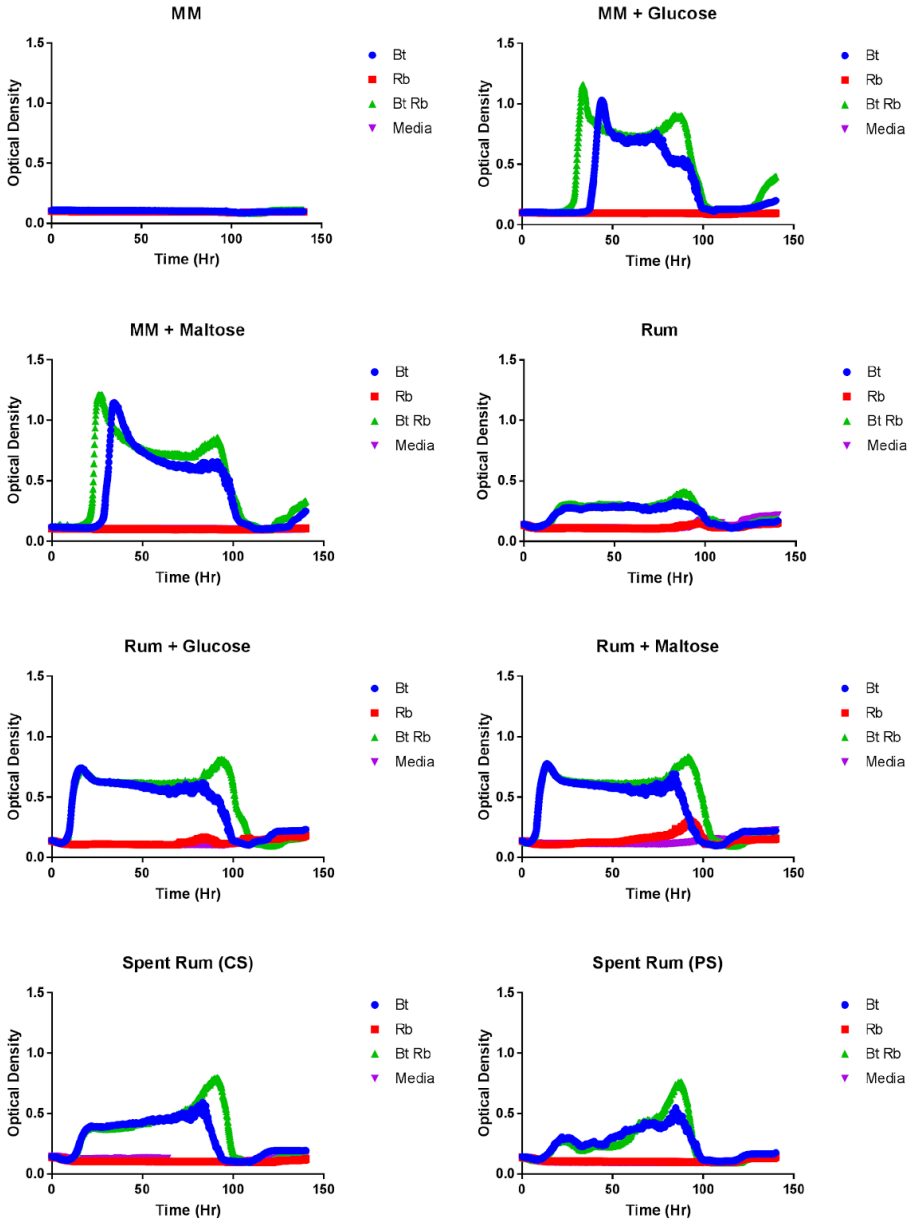

Figure 4.3 Growth curves obtained from *B. theta*, *R. bromii*, and *B. theta/R. bromii* co-culture inoculated in minimal media (MM), Rum media, and spent rum isolated from *R. bromii* grown with corn starch (CS) or potato starch (PS). The samples denoted MM and Rum did not include additional sugar, but instead was diluted with sterile water to make 1X media. The curves called "Media" in each panel indicate the OD_{600} reading with no inoculated cells.

4.2.3 Identification of bacteria by sizes and shapes

To visualize and examine the gut microbiome using microscopy, I developed a more faithful *in vitro* model of the bacterial communities constituting the gut microbiome. I grew liquid co-cultures of *B. theta* and *R. bromii*, and through qualitative observations, I distinguished the smaller, rounder *R. bromii* from the bigger, more elongated *B. theta* **(Figure 4.4a vs. b)**. There was growth for both bacteria in monocultures over the course of a 24-h period and in the co-cultures. Though it was easy to distinguish these two bacteria in low growth densities based on their cell morphologies, in higher bacterial densities there were ambiguities in determining bacterial sizes **(Figure 4.4c vs d).** Since bacteria were at different stages of cell division, it was hard to determine a dividing cell from one that was not dividing. Furthermore, there was more growth of *B. theta* relative to *R. bromii*, which is not surprising since *B. theta* doubles more quickly than *R. bromii* **(Figure 4.3)**.

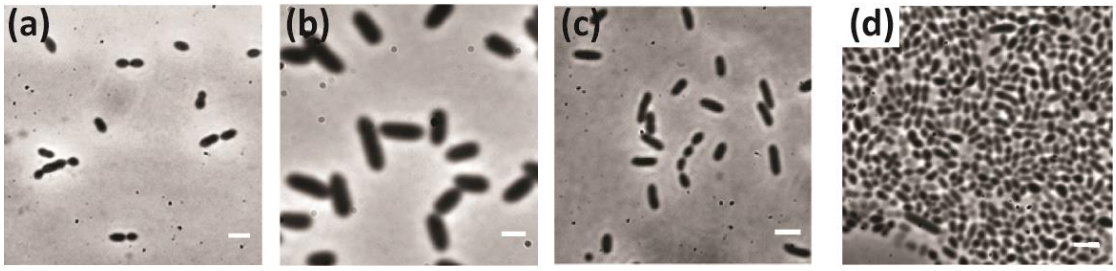

Figure 4.4 Growth of co-cultures on a coverslip. **(a)** A monoculture of *R. bromii* in Rum media. **(b)** A monoculture of *B. theta* in minimal media. A co-culture of *R. bromii* and *B. theta* in spent Rum media at **(c)** 0 h of growth and at **(d)** 24 h of growth. Scales bars: 2 µm.

Additionally, there was occasional contamination in some of these co-cultures; I attribute these species to cross-contamination from experiments in my collaborators' labs. Though I determined that wildtype *B. theta* was unable to use potato starch as a carbon source, I observed

some bacterial growth of rod-shaped bacteria **(Figure 4.5a)**. In the co-culture **(Figure 4.5b)**, there were growths of *B. theta* (green), *R. bromii* (purple), and an additional rod-shaped bacteria (red). I suspect that this culture contamination may be from *Bacillus* spp due to the size and shape. However, the sizes and shapes of this contaminant and *B. theta* were similar, and so there was a risk for potential misidentification. It was therefore critical to use a more definitive approach to characterizing bacterial species in mixed cultures.

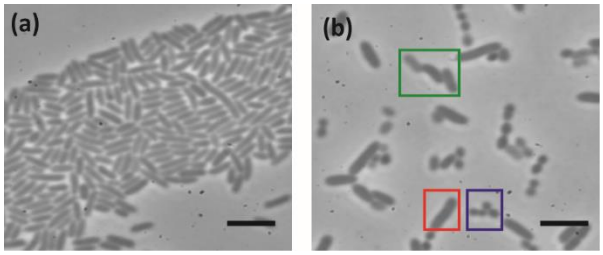

Figure 4.5 Contamination of cultures grown in the anaerobic chamber. **(a)** Growth of wildtype *B. theta* with potato starch. **(b)** A co-culture of *B. theta* (green) and *R. bromii* (purple) with contamination by another bacterial species (red). Scale bars: 4µm.

4.2.4 Selective labeling of *B. theta* for imaging of co-cultures

Due to the oxygen sensitivity of these anaerobic microbes, traditional fluorescent proteins, such as GFP and mCherry, cannot be used in the experiments, as the aforementioned proteins require oxygen in their biochemical reactions. Specifically, oxygen is needed by the chromophore to oxidize the α,β bond of tyrosine 66 during the self-catalyzing process to cause fluorescence[37]. To overcome this limitation in obligate anaerobic bacteria, a novel class of flavin-mononucleotide (FMN)-based fluorescent proteins (FbFPs) was developed by genetically engineering the bacterial light, oxygen, and voltage (LOV) sensing proteins from photoreceptors YtvA from *Bacillus subtilis*[38] and SB2 from *Pseudomonas putida*[39]. Therefore, I labeled the cells with FbFPs to preserve the oxygen-limiting environment required for the co-culture of *B. theta*

and *R. bromii*. FbFPs have been previously shown to be suitable fluorescent reporter proteins for quantitative analysis of microbial processes in both the presence and absence of oxygen[39-41]. Therefore, I used an engineered version of the light, oxygen, and voltage (LOV) sensing protein from *Chlamydomonas reinhardtii*[42] (CreiLOV) that was codon optimized for *B. theta* (BtCreiLOV).

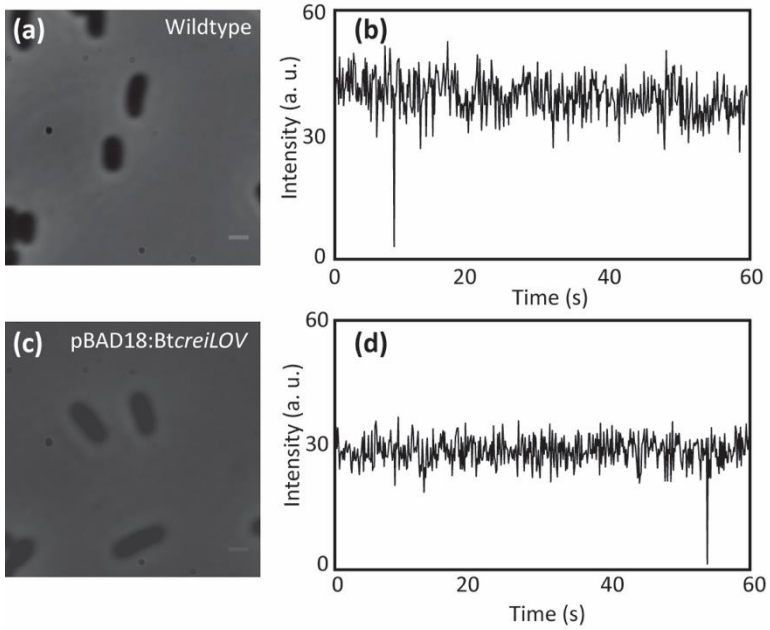

Figure 4.6 Fluorescence detection of BtCreiLOV in *E. coli.* Phase-contrast images were acquired for **(a)** wildtype *E. coli* and **(c)** *E. coli* pBAD18:BtcreiLOV. **(b)** Fluorescence intensity traces were measured for one cell in (a), and similarly plotted for *E. coli* pBAD18:Bt*creiLOV* after arabinose-induction in **(d)**. Scale bars: 1 µm.

I investigated the fluorescent properties of FbFP with my microscope setup and imaging conditions by observing the BtCreiLOV expression in *E. coli*. I cloned the Bt*creiLOV* gene into *E. coli* under an arabinose-inducible promoter pBAD18. Here, I used arabinose induction at 0.1% final concentration (v/v) to ensure high expression of BtCreiLOV. I imaged *E. coli* containing pBAD18:Bt*creiLOV* under both aerobic and anaerobic conditions, and detected no

discernible difference in fluorescence among wildtype *E. coli* cells, arabinose non-induced pBAD18:Bt*creiLOV E. coli* cells, and arabinose-induced pBAD18:Bt*creiLOV E. coli* cells. The introduction of Bt*creiLOV* did not affect the phenotype of *E. coli* **(Figure 4.6a vs. c)**. To determine if the fluorescence of BtCreiLOV can be detected in *E. coli* under my imaging conditions, I measured the fluorescence signal from *E. coli* cells nominally expressing BtCreiLOV and compared the signal against the autofluorescence of non-transfected *E. coli* illuminated with 488-nm laser light using the same excitation power **(Figure 4.6b vs. d)**. By comparing the fluorescence intensity traces over time, I observed that the fluorescence signal of BtCreiLOV was not distinguishable from the background fluorescence in wildtype *E. coli*. Though it had been reported in literature that fluorescence intensities from BtCreiLOV are comparable to eGFP[41], my data suggests otherwise. One difficulty here is that the blue color of the BtCreiLOV protein coincides with the spectral region where cells exhibit autofluorescence, due to the flavins that are naturally present in the cell. Though absorbance maximum of BtCreiLOV is 440 nm, I selected a 488-nm excitation laser to avoid background autofluorescence in this color region. Still, under the imaging conditions used in **Figure 4.6**, there was no detectable fluorescence. However, there was a tradeoff with 488-nm excitation: the cellular background will be decreased, but the fluorescence of the LOV protein will also decrease since I am not optimally exciting the LOV proteins at the right wavelength. Therefore, I speculate that the LOV protein fluorescence signals were overwhelmed by cellular autofluorescence signals in this imaging setup.

I also examined the fluorescence of these *E. coli* cells with 440-nm excitation in a different microscope setup (CFP filters; Olympus BX61 microscope using an Olympus 100× oil immersion 1.45-numerical aperture (NA) total internal reflection fluorescence microscopy

(TIRFM) objective lens), but again detected no difference between the wildtype and pBAD18:Bt*creiLOV E. coli* cells, perhaps due to high cellular autofluorescence. In the future, it may be necessary to excite the samples using 514-nm laser light where cellular autofluorescence is minimized. However, since this longer wavelength is the peak of CreiLOV emission, some of the signals will get filtered out in the measurements **(Figure 4.7)**.

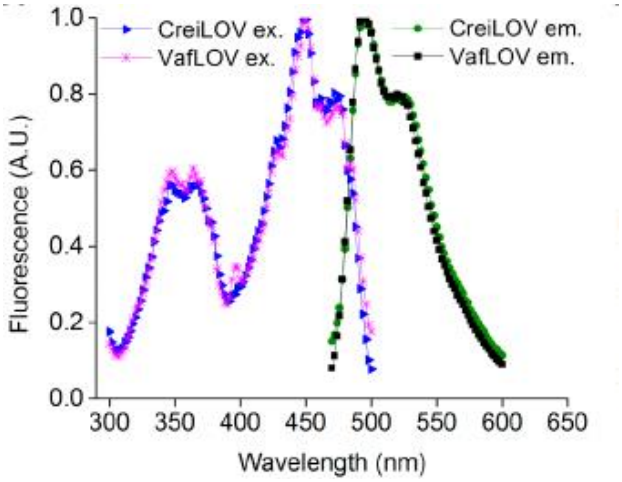

Figure 4.7 Fluorescence excitation and emission spectra of purified CreiLOV and VafLOV from *Chlamydomonas reinhardtii* and *Vaucheria frigida*, respectively. This figure was reprinted from Mukherjee et al., *ACS Syn. Bio*. 2014[42].

To investigate the feasibility of using an FbFP in *B. theta*, I acquired the Bt*creiLOV* gene from the *E. coli* S17 strain by PCR and did conjugation with *B. theta* to facilitate homologous recombination, putting the Bt*creiLOV* gene under the constitutive promoter *usBT1311*. Because BtCreiLOV expression is constitutive, all cells should express the FbFP since expression level here does not vary with cell cycle. The successful transfer of the gene into *B. theta* was verified by PCR and sequencing. Additionally, I cloned two other variants of FbFP (Evoglow[43]) onto the *usBT1331* promoter. These FbFPs were codon optimized for *B. theta (BtfbFP)* and *E. coli (EcfbFP).* From the movies acquired with my microscope setup and imaging conditions, I did not

detect significant differences in fluorescence signals in wildtype *B. theta* from the three *B. theta* strains expressing FbFPs **(Figure 4.8).** These results suggest that these flavin-based reporters are not appropriate fluorescent proteins to label *B. theta* cells.

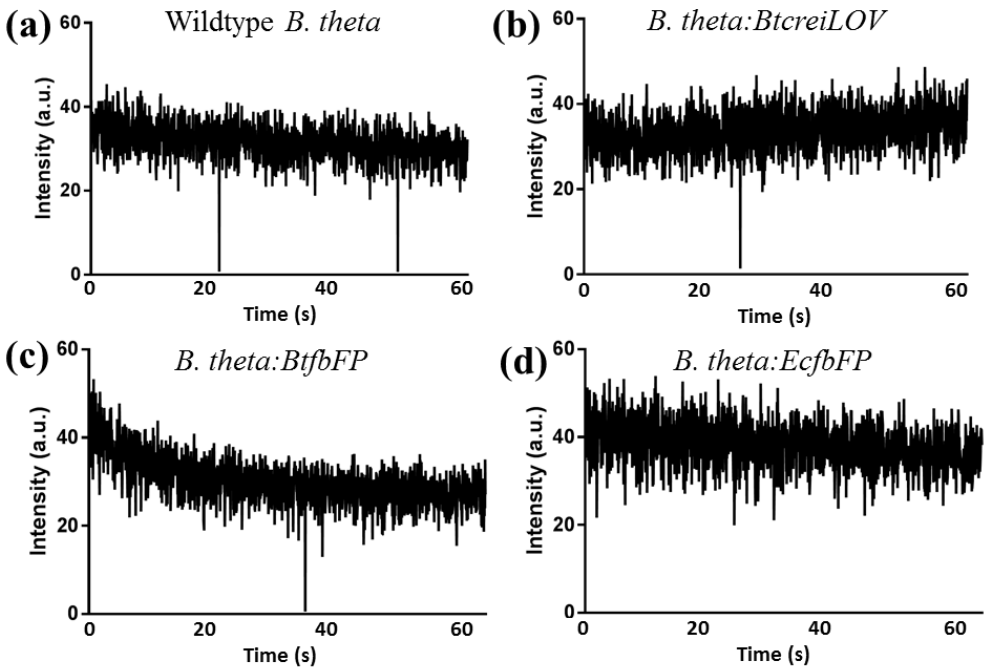

Figure 4.8 Fluorescence detection of FbFPs in *B. theta.* Fluorescence intensity traces were measured for **(a)** wildtype *B. theta*, **(b)** *B. theta* expressing codon-optimized CreiLOV, **(c)** *B. theta* expressing codon-optimized Evoglow, and **(d)** *B. theta* expressing Evoglow optimized for *E. coli*. These intensity traces were from single-cell measurements.

4.2.5 Selective labeling of *R. bromii* for imaging co-cultures

In addition to the selective labeling of *B. theta*, I used immunofluorescence to identify *R. bromii* in a mixed culture. A culture of *R. bromii* was probed with antibodies against starch degrading enzymes on *R. bromii* surface (either α4T, α9T, or α12T) before a second antibody containing an organic dye was used for secondary labeling. To maintain anoxic conditions, all antibody labeling done on living cells was performed in the anaerobic chamber. 488-nm laser

light was used to detect fluorescence from antibody-labeled *R. bromii*. Though *R. bromii* does exhibit background fluorescence at 488 nm, these signals were not as strong and could be bleached quite rapidly. By imaging a co-culture containing labeled *R. bromii* and unlabeled *B. theta* (**Figure 4.9**), I detected fluorescence in *R. bromii* and minimal specific interactions between the *anti-R. bromii* antibodies and *B. theta* cells, which suggests the feasibility of this antibody-labeling method to study the composition of a co-culture at a specific time point. Future experiments will further optimize antibody labeling to minimize nonspecific binding and eliminate free, unbounded dyes in the sample.

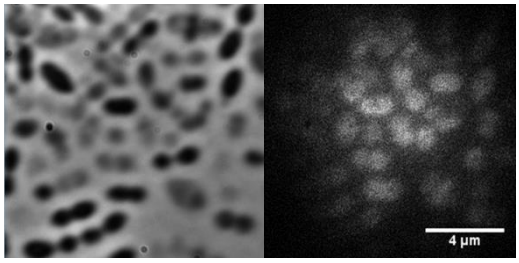

Figure 4.9 Direct imaging of *R. bromii/B. theta* co-culture by immunofluorescence microscopy. A phase-contrast image (left) and a fluorescence image (right) of this co-culture grown in spent Rum media.

4.3 Conclusions

In this chapter, I have shown that *B. theta* and *R. bromii* can grow in a commensal fashion under growth conditions where *R. bromii* initially breaks down RS and releases digestible starches. Before I can accurately measure growth of specific bacterial species in a mixed culture, optimizations in the growth conditions to minimize contaminations and methods development to grow co-cultures with similar starting densities for different bacterial species need to be done. To determine which metabolic byproducts from RS are important for growth of *B. theta*, future experiments will also need to include qualitative and quantitative measurements

of the byproducts based on thin-layer chromatography, mass spectrometry, and high pressure liquid chromatography. By characterizing byproducts, it may be possible to grow different sets of bacterial species to differentiate the major degraders of certain starches from the minor degraders in this microbial community. In addition to growth in a test tube, I have shown first images of two live, anaerobic bacterial species grown on a coverslip and imaged using a benchtop microscope. Because of similarity in shapes of these two bacterial species, phase-contrast images were not enough to definitively distinguish these two bacteria. Nevertheless, this preliminary single-cell imaging data suggests that it is possible to detect multiple species in co-culture, and perhaps visualize cross-feeding interactions between *B. theta* and *R. bromii*. Fluorescence markers may be useful to detect individual species in a mixed culture, but the availability of probes for imaging in anaerobic conditions make this endeavor a bit challenging.

The complex network of the human gut microbiota is complicated, and therefore it is important to increase the complexity of imaging samples to better understand the processes that make biofilm development crucial to microbes. Biofilms are surface-attached multi-species microbial communities that are up to 1000-fold less susceptible to antimicrobials and antibiotics[44]. This reduced susceptibility is due to retarded antimicrobial penetration into the biofilm, altered growth rates, intraspecies and interspecies metabolite and/or cell–cell signaling interactions, and cross-species protection[44]. Here, I describe several approaches to growing *B. theta/R. bromii* biofilms **(Table 4.2)**. The static nature of these systems inhibits continuous supply of fresh medium and thus limit nutrients, and makes it hard to generate mature biofilms. Still, method developments in continuous-flow and chemostat systems for the production of mature biofilms will hopefully address these limitations[45].

Table 4.2 Different methods to grow a *B. theta/R. bromii* biofilm

Method	Ease of Use	Possibility of Working
Cube of coverslips held together by epoxy	Extremely hard	Possible
Cube of coverslips held together by Blu-Tack	Hard	Possible
Immersing coverslip in liquid culture	Easy	Unlikely
Growing *B. theta* between two coverslips	Medium	Possible

.

4.4 Methods

4.4.1 Bacterial growth

Monocultures of *R. bromii* were grown anaerobically at 37 °C in Ruminococcus (Rum) media with corn or potato starches (1-2% wt/vol). See Rum media recipe below. After 2-3 days of growth in Rum media, *R. bromii* cultures were spun down to pellet the starches and bacteria. To make spent Rum media, which is a media containing breakdown product of *R. bromii* digestion of resistant starches (RS), the supernatant from this separation step was sterilized with a 0.22 μm filter. This separation step removed *R. bromii*, as well as any unprocessed RS, from the media, leaving behind only soluble byproducts as the only carbon source. Monocultures of *B. theta* were similarly grown under anaerobic conditions at 37 °C in TYG media (see recipe below) with glucose or maltose (0.5% wt/vol). After overnight growth to stationary phase in TYG media, *B. theta* was subsequently back-diluted into minimal media with glucose or maltose. Bacterial co-cultures were made from mixing different aliquots of the overnight cultures of *R. bromii* in Rum media and *B. theta* in minimal media (MM) into spent Rum media, and grown anaerobically for 1-3 days at 37 °C. Growth curves were obtained by taking optical density measurements at 600 nm on a high-throughput plate reader. Media was deposited into 96-well plates, and were allowed to equilibrate in anaerobic conditions before the addition of *B. theta* or *R. bromii* (1:200 dilution), with triplicates of each bacteria/media combination. OD_{600} readings

were taken every 10 minutes for six days. Growth curves were plotted and analyzed using GraphPad Prism.

Recipes for the growth media used in this study

TYG (1x, 50 mL) [46]

5 mL 10x Bacteriodes salts (KH_2PO_4, $(NH_4)_2SO_4$ and NaCl)

1 g TYG powder mix (HIMEDIA)

50 µL $FeSO_4$ with 10 mM HCl

50 µL 0.08% $CaCl_2$

50 µL 0.1 M $MgCl_2$

50 µL 1.9 mM Hematin with 0.2 M histidine

50 µL 1 mg/mL Vitamin K3

50 µL Vitamin B12

25 mg Cysteine

MM (2x, 50 mL)

10 mL 10x Bacteriodes salts (KH_2PO_4, $(NH_4)_2SO_4$ and NaCl)

100 µL $FeSO_4$ with 10 mM HCl

100 µL 0.08% $CaCl_2$

100 µL 0.1 M $MgCl_2$

100 µL 1.9 mM Hematin with 0.2 M histidine

100 µL 1 mg/mL Vitamin K3

100 µL Vitamin B12

100 mg Cysteine

<u>100x vitamin mix</u>

Dissolve 1 mg biotin, 1 mg cobalamin, 3 mg p-aminobenzoic acid, 5 mg folic acid, 15 mg pyridoxamine, 5 mg thiamine, 5 mg riboflavin in 100 mL water. Solution is stored in the dark at 4 °C.

Hematin/L-histidine

Dissolve 1.9 mM (1.2 mg/mL) hematin in 0.2 M L-histidine, pH 8.0. Hematin must be pre-dissolved in 1 M NaOH and neutralized with equal volume of 1 M HCl before L-histidine is added. Solution is stored in the dark at 4 °C.

Rum media (2x, 50 mL)

This recipe was modified from Ze et al., mBio 2015[47].

5 mL K/Na salts (20x)

500 µL $MgSO_4$ (200x)

500 µL $CaCl_2$ (200x)

1 mL Vitamin mix (100x)

0.8 mL Hematin/L-histidine

0.25 g Yeast extract

0.4 g $NaHCO_3$

0.1 g L-cysteine

0.09 g $(NH_4)_2SO_4$

0.1 mg D-Pantothenoic acid hemicalcium salt

0.1 mg Nicotinamide

183 µL Acetic acid

67 µL Propionic acid

26.4 µL Isobutyric acid

10.8 µL Isovaleric acid

10.8 µL Valeric acid

0.05 mg Resazurin

To make media, add ingredients in the order as listed above. Adjust all volumes with milliQ H_2O to a final volume of 50 mL. Filter sterilize the media with 0.22 µm filter and equilibrate in the anaerobic chamber before use. TYG media will store for 2 days, MM media for 2 days, and Rum media will store for 5-7 days in the dark. MM was diluted with carbohydrate sources to make 1X final solution. Rum media was adjusted to 1x by adding equal volumes of

filter sterilized solutions of glucose or maltose, autoclaved solutions of corn or potato starch, or filtered water mixed with ethanol sterilized corn or potato starch (final starch concentration of ~5 mg/mL).

4.4.2 Bacterial mating of *E. coli* and *B. theta*

Wildtype *B.theta* was grown at 37 °C under anaerobic conditions in TYG media. *E.coli* S17 harboring the FbFP gene was grown in LB with ampicillin (final concentration 100 μg/mL). The bacteria cultures were subsequently back-diluted and allowed to grow to mid-log phase before they were spun down together. The mixed pellet was resuspended, plated on BHI/blood plates with no antibiotics, and grown at 37 °C with shaking. The resulting bacterial film on top of the plate was scraped off and resuspended. This mixture (slurry consistency) was plated on BHI/blood plates containing gentamycin (200 μg/mL) and erythromycin (25 μg/mL) and grown at 37 °C anaerobically. The resulting colonies were restreaked on BHI/blood plates with gentamycin and erythromycin to eliminate background wild type *B.theta*. PCR was used to verify the successful transfer of genes into *B. theta*.

4.4.3 Imaging live bacterial cells

For live-cell imaging of wildtype *B. theta and R. bromii*, small aliquots of bacterial cells were deposited onto pads of 2% agarose in the same medium for imaging. The coverslip edges were sealed with epoxy (Devcon) to maintain an oxygen-free environment. These cells were imaged on an Olympus IX71 inverted fluorescence microscope equipped with a 1.40 numerical aperture (NA), 100× oil immersion wide-field phase-contrast objective. To image *B. theta* containing SusG labeled with photoactivatable mCherry (PAmCherry), the sample was activated with a 405-nm laser (Coherent 405-100) and excited with a 561-nm laser (Coherent Sapphire

561-50), and fluorescence emission intensities were detected by a Photometrics Evolve electron-multiplying charge-coupled device (EMCCD) camera at 25 frames per second. Because fluorescent proteins cannot mature in an anaerobic environment, *B. theta* cells containing fluorescent proteins were brought outside of the anaerobic chamber and exposed to oxygen (shaking) for 0.5-1 h, before being brought back to the chamber to equilibrate. *B. theta* goes dormant in O_2 and recovers on the timescale of 0.5 – 1 h.

4.4.3 Antibody labeling

To distinguish *R. bromii* from other bacteria grown in the same culture, we did antibody labeling of *R. bromii* bacterial cells. A 1 mL culture of *R. bromii* in early or late stationary phase was spun down, and the supernatant decanted. The pellet was resuspended in antibodies specific to *R. bromii* surface proteins (acquired from Nicole Koropatkin) and incubated in the anaerobic chamber for 30 min. After being washed twice with PBS, the cells were incubated in Alexa 488-conjugated goat anti-rabbit IgG secondary antibodies (Molecular Probes). Antibody-labeled cells were washed 3X with PBS and resuspended in PBS for cellular imaging. A small aliquot of bacterial cells was deposited onto pads of 2% agarose in for imaging. The coverslip edges were sealed with epoxy before being transported out of the anaerobic chamber.

4.5 Acknowledgements

I thank the members of Nicole Koropatkin's and Eric Marten's labs for help with growing and maintaining anaerobes.

4.6 References

1. Hooper, L. V.; Macpherson, A. J. Immune Adaptations that Maintain Homeostasis with the Intestinal Microbiota. *Nat. Rev. Immunol.* **2010**, *10*, 159-169.

2. Mackie, R. I.; Sghir, A.; Gaskins, H. R. Developmental Microbial Ecology of the Neonatal Gastrointestinal Tract. *Am. J. Clin. Nutr.* **1999**, *69*, 1035S-1045S.

3. Cerf-Bensussan, N.; Gaboriau-Routhiau, V. The Immune System and the Gut Microbiota: Friends Or Foes? *Nat. Rev. Immunol.* **2010**, *10*, 735-744.

4. Khanna, S.; Tosh, P. K. A Clinician's Primer on the Role of the Microbiome in Human Health and Disease. *Mayo Clin. Proc.* **2014**, *89*, 107-114.

5. Bull, M. J.; Plummer, N. T. Part 1: The Human Gut Microbiome in Health and Disease. *Integr. Med. (Encinitas)* **2014**, *13*, 17-22.

6. Round, J. L.; Mazmanian, S. K. The Gut Microbiota Shapes Intestinal Immune Responses during Health and Disease. *Nat. Rev. Immunol.* **2009**, *9*, 313-323.

7. Wardwell, L. H.; Huttenhower, C.; Garrett, W. S. Current Concepts of the Intestinal Microbiota and the Pathogenesis of Infection. *Curr. Infect. Dis. Rep.* **2011**, *13*, 28-34.

8. Collins, S. M.; Surette, M.; Bercik, P. The Interplay between the Intestinal Microbiota and the Brain. *Nat. Rev. Microbiol.* **2012**, *10*, 735-742.

9. Mayer, E. A. Gut Feelings: The Emerging Biology of Gut-Brain Communication. *Nat. Rev. Neurosci.* **2011**, *12*, 453-466.

10. Garrett, W. S.; Gallini, C. A.; Yatsunenko, T.; Michaud, M.; DuBois, A.; Delaney, M. L.; Punit, S.; Karlsson, M.; Bry, L.; Glickman, J. N.; Gordon, J. I.; Onderdonk, A. B.; Glimcher, L. H. Enterobacteriaceae Act in Concert with the Gut Microbiota to Induce Spontaneous and Maternally Transmitted Colitis. *Cell. Host Microbe* **2010**, *8*, 292-300.

11. Packey, C. D.; Sartor, R. B. Commensal Bacteria, Traditional and Opportunistic Pathogens, Dysbiosis and Bacterial Killing in Inflammatory Bowel Diseases. *Curr. Opin. Infect. Dis.* **2009**, *22*, 292-301.

12. Sheehan, D.; Shanahan, F. The Gut Microbiota in Inflammatory Bowel Disease. *Gastroenterol. Clin. North Am.* **2017**, *46*, 143-154.

13. Hamer, H. M.; Jonkers, D.; Venema, K.; Vanhoutvin, S.; Troost, F. J.; Brummer, R. -. Review Article: The Role of Butyrate on Colonic Function. *Aliment. Pharmacol. Ther.* **2008**, *27*, 104-119.

14. Warren, R. L.; Freeman, D. J.; Pleasance, S.; Watson, P.; Moore, R. A.; Cochrane, K.; Allen-Vercoe, E.; Holt, R. A. Co-Occurrence of Anaerobic Bacteria in Colorectal Carcinomas. *Microbiome* **2013**, *1*, 16-2618-1-16.

15. Khoruts, A.; Dicksved, J.; Jansson, J. K.; Sadowsky, M. J. Changes in the Composition of the Human Fecal Microbiome After Bacteriotherapy for Recurrent Clostridium Difficile-Associated Diarrhea. *J. Clin. Gastroenterol.* **2010**, *44*, 354-360.

16. Qin, J.; Li, Y.; Cai, Z.; Li, S.; Zhu, J.; Zhang, F.; Liang, S.; Zhang, W.; Guan, Y.; Shen, D.; Peng, Y.; Zhang, D.; Jie, Z.; Wu, W.; Qin, Y.; Xue, W.; Li, J.; Han, L.; Lu, D.; Wu, P.; Dai, Y.; Sun, X.; Li, Z.; Tang, A.; Zhong, S.; Li, X.; Chen, W.; Xu, R.; Wang, M.; Feng, Q.; Gong, M.; Yu, J.; Zhang, Y.; Zhang, M.; Hansen, T.; Sanchez, G.; Raes, J.; Falony, G.; Okuda, S.; Almeida, M.; LeChatelier, E.; Renault, P.; Pons, N.; Batto, J. M.; Zhang, Z.; Chen, H.; Yang, R.; Zheng, W.; Li, S.; Yang, H.; Wang, J.; Ehrlich, S. D.; Nielsen, R.; Pedersen, O.; Kristiansen, K.; Wang, J. A Metagenome-Wide Association Study of Gut Microbiota in Type 2 Diabetes. *Nature* **2012**, *490*, 55-60.

17. Ley, R. E.; Turnbaugh, P. J.; Klein, S.; Gordon, J. I. Microbial Ecology: Human Gut Microbes Associated with Obesity. *Nature* **2006**, *444*, 1022-1023.

18. Martens, E. C.; Lowe, E. C.; Chiang, H.; Pudlo, N. A.; Wu, M.; McNulty, N. P.; Abbott, D. W.; Henrissat, B.; Gilbert, H. J.; Bolam, D. N.; Gordon, J. I. Recognition and Degradation of Plant Cell Wall Polysaccharides by Two Human Gut Symbionts. *PLoS Biol* **2011**, *9*, e1001221.

19. Shipman, J. A.; Cho, K. H.; Siegel, H. A.; Salyers, A. A. Physiological Characterization of SusG, an Outer Membrane Protein Essential for Starch Utilization by Bacteroides Thetaiotaomicron. *J. Bacteriol.* **1999**, *181*, 7206-7211.

20. Shipman, J. A.; Berleman, J. E.; Salyers, A. A. Characterization of Four Outer Membrane Proteins Involved in Binding Starch to the Cell Surface of Bacteroides Thetaiotaomicron. *J. Bacteriol.* **2000**, *182*, 5365-5372.

21. Cho, K. H.; Salyers, A. A. Biochemical Analysis of Interactions between Outer Membrane Proteins that Contribute to Starch Utilization by Bacteroides Thetaiotaomicron. *J. Bacteriol.* **2001**, *183*, 7224-7230.

22. Tancula, E.; Feldhaus, M. J.; Bedzyk, L. A.; Salyers, A. A. Location and Characterization of Genes Involved in Binding of Starch to the Surface of Bacteroides Thetaiotaomicron. *J. Bacteriol.* **1992**, *174*, 5609-5616.

23. Cameron, E. A.; Maynard, M. A.; Smith, C. J.; Smith, T. J.; Koropatkin, N. M.; Martens, E. C. Multidomain Carbohydrate-Binding Proteins Involved in Bacteroides Thetaiotaomicron Starch Metabolism. *J. Biol. Chem.* **2012**, *287*, 34614-34625.

24. Karunatilaka, K. S.; Cameron, E. A.; Martens, E. C.; Koropatkin, N. M.; Biteen, J. S. Superresolution Imaging Captures Carbohydrate Utilization Dynamics in Human Gut Symbionts. *mBio* **2014**, *5*, e02172-14.

25. El Kaoutari, A.; Armougom, F.; Gordon, J. I.; Raoult, D.; Henrissat, B. The Abundance and Variety of Carbohydrate-Active Enzymes in the Human Gut Microbiota. *Nat Rev Microbiol* **2013**, *11*, 497-504.

26. Englyst, H. N.; Kingman, S. M.; Cummings, J. H. Classification and Measurement of Nutritionally Important Starch Fractions. *Eur. J. Clin. Nutr.* **1992**, *46 Suppl 2*, S33-50.

27. Leitch, E. C.; Walker, A. W.; Duncan, S. H.; Holtrop, G.; Flint, H. J. Selective Colonization of Insoluble Substrates by Human Faecal Bacteria. *Environ. Microbiol.* **2007**, *9*, 667-679.

28. Abell, G. C. J.; Cooke, C. M.; Bennett, C. N.; Conlon, M. A.; McOrist, A. L. Phylotypes Related to Ruminococcus Bromii are Abundant in the Large Bowel of Humans and Increase in Response to a Diet High in Resistant Starch. *FEMS Microbiol. Ecol.* **2008**, *66*, 505-515.

29. Ze, X.; Duncan, S. H.; Louis, P.; Flint, H. J. Ruminococcus Bromii is a Keystone Species for the Degradation of Resistant Starch in the Human Colon. *ISME J.* **2012**, *6*, 1535-1543.

30. Robertson, M. D.; Bickerton, A. S.; Dennis, A. L.; Vidal, H.; Frayn, K. N. Insulin-Sensitizing Effects of Dietary Resistant Starch and Effects on Skeletal Muscle and Adipose Tissue Metabolism. *Am. J. Clin. Nutr.* **2005**, *82*, 559-567.

31. Niderman-Meyer, O.; Zeidman, T.; Shimoni, E.; Kashi, Y. Mechanisms Involved in Governing Adherence of Vibrio Cholerae to Granular Starch. *Appl. Environ. Microbiol.* **2010**, *76*, 1034-1043.

32. Le Leu, R. K.; Hu, Y.; Brown, I. L.; Woodman, R. J.; Young, G. P. Synbiotic Intervention of Bifidobacterium Lactis and Resistant Starch Protects Against Colorectal Cancer Development in Rats. *Carcinogenesis* **2010**, *31*, 246-251.

33. Bird, A. R.; Conlon, M. A.; Christophersen, C. T.; Topping, D. L. Resistant Starch, Large Bowel Fermentation and a Broader Perspective of Prebiotics and Probiotics. *Benef Microbes* **2010**, *1*, 423-431.

34. Lobo, L. A.; Smith, C. J.; Rocha, E. R. Flavin Mononucleotide (FMN)-Based Fluorescent Protein (FbFP) as Reporter for Gene Expression in the Anaerobe Bacteroides Fragilis. *FEMS Microbiol. Lett.* **2011**, *317*, 67-74.

35. Karunatilaka, K. S.; Coupland, B. R.; Cameron, E. A.; Martens, E. C.; Koropatkin, N. M.; Biteen, J. S. Single-Molecule Imaging can be Achieved in Live Obligate Anaerobic Bacteria. *Proc. SPIE* **2013**, *8590*, 85900K.

36. Yan, J.; Sharo, A. G.; Stone, H. A.; Wingreen, N. S.; Bassler, B. L. Vibrio Cholerae Biofilm Growth Program and Architecture Revealed by Single-Cell Live Imaging. *Proc. Natl. Acad. Sci. U. S. A.* **2016**, *113*, E5337-43.

37. Tsien, R. Y. The Green Fluorescent Protein. *Annu. Rev. Biochem.* **1998**, *67*, 509-544.

38. Losi, A.; Polverini, E.; Quest, B.; Gartner, W. First Evidence for Phototropin-Related Blue-Light Receptors in Prokaryotes. *Biophys. J.* **2002**, *82*, 2627-2634.

39. Krauss, U.; Losi, A.; Gartner, W.; Jaeger, K. E.; Eggert, T. Initial Characterization of a Blue-Light Sensing, Phototropin-Related Protein from Pseudomonas Putida: A Paradigm for an Extended LOV Construct. *Phys. Chem. Chem. Phys.* **2005**, *7*, 2804-2811.

40. Drepper, T.; Huber, R.; Heck, A.; Circolone, F.; Hillmer, A.; Buechs, J.; Jaeger, K. Flavin Mononucleotide-Based Fluorescent Reporter Proteins Outperform Green Fluorescent Protein-Like Proteins as Quantitative in Vivo Real-Time Reporters. *Appl. Environ. Microbiol.* **2010**, *76*, 5990-5994.

41. Tielker, D.; Eichhof, I.; Jaeger, K. E.; Ernst, J. F. Flavin Mononucleotide-Based Fluorescent Protein as an Oxygen-Independent Reporter in Candida Albicans and Saccharomyces Cerevisiae. *Eukaryot. Cell.* **2009**, *8*, 913-915.

42. Mukherjee, A.; Weyant, K. B.; Agrawal, U.; Walker, J.; Cann, I. K.; Schroeder, C. M. Engineering and Characterization of New LOV-Based Fluorescent Proteins from Chlamydomonas Reinhardtii and Vaucheria Frigida. *ACS Synth. Biol.* **2015**, *4*, 371-377.

43. Landete, J. M.; Langa, S.; Revilla, C.; Margolles, A.; Medina, M.; Arques, J. L. Use of Anaerobic Green Fluorescent Protein Versus Green Fluorescent Protein as Reporter in Lactic Acid Bacteria. *Appl. Microbiol. Biotechnol.* **2015**, *99*, 6865-6877.

44. Mah, T. F.; O'Toole, G. A. Mechanisms of Biofilm Resistance to Antimicrobial Agents. *Trends Microbiol.* **2001**, *9*, 34-39.

45. Ludecke, C.; Jandt, K. D.; Siegismund, D.; Kujau, M. J.; Zang, E.; Rettenmayr, M.; Bossert, J.; Roth, M. Reproducible Biofilm Cultivation of Chemostat-Grown Escherichia Coli and Investigation of Bacterial Adhesion on Biomaterials using a Non-Constant-Depth Film Fermenter. *PLoS One* **2014**, *9*, e84837.

46. Martens, E. C.; Chiang, H. C.; Gordon, J. I. Mucosal Glycan Foraging Enhances Fitness and Transmission of a Saccharolytic Human Gut Bacterial Symbiont. *Cell Host Microbe* **2008**, *4*, 447-457.

47. Ze, X.; Ben David, Y.; Laverde-Gomez, J. A.; Dassa, B.; Sheridan, P. O.; Duncan, S. H.; Louis, P.; Henrissat, B.; Juge, N.; Koropatkin, N. M.; Bayer, E. A.; Flint, H. J. Unique Organization of Extracellular Amylases into Amylosomes in the Resistant Starch-Utilizing Human Colonic Firmicutes Bacterium Ruminococcus Bromii. *MBio* **2015**, *6*, e01058-15.

Chapter 5: Final Conclusions and Perspectives

Portions of this chapter (written by CS) have been adapted from the following publication:

Lee, S.A.[§]; Ponjavic, A. [§]; Siv, C. [§]; Lee, S,F.; and Biteen, J.S. Nanoscopic Cellular Imaging: Confinement Broadens Understanding. ACS Nano **2016**, 10, 8143-8153.

[§]Authors have contributed equally to this work.

The focus of this thesis was to apply high-resolution imaging methods to study non-model bacterial systems. In order to elucidate biological processes in living bacteria with nanometer-scale resolution, essential biological controls must be carried out to ensure that protein localizations and dynamics in cells are examined in the least perturbed way possible. In this chapter, I summarize my findings pertaining to single- and dual-color fluorescence imaging in live *V. cholerae* cells. The results provided here support a more rigorous testing of controls that the single-molecule fluorescence bacterial imaging field has overlooked. In addition to visualizing a pathogen, I tested the feasibility of fluorescence imaging for investigating anaerobes in a single-bacterial species culture and in a mixed-bacterial species culture, and provided evidence for the first-imaging studies of a microbiome. Finally, I conclude this chapter by highlighting some current methods development in the single-molecule fluorescence imaging field to image samples with greater complexity in the hope of visualizing a biological process in its most natural state.

5.1 Summary

In studying non-model bacteria like pathogens, I have witnessed the difficulty of labeling biomolecules in living systems[1-4]. Because single-molecule imaging requires native or controlled expression of fused biomolecules, I have addressed the consequences of using different protein expression systems on protein dynamics in live bacterial cells. I have shown that protein dynamics are altered if expression levels are not controlled to reflect native expression levels. However, if difficulties arise from genetic engineering that prevent endogenous expression of functional protein fusions, single-molecule tracking is still a highly sensitive method to detect subtle dynamic changes from changing growth conditions in ectopic-expressed systems. By studying an endogenous TcpP fluorescent fusion in different growth conditions, I uncovered a slow subpopulation that may be involved in interactions with other proteins and the DNA to activate gene expression. This result gets us closer to determining the mechanism *toxT* transcription activation[5-9]. This slow subpopulation was not previously elucidated based on only ectopic expression of a TcpP fluorescent fusion[10]. In addition, I identified that when fluorescent protein fusions are expressed from a plasmid, dynamics are altered and result in subdiffusive motion. This consequence of plasmid-expression systems may interfere or mask relevant dynamics in the cell[11,12]. Furthermore, I provided evidence that suggested that dynamics of TcpP in *V. cholerae* were not consistent with TcpP dynamics in *E. coli.* These results have implications for studying biological processes in a heterologous host[13-15]. In general, I have shown that single-molecule imaging can be very useful for understanding bacterial behavior as long as proper controls are performed to validate the findings. Overall, the work in Chapter 2 provides precautions for the single-molecule imaging community to minimize perturbations when visualizing biological processes in real-time.

Though it is possible to extract and infer relevant biological mechanisms like protein-protein interactions from the dynamics of a single protein in different conditions and knockout strains, the result is more convincing if protein-protein interactions can be directly probed with nm-precision. FRET[16-18] is a good measure for short range interactions between labeled proteins—providing information on length scales between 1 and 10 nm depending on the fluorophore—but FRET in live bacterial systems is difficult given the weak properties of fluorescent proteins at FRET pairs. Therefore, two-color single particle tracking may be a useful method to infer protein-protein interactions below the diffraction limit[19,20]. I set out to do just that when I fused orthogonal fluorescent proteins to ToxR and TcpP in *V. cholerae*. I provided evidence that the N-terminus of a protein is not always the most stable location to place a fluorescent tag, and endogenous labeling of interacting pairs of proteins may not always result in native interactions due to sterics caused by bulkiness of tags. Furthermore, I showed that PAGFP[21] is not a good fluorophore for use in *V. cholerae* due to its poor properties in this system. Though I have shown in Chapter 2 that endogenous expression of protein fusions is the least perturbed method of expression in *V. cholerae*, nevertheless plasmid expression of protein fusions may be the only feasible method when endogenous expression is not possible. By tracking the dynamics of plasmid-expressed ToxR-mCitrine and TcpP-PAmCherry, I verified the capability of our imaging to detect simultaneous emission signals from these two biomolecules. Though biochemical and genetic studies have revealed that there are ToxR and TcpP binding sites on the *toxT* promoter[5,22], it is still not known what the mechanisms of these proteins are in relation to the toxin pathway in *V. cholerae*. The data provided in Chapter 3 proved the feasibility of simultaneous two-color fluorescence imaging in *V. cholerae* that may be further exploited to determine the spatial co-locations and correlated dynamics of ToxR and TcpP.

Because bacterial species do not live alone in the environment, in Chapter 4 I tested the feasibility of fluorescence imaging within a microbiome. Because the human gut microbiome has implications for health and disease[23-25], I visualized anaerobic bacteria commonly found in the human gut microbiome. Since anaerobes mostly reside in the gut, high-resolution methods like single-molecule fluorescence imaging have not been readily applied to studying anaerobes[26,27]. Fluorescent proteins have been very valuable in bacterial cell imaging for its ease of genetic encoding, but fluorescent proteins require oxygen to properly fold and mature, and thus the use of fluorescent proteins is precluded in live anaerobes. Though *B. theta* and *R. bromii*—two bacteria that may exhibit cross-feeding mechanisms in the human gut microbiome[28]—could be distinguished under a phase-contrast microscope by their cell shapes and sizes in low cell densities, this identification method was not applicable in high cell densities. Therefore, I aimed to develop a fluorescence-based system to distinguish these bacteria species. Though the literature has shown that the flavin-based fluorescent proteins (Fbfp) exhibit eGFP-like properties in anaerobic imaging conditions in terms of fluorescence intensities[29], I found that these fluorophores exhibit low fluorescence that cannot be detected above intrinsic cellular autofluorescence. I also found that codon-optimized versions of the Fbfp did not increase the fluorescence intensities. Though we have yet to identify the best fluorophores for use in anaerobic imaging of the human gut microbiome, I provided here the first experiments to grow and image co-cultures of bacteria on a coverslip. These studies lay the groundwork for further investigation of the composition and growth patterns in microbiomes. Once fluorophore optimization for anaerobic imaging is achieved, it may be possible to probe the cross-feeding mechanism important for understanding the mechanism of collaborative starch degradation among species in the human gut microbiota.

5.2 Outlook

Advances in single-molecule imaging have enabled us to understand biological events one molecule at a time. The high sensitivity, specificity and spatial resolution of single-molecule fluorescence tracking and super-resolution imaging allow us to visualize intracellular activity that cannot be measured by conventional ensemble-averaged measurements, and thereby elucidating tremendous knowledge about cellular processes. By capturing, measuring and analyzing motion of single molecules in live systems, it is possible to uncover motion heterogeneities that provide clues to identifying rare mechanisms. While imaging single molecules in cells has been well optimized for mammalian cells, there is a growing increase in improving imaging conditions and controls to study bacterial cells. The work demonstrated in this thesis has allowed us to address some of those challenges associated with imaging bacteria. Below, I outline some of the exciting opportunities and technologies that are coming online to facilitate cellular imaging of more complex biological samples, such as biofilms, tissues, and in organisms. In addition to measuring protein dynamics with single-molecule fluorescence imaging and tracking, new labeling methods are now becoming available to detect DNA and RNA *in vivo*[2,30-33]. Therefore, it may be possible in the near future to probe the entire ToxR regulon, and visualize the whole process of virulence regulation from start to end. Furthermore, methods to enhance spectroscopic properties of fluorescent emitters are now being used for live-cell imaging[34-36], which will ultimately allow us to detect single-molecules with nanometer resolutions and track them for longer periods of time to better access their motion heterogeneities. As I have shown in Chapter 4, a better signal-to-noise ratio is needed in order to use fluorescence as a marker to distinguish anaerobes in a mixed culture.

5.21 High-resolution imaging of thicker samples.

As microscopes become more complicated, more intricate sample geometries are required. Light sheet microscopy, also referred to as single plane illumination microscopy, is a gentle way of imaging thick samples and fast biological processes *in vivo*. Since light-sheet microscopy can be adapted for our microscope setup with our existing cameras to get optical sectioning without a confocal setup, this techniques makes it possible for us to study biofilm compositions as well as interactions in the human gut microbiota with less photobleaching and and minimal phototoxicity. Ultimately, leaving the surface has made it possible to study both live and synthetic tissue at the single-molecule level; the combination of optical trapping[37] or 3D-printed tissues[38] with off-surface optical sectioning provides a unique platform for investigating interactions between cells. Application of these biophysical tools will lead to a wealth of discoveries about how signaling works on an intercellular scale.

5.22 Probing macromolecular interactions to understand cause and effect more completely.

While most single-molecule work has focused on proteins, for which labeling schemes are more well developed,[39] improving the level of subcellular complexity accessible to single-molecule fluorescence (SMF) imaging requires the development of labeling and imaging methods that simultaneously and directly visualize the complex interactions between DNA, RNA, proteins, and lipids in live cells. The CRISPR/Cas9 system is now a near-ubiquitous tool for genome editing in biology.[40] Excitingly, fluorescent protein fusions to the endonuclease-defective mutant dCas9 create an irreversibly bound probe capable of localizing a specific chromosomal locus.[31] Ongoing research will continue to improve the sgRNA specificity[41,42] and will provide multiple dCas9 probes for multi-color imaging.[30,43] To visualize RNA, single-molecule fluorescence *in situ* hybridization (smFISH) targets mRNA transcripts with

oligonucleotide fluorescent probes which is used to monitor transcriptional regulation.[44] Super-resolution imaging based on smFISH permits precise quantification of gene expression even in bacteria,[45] and can be extended for efficient multiplexing.[33,46,47]

Another important frontier in bacterial super-resolution imaging is the ability to combine chemical sensing with imaging,[48] thereby merging high spatial resolution and accurate chemical specificity. pH- and force-sensing dyes can also be incorporated into single-molecule experiments,[49] combining imaging with vibrational spectroscopy permits non-invasive chemical identification,[50,51] and complementing non-destructive optical imaging with matrix-assisted laser desorption ionization (MALDI) mass spectrometry imaging maps molecular distributions with high specificity.[52] These technical capabilities now open up avenues for us to explore biological processes with multiple variables simultaneously to see biology as a whole. In microbiology in particular, it will be exciting to finally probe the complex communication among cells to understand why individual bacteria join together to create bacterial communities.

5.2.3 Nanotechnology solutions to widen the scope of super-resolution imaging in mixed-species bacterial cultures

Advances in nanotechnology and microfluidics[53,54] will continue to increase opportunities for SMF imaging of bacterial cells through cell sorting. Recent advances in fluorescence activated cell sorting (FACS) are improving bacterial cell sorting,[55] which is vitally important for studying heterogeneous cell populations. Microfluidic devices allow single cell manipulation and analysis[56] to enable multiple experiments on a single cell. In addition to sorting, microfluidics have made physiologically relevant conditions much more accessible. For instance, gradient hydrogels produced by a microfluidic mixing system enabled a study of hematopoietic stem cell

differentiation as a function of niche cell concentration.[57] As an alternative to chip-based microfluidics, individual cells identified by optical microscopy can be selected, manipulated, and sorted with a modified atomic force microscope with a microchanneled cantilever in fluidic force microscopy.[58]

Furthermore, though single-cell super-resolution experiments are common, bacterial cells do not exist in isolation; rather it is becoming increasingly obvious that most bacteria function as a part of a microbiome. I envision single-molecule imaging as a bridge for the gap between community-level observations and nanoscale biophysics. On one hand, tools like optical sectioning will find their place in studies of thick biofilms. On the other hand, 2D bacterial biofilm models[59,60] will provide confinement in the axial direction while maintaining intercellular connectivity. Alternatively, sample confinement can make single cells behave as if they were in communities: for instance, volumetrically confined single *Pseudomonas aeruginosa* cells will undergo auto-induced quorum sensing, in an effective community of one.[61]

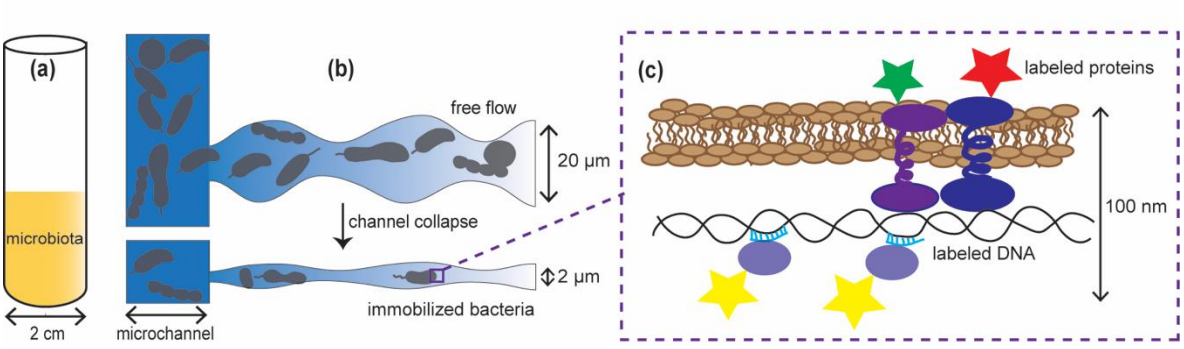

Figure 5.1 Single-molecule imaging of microbial community members. (a) A microbiota is grown in a culture flask, (b) an aliquot of the co-culture is flowed through a nanofluidic device capable of separating and immobilizing bacteria by channel closing, and (c) labeled molecules within individual cells are imaged *in situ* using SMF microscopy.

I envision a simple apparatus for studying protein function at the single-molecule level in single cells from a microbiome (**Figure 5.1**). This sample connects a microbial community co-culture[62] to a nanofluidic sorting mechanism[63] that prepares the sample for imaging. A more elaborate experiment might include tissue sectioning or imaging through mice[64] or rabbits[65] to understand how a microbiota interacts with a host.[66] Overall, with the use of microfluidics, researchers can multiplex studies on individual cells in a variety of environments and with different stimuli, and extend single-cell measurements to the regime of cellular communities.

5.3.4 The properties of plasmon-enhanced fluorescence applied to improving live-cell imaging.

Finally, looking forward, plasmonics will allow a variety of spectroscopies to be performed on the subcellular level to obtain dynamic chemical and structural information with higher spatial resolutions. Plasmonic nanoparticle arrays, in particular, will improve the resolution of fluorescence microscopy to the order of the size of the emitter and reduce photobleaching for monitoring real-time protein dynamics.[67] For instance, I envision combining plasmonics and nanofluidics to produce a platform for confined, physiological, enhanced imaging in bacteria (**Figure 5.2**). Overall, as technologies improve, all of the tools discussed here can be combined to reach higher levels of understanding about fundamental, subcellular biology. Through innovative combinations of confinement approaches, imaging modalities, and nanotechnologies, it will be possible to finally close the mismatch between the spatial resolution of light microscopy and the nanoscale world of cellular biophysics to enable a wealth of discoveries.

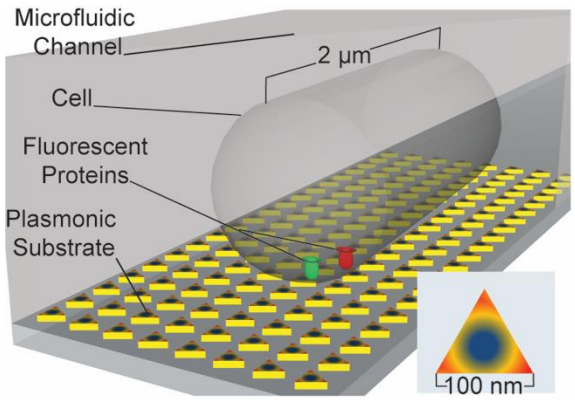

Figure 5.2 Single-cell analysis on a plasmonic substrate within a microfluidic channel will permit active control of the cellular environment. Two intracellular fluorescent proteins (red and green) couple to the plasmonic substrate for plasmon-enhanced two-color single-molecule imaging. (Inset) Electric field enhancement above each plasmonic nanotriangle.

5.3.5 Concluding remarks

Single-molecule imaging in live bacteria is in an era beyond the novelty of the technique. This method has the potential to answer many questions not previously addressed by bulk techniques in microbiology. This method has already been successfully applied to understand bacterial cytoskeleton, nucleoid organization and partitioning, transcription and translation in model bacterial systems; it is now just starting to be rapidly applied to non-model bacterial systems. The work presented in this thesis present some early applications of single-molecule imaging in non-model bacterial systems. By capturing, measuring and analyzing the motion of single molecules, it is now possible to directly probe essential biological processes. When coupled with complementary *in vitro* biochemical assays and strategic manipulation of the organism, single-molecule imaging opens the door to quantitative imaging-based research that will ultimately reveal answers to unanswered, burning biomedical questions.

5.3 References

1. Prescher, J. A.; Bertozzi, C. R. Chemistry in Living Systems. *Nat. Chem. Biol.* **2005**, *1,* 13-21.

2. Dean, K. M.; Palmer, A. E. Advances in Fluorescence Labeling Strategies for Dynamic Cellular Imaging. *Nat. Chem. Biol.* **2014**, *10,* 512-523.

3. Dragulescu-Andrasi, A.; Rao, J. Chemical Labeling of Proteins in Living Cells. *ChemBioChem* **2007**, *8,* 1099-1101.

4. Chamberlain, C.; Hahn, K. M. Watching Proteins in the Wild: Fluorescence Methods to Study Protein Dynamics in Living Cells. *Traffic* **2000**, *1,* 755-762.

5. Goss, T. J.; Seaborn, C. P.; Gray, M. D.; Krukonis, E. S. Identification of the TcpP-Binding Site in the *toxT* Promoter of *Vibrio Cholerae* and the Role of ToxR in TcpP-Mediated Activation. *Infect. Immun.* **2010**, *78,* 4122-4133.

6. Brown, R. C.; Taylor, R. K. Organization of Tcp, Acf, and toxT Genes within a ToxT-Dependent Operon. *Mol. Microbiol.* **1995**, *16,* 425-439.

7. DiRita, V. J.; Parsot, C.; Jander, G.; Mekalanos, J. J. Regulatory Cascade Controls Virulence in Vibrio Cholerae. *Proc. Natl. Acad. Sci. U. S. A.* **1991**, *88,* 5403-5407.

8. Häse, C. C.; Mekalanos, J. J. TcpP Protein is a Positive Regulator of Virulence Gene Expression in *Vibrio Cholerae*. *Proc. Natl. Acad. Sci. U. S. A.* **1998**, *95,* 730-734.

9. Krukonis, E. S.; Yu, R. R.; DiRita, V. J. The *Vibrio Cholerae* ToxR/TcpP/ToxT Virulence Cascade: Distinct Roles for Two Membrane-Localized Transcriptional Activators on a Single Promoter. *Mol. Microbiol.* **2000**, *38,* 67-84.

10. Haas, B. L.; Matson, J. S.; DiRita, V. J.; Biteen, J. S. Single-Molecule Tracking in Live *Vibrio Cholerae* Reveals that ToxR Recruits the Membrane-Bound Virulence Regulator TcpP to the *toxT* Promoter. *Mol. Microbiol.* **2015**, *96,* 4-13.

11. Brieger, A.; Plotz, G.; Hinrichsen, I.; Passmann, S.; Adam, R.; Zeuzem, S. C-Terminal Fluorescent Labeling Impairs Functionality of DNA Mismatch Repair Proteins. *PLoS One* **2012**, *7,* e31863.

12. Burgert, A.; Letschert, S.; Doose, S.; Sauer, M. Artifacts in Single-Molecule Localization Microscopy. *Histochem. Cell Biol.* **2015**, *144,* 123-131.

13. Miller, V. L.; DiRita, V. J.; Mekalanos, J. J. Identification of toxS, a Regulatory Gene Whose Product Enhances toxR-Mediated Activation of the Cholera Toxin Promoter. *J. Bacteriol.* **1989**, *171,* 1288-1293.

14. Miller, V. L.; Mekalanos, J. J. Synthesis of Cholera Toxin is Positively Regulated at the Transcriptional Level by toxR. *Proc. Natl. Acad. Sci. U. S. A.* **1984**, *81*, 3471-3475.

15. Pearson, G. D.; Mekalanos, J. J. Molecular Cloning of Vibrio Cholerae Enterotoxin Genes in Escherichia Coli K-12. *Proc. Natl. Acad. Sci. U. S. A.* **1982**, *79*, 2976-2980.

16. Robinson, A.; van Oijen, A. M. Bacterial Replication, Transcription and Translation: Mechanistic Insights from Single-Molecule Biochemical Studies. *Nat. Rev. Microbiol.* **2013**, *11*, 303-315.

17. Lorenz, M.; Diekmann, S. Distance Determination in Protein-DNA Complexes using Fluorescence Resonance Energy Transfer. *Methods Mol. Biol.* **2006**, *335*, 243-255.

18. Akrap, N.; Seidel, T.; Barisas, B. G. Förster Distances for Fluorescent Resonant Energy Transfer between mCherry and Other Visible Fluorescent Proteins. *Anal. Biochem.* **2010**, *402*, 105-106.

19. Subach, F. V.; Patterson, G. H.; Manley, S.; Gillette, J. M.; Lippincott-Schwartz, J.; Verkhusha, V. V. Photoactivatable mCherry for High-Resolution Two-Color Fluorescence Microscopy. *Nat. Methods* **2009**, *6*, 153-159.

20. Bock, H.; Geisler, C.; Wurm, C. A.; von Middendorff, C.; Jakobs, S.; Schönle, A.; Egner, A.; Hell, S. W.; Eggeling, C. Two-Color Far-Field Fluorescence Nanoscopy Based on Photoswitchable Emitters. *Appl. Phys. B* **2007**, *88*, 161-165.

21. Patterson, G. H.; Lippincott-Schwartz, J. A Photoactivatable GFP for Selective Photolabeling of Proteins and Cells. *Science* **2002**, *297*, 1873-1877.

22. Miller, V. L.; Taylor, R. K.; Mekalanos, J. J. Cholera Toxin Transcriptional Activator ToxR is a Transmembrane DNA Binding Protein. *Cell* **1987**, *48*, 271-279.

23. Khanna, S.; Tosh, P. K. A Clinician's Primer on the Role of the Microbiome in Human Health and Disease. *Mayo Clin. Proc.* **2014**, *89*, 107-114.

24. Martens, E. C.; Sonnenburg, J. L.; Relman, D. A. Editorial Overview: Insights into Molecular Mechanisms of Microbiota. *J. Mol. Biol.* **2014**, *426*, 3827-3829.

25. Bull, M. J.; Plummer, N. T. Part 1: The Human Gut Microbiome in Health and Disease. *Integr. Med. (Encinitas)* **2014**, *13*, 17-22.

26. Karunatilaka, K. S.; Coupland, B. R.; Cameron, E. A.; Martens, E. C.; Koropatkin, N. M.; Biteen, J. S. Single-Molecule Imaging can be Achieved in Live Obligate Anaerobic Bacteria. *Proc. SPIE* **2013**, *8590*, 85900K.

27. Karunatilaka, K. S.; Cameron, E. A.; Martens, E. C.; Koropatkin, N. M.; Biteen, J. S. Superresolution Imaging Captures Carbohydrate Utilization Dynamics in Human Gut Symbionts. *mBio* **2014**, *5*, e02172-14.

28. Turroni, F.; Özcan, E.; Milani, C.; Mancabelli, L.; Viappiani, A.; van Sinderen, D.; Sela, D.; Ventura, M. Glycan Cross-Feeding Activities between Bifidobacteria Under *in Vitro* Conditions. *Front Microbiol* **2015**, *6*, 1030.

29. Walter, J.; Hausmann, S.; Drepper, T.; Puls, M.; Eggert, T.; Dihne, M. Flavin Mononucleotide-Based Fluorescent Proteins Function in Mammalian Cells without Oxygen Requirement. *PLoS One* **2012**, *7*, e43921.

30. Deng, W.; Shi, X.; Tjian, R.; Lionnet, T.; Singer, R. H. CASFISH: CRISPR/Cas9-Mediated in Situ Labeling of Genomic Loci in Fixed Cells. *Proc. Natl. Acad. Sci. U. S. A.* **2015**, *112*, 11870-11875.

31. Chen, B.; Gilbert, L. A.; Cimini, B. A.; Schnitzbauer, J.; Zhang, W.; Li, G. W.; Park, J.; Blackburn, E. H.; Weissman, J. S.; Qi, L. S.; Huang, B. Dynamic Imaging of Genomic Loci in Living Human Cells by an Optimized CRISPR/Cas System. *Cell* **2013**, *155*, 1479-1491.

32. Ji, N.; van Oudenaarden, A. Single Molecule Fluorescent in Situ Hybridization (smFISH) of C. Elegans Worms and Embryos. *WormBook* **2012**, 1-16.

33. Chen, K. H.; Boettiger, A. N.; Moffitt, J. R.; Wang, S.; Zhuang, X. Spatially Resolved, Highly Multiplexed RNA Profiling in Single Cells. *Science* **2015**, *348*, aaa6090.

34. Lakowicz, J. R. Plasmonics in Biology and Plasmon-Controlled Fluorescence. *Plasmonics* **2006**, *1*, 5-33.

35. Moal, E. L.; Fort, E.; Lévêque-Fort, S.; Cordelières, F. P.; Fontaine-Aupart, M. -.; Ricolleau, C. Enhanced Fluorescence Cell Imaging with Metal-Coated Slides. *Biophys. J.* **2007**, *92*, 2150-2161.

36. He, R. Y.; Chang, G. L.; Wu, H. L.; Lin, C. H.; Chiu, K. C.; Su, Y. D.; Chen, S. J. Enhanced Live Cell Membrane Imaging using Surface Plasmon-Enhanced Total Internal Reflection Microscopy. *Opt. Express* **2006**, *14*, 9307-9316.

37. Oddos, S.; Dunsby, C.; Purbhoo, M. A.; Chauveau, A.; Owen, D. M.; Neil, M. A. A.; Davis, D. M.; French, P. M. W. High-Speed High-Resolution Imaging of Intercellular Immune Synapses using Optical Tweezers. *Biophys. J.* **2008**, *95*, L66-L68.

38. Villar, G.; Graham, A. D.; Bayley, H. A Tissue-Like Printed Material. *Science* **2013**, *340*, 48-52.

39. Fernández-Suárez, M.; Ting, A. Y. Fluorescent Probes for Super-Resolution Imaging in Living Cells. *Nat. Rev. Mol. Cell Biol.* **2008**, *9*, 929-943.

40. Jinek, M.; Chylinski, K.; Fonfara, I.; Hauer, M.; Doudna, J. A.; Charpentier, E. A Programmable Dual-RNA–Guided DNA Endonuclease in Adaptive Bacterial Immunity. *Science* **2012**, *337*, 816-821.

41. Taylor, D. W.; Zhu, Y.; Staals, R. H.; Kornfeld, J. E.; Shinkai, A.; van der Oost, J.; Nogales, E.; Doudna, J. A. Structural Biology. Structures of the CRISPR-Cmr Complex Reveal Mode of RNA Target Positioning. *Science* **2015**, *348*, 581-585.

42. Wu, X.; Kriz, A. J.; Sharp, P. A. Target Specificity of the CRISPR-Cas9 System. *Quant. Biol.* **2014**, *2*, 59-70.

43. Ma, H.; Naseri, A.; Reyes-Gutierrez, P.; Wolfe, S. A.; Zhang, S.; Pederson, T. Multicolor CRISPR Labeling of Chromosomal Loci in Human Cells. *Proc. Natl. Acad. Sci. U. S. A.* **2015**, *112*, 3002-3007.

44. Femino, A. M.; Fay, F. S.; Fogarty, K.; Singer, R. H. Visualization of Single RNA Transcripts in Situ. *Science* **1998**, *280*, 585-590.

45. Skinner, S. O.; Sepulveda, L. A.; Xu, H.; Golding, I. Measuring mRNA Copy Number in Individual Escherichia Coli Cells using Single-Molecule Fluorescent in Situ Hybridization. *Nat. Protoc.* **2013**, *8*, 1100-1113.

46. Lubeck, E.; Cai, L. Single-Cell Systems Biology by Super-Resolution Imaging and Combinatorial Labeling. *Nat Meth.* **2012**, *9*, 743-748.

47. Lubeck, E.; Coskun, A. F.; Zhiyentayev, T.; Ahmad, M.; Cai, L. Single-Cell in Situ RNA Profiling by Sequential Hybridization. *Nat Meth* **2014**, *11*, 360-361.

48. Biteen, J. S.; Blainey, P. C.; Cardon, Z. G.; Chun, M.; Church, G. M.; Dorrestein, P. C.; Fraser, S. E.; Gilbert, J. A.; Jansson, J. K.; Knight, R.; Miller, J. F.; Ozcan, A.; Prather, K. A.; Quake, S. R.; Ruby, E. G.; Silver, P. A.; Taha, S.; van, d. E.; Weiss, P. S.; Wong, G. C. L.; Wright, A. T.; Young, T. D. Tools for the Microbiome: Nano and Beyond. *ACS Nano* **2016**, *10*, 6-37.

49. Schaferling, M. Nanoparticle-Based Luminescent Probes for Intracellular Sensing and Imaging of pH. *Wiley Interdiscip. Rev. Nanomed. Nanobiotechnol.* **2016**, *8*, 378-413.

50. Watanabe, K.; Palonpon, A. F.; Smith, N. I.; Chiu, L. D.; Kasai, A.; Hashimoto, H.; Kawata, S.; Fujita, K. Structured Line Illumination Raman Microscopy. *Nat. Commun.* **2015**, *6*, 10095.

51. Cheng, J.; Xie, X. S. Vibrational Spectroscopic Imaging of Living Systems: An Emerging Platform for Biology and Medicine. *Science* **2015**, *350*, 1054.

52. Hanrieder, J.; Phan, N. T.; Kurczy, M. E.; Ewing, A. G. Imaging Mass Spectrometry in Neuroscience. *ACS Chem. Neurosci.* **2013**, *4*, 666-679.

53. Bell, L.; Seshia, A.; Lando, D.; Laue, E.; Palayret, M.; Lee, S. F.; Klenerman, D. A Microfluidic Device for the Hydrodynamic Immobilisation of Living Fission Yeast Cells for Super-Resolution Imaging. *Sensor. Actuat. B: Chem.* **2014**, *192*, 36-41.

54. Zhou, Y.; Basu, S.; Wohlfahrt, K. J.; Lee, S. F.; Klenerman, D.; Laue, E. D.; Seshia, A. A. A Microfluidic Platform for Trapping, Releasing and Super-Resolution Imaging of Single Cells. *Sensor. Actuat. B: Chem.* **2016**, *232*, 680-691.

55. Chen, C. H.; Cho, S. H.; Chiang, H.; Tsai, F.; Zhang, K.; Lo, Y. Specific Sorting of Single Bacterial Cells with Microfabricated Fluorescence-Activated Cell Sorting and Tyramide Signal Amplification Fluorescence in Situ Hybridization. *Anal. Chem.* **2011**, *83*, 7269-7275.

56. Shields, C. W.; Reyes, C. D.; Lopez, G. P. Microfluidic Cell Sorting: A Review of the Advances in the Separation of Cells from Debulking to Rare Cell Isolation. *Lab Chip* **2015**, *15*, 1230-1249.

57. Mahadik, B. P.; Wheeler, T. D.; Skertich, L. J.; Kenis, P. J. A.; Harley, B. A. C. Microfluidic Generation of Gradient Hydrogels to Modulate Hematopoietic Stem Cell Culture Environment. *Adv. Healthc. Mater.* **2014**, *3*, 449-458.

58. Stiefel, P.; Zambelli, T.; Vorholt, J. A. Isolation of Optically Targeted Single Bacteria by Application of Fluidic Force Microscopy to Aerobic Anoxygenic Phototrophs from the Phyllosphere. *Appl. Environ. Microbiol.* **2013**, *79*, 4895-4905.

59. Sadanandan, S. K.; Baltekin, O.; Magnusson, K. E. G.; Boucharin, A.; Ranefall, P.; Jalden, J.; Elf, J.; Wahlby, C. Segmentation and Track-Analysis in Time-Lapse Imaging of Bacteria. *Selected Topics in Signal Processing, IEEE Journal of* **2016**, *10*, 174-184.

60. Liu, J.; Prindle, A.; Humphries, J.; Gabalda-Sagarra, M.; Asally, M.; Lee, D. D.; Ly, S.; Garcia-Ojalvo, J.; Suel, G. M. Metabolic Co-Dependence Gives Rise to Collective Oscillations within Biofilms. *Nature* **2015**, *523*, 550-554.

61. Boedicker, J. Q.; Vincent, M. E.; Ismagilov, R. F. Microfluidic Confinement of Single Cells of Bacteria in Small Volumes Initiates High-Density Behavior of Quorum Sensing and Growth and Reveals its Variability. *Angew. Chem. , Int. Ed.* **2009**, *48*, 5908-5911.

62. Ze, X.; Duncan, S. H.; Louis, P.; Flint, H. J. Ruminococcus Bromii is a Keystone Species for the Degradation of Resistant Starch in the Human Colon. *ISME J.* **2012**, *6*, 1535-1543.

63. Cheng, M. C.; Leske, A. T.; Matsuoka, T.; Kim, B. C.; Lee, J.; Burns, M. A.; Takayama, S.; Biteen, J. S. Super-Resolution Imaging of PDMS Nanochannels by Single-Molecule Micelle-Assisted Blink Microscopy. *J. Phys. Chem. B* **2013**, *117*, 4406-4411.

64. Bolea, I.; Gan, W. B.; Manfedi, G.; Magrane, J. Imaging of Mitochondrial Dynamics in Motor and Sensory Axons of Living Mice. *Methods Enzymol.* **2014**, *547*, 97-110.

65. Abran, M.; Stahli, B. E.; Merlet, N.; Mihalache-Avram, T.; Mecteau, M.; Rheaume, E.; Busseuil, D.; Tardif, J. C.; Lesage, F. Validating a Bimodal Intravascular Ultrasound (IVUS) and Near-Infrared Fluorescence (NIRF) Catheter for Atherosclerotic Plaque Detection in Rabbits. *Biomed. Opt. Express* **2015**, *6*, 3989-3999.

66. Earle, K.; Billings, G.; Sigal, M.; Lichtman, J.; Hansson, G.; Elias, J.; Amieva, M.; Huang, K.; Sonnenburg, J. Quantitative Imaging of Gut Microbiota Spatial Organization. *Cell Host Microbe* **2015**, *18*, 478-488.

67. Donehue, J. E.; Wertz, E.; Talicska, C. N.; Biteen, J. S. Plasmon-Enhanced Brightness and Photostability from Single Fluorescent Proteins Coupled to Gold Nanorods. *J. Phys. Chem. C* **2014**, *118*, 15027-15035.

Appendix

A.1 Super-resolution microscopy

Super-resolution methods circumvent the diffraction limit that restricts conventional light microscopy to enable the investigation of biological questions within living cells at millisecond and nanometer-scale resolution. The most significant advances in super-resolution imaging in the last 20 or so years break the diffraction limit by physically reducing the size of the point spread function (PSF), or by spatially separating single molecules through switching fluorophores on and off over time. Structured Illumination Microscopy (SIM)[1] and Stimulated Emission Depletion (STED)[2] are two methods to apply PSF modification for improved resolution commonly used in biology. In SIM, a grid pattern is generated through interference of diffracted light and superimposed on the specimen while capturing images. The grid pattern is then rotated and shifted to generate image subsets. This patterned illumination method gains resolution by accessing higher frequency information. In STED microscopy, a doughnut-shaped depletion beam forces excited fluorophores to relax by saturated emission depletion. The red-shifted stimulated emission can be filtered out spectrally or temporally. The doughnut-shaped depletion beam effectively narrows the point-spread function of the excitation to increase lateral resolution down to ~20 nanometers. Because fluorophores used in STED microscopy are organic dyes, this imaging method has been infrequently applied to bacterial imaging[3].

The second class of super-resolution methods, which is used throughout this thesis, achieves super-resolution information by imaging single molecules one at a time. Though there are many single-molecule localization-based methods, biological imaging has relied heavily on a group of approaches that achieve single-molecule detection through fluorophore photoswitching and photoactivation—such as Photoactivated Localization Microscopy (PALM)[4], Fluorescence Photoactivation Localization Microscopy (FPALM)[5], Stochastic Optical Reconstruction Microscopy (STORM)[6]. Here I focus on a method that combines PALM with live-cell single-particle tracking (sptPALM)[7]. The principle surrounding PALM rests on imaging isolated photoactivatable fluorescent proteins by controllably activating and sampling sparse subsets of these labels over time. To perform PALM in bacteria, a biomolecule of interest is labeled with a fluorescent tag that has this photoswitching/photoactivating property[8]. This kind of fluorophore begins in a "dark" (non-absorbing) state and can be switched to a fluorescent state using violet (405-nm) laser light. The fluorescence is observed and molecules localized by separating the emission of individual fluorophores in space and time. The position of a single molecule can be localized with an accuracy of several nanometers (or better) if enough photons can be gathered. sptPALM builds on the subsets of molecules photoactivated in PALM by tracking each single molecule after activation. Thus, sptPALM can access information on heterogeneities in the motions of individual proteins to provide insights into subcellular events.

A.1.1 The optical set-up

In order to detect fluorescence signals from a single-molecule emitter, the optical setup has to be carefully designed to minimize background noise, such as reflected and scattered source light. A schematic of a typical widefield single-molecule epifluorescence microscope set-

up is depicted in **Figure A.1.** Each laser beam is initially passed through an excitation filter and then a quarter-wave plate to become circularly polarized. A telescope widens the laser beam to fill up the back aperture of a 100x 1.40 N.A. oil-immersion objective, and makes the illumination area larger. Adjustable mirrors and a periscope (CVI Melles Griot) direct the laser beam into a standard widefield inverted epifluorescence microscope (Olympus IX71). The emitted light then detected by an electron-multiplying charge-coupled device (EMCCD) detector (Photometrics Evolve) that connects to a computer. Due to the Stokes shift, reflected or scattered laser lights can be removed by a dichroic filter and a long-pass emission filter before detection by the camera sensor. A 3x beam expander is placed between the microscope and the camera, producing a pixel size of 49 nm/pixel (~20 pixels/μm) that is suitable for imaging single molecules in bacterial cells.

Depending on the application, this optical set-up can be modified to meet specific needs of the experiments. Because I used a photoactivatable fluorophore throughout my thesis, it was necessary to alternate the incoming light between an activation beam (406-nm) and an excitation beam (488-nm or 561-nm) to allow for photoactivation events before fluorophore excitation. For two-color imaging, I inserted a beam splitter between the microscope and the 3x beam expander to allow for simultaneous acquisition of signals of two distinct emission colors. Because this is a custom-built free-standing optical setup, lasers always had to be aligned before each new experiment.

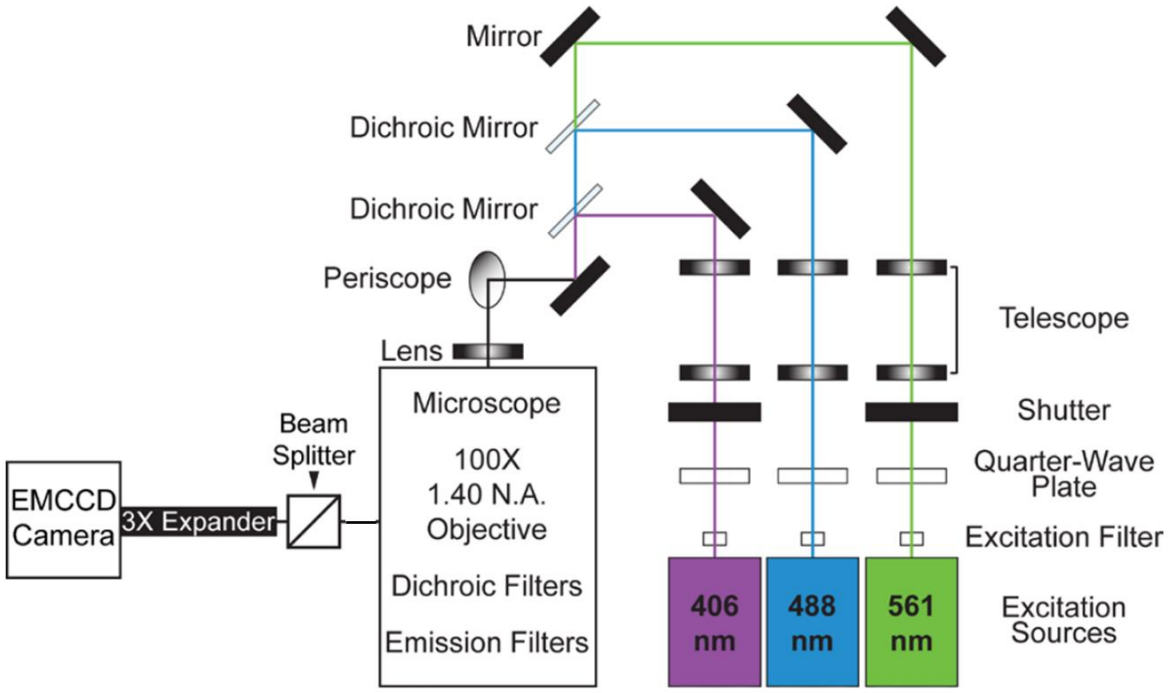

Figure A.1 Optical set-up for single-molecule fluorescence imaging. This figure is adapted and modified from Tuson et al., *Anal. Chem* 2015[9].

A.1.2 Fluorescent proteins

A wide variety of fluorescent proteins are now available for use in various biological applications. Fluorescent proteins come in numerous colors (blue to far-red) and in different oligomeric forms (monomer, dimer and tetramer). The green fluorescent protein GFP is naturally a monomer[10], but other fluorescent proteins such as DsRed and tdTomato have tendencies to oligomerize at high concentrations[11]. The basic strategy for overcoming oligomerization artifacts is to modify the fluorescent protein amino acid sequence to include residues that disrupt intermolecular binding, but this has yet to be done for all fluorescent proteins. For the work in Chapter 3, I used a monomeric mCitrine fluorophore [12]. It is often recommended to use monomeric forms of fluorescent proteins since fluorescent protein oligomerization may give rise to mislocalization artifacts[13].

PAmCherry[14] is a photoactivatable fluorescent protein that I used throughout Chapters 2 and 3. PAmCherry, after activation with violet light (405 nm), absorbs yellow-green light (excitation max = 564 nm) and emits red light (emission max = 595 nm). In contrast, a photoswitchable fluorophore, like EYFP, can initially undergo bleaching and gets reactivated upon excitation with violet laser light[15]. Because of their ability to undergo repeated cycles of activation and reactivation, photoswitchable fluorescent proteins have found unique applications in super-resolution measurements of subcellular structures.

Fluorescent protein tags allow highly specific labeling of the target by genetic encoding, but this advantage must be weighed against the poor quantum yields (e.g. 0.46 for PAmCherry, 0.76 for mCitrine, and 0.79 for PAGFP)[12] of these labels compared to organic dyes (e.g. 0.95 for rhodamine 6 and 0.92 for Alexa Fluor 488)[16]. Though PAGFP exhibits the highest quantum yield out of the fluorophores used in this thesis, I have not been able to detect signals from this fluorescent protein with our microscope setup, likely due to high cellular autofluorescence in the color channel used to image PAGFP. Another factor to consider when choosing fluorophores is how long the fluorescence remains emissive. I want excellent photo-stability for fluorophores in order to obtain longer trajectories for the molecule. With mCitrine and PAmCherry probes, I can get track lengths of more than 5s. One of the issues associated with photoactivatable FPs is that only about 50% of the molecules can be photoactivated into a fluorescent state[17]. However, this problem did not affect us since I was not measuring low copy-number proteins. Another typical problem encountered in fluorescence imaging that did not affect our experiments was the maturation time of fluorescent proteins (~15-30 min) since I imaged fluorescent proteins after allowing them to mature for 4 h or longer.

A.1.3 Data analysis

After collecting single-molecule fluorescence movies, I used custom Matlab code written in the lab to do data analysis. This analysis procedure utilizes a multi-stage post-processing routine. First, a watershed algorithm is applied to segment cells in phase-contrast images. V. cholerae cells were diluted so that overlapping areas between cells were minimized. All subsequent analyses are only performed within the boundary defined by the cell segmentation masks. Then, I applied an *ad hoc* threshold to remove all pixels with intensities comparable to that of autofluorescence, and band-pass filtering was applied to exclude uncorrelated noise signals and to retain correlated ones. Finally, shrinking removes pixels on the edge of objects until only one pixel remains. By taking these peak pixels as a guess, I use a 2D asymmetric Gaussian function to fit the raw intensity values within a box of 15x15 pixels (735 x 735 nm) around each putative peak to obtain the sub-diffraction-limited coordinates of each fluorescent molecule. Candidate molecules with amplitudes lower than the average cell intensity or with center-position uncertainties larger than 300 nm are considered bad fits and excluded from further analyses.

Single-molecule positions can be linked temporally to produce single-molecule trajectories, but a number of factors affect the complexity of single-particle tracking. Though approaches like the simple nearest-neighbor method have addressed challenges associated with fluorophore blinking and molecules crossing, our single-molecule trajectories were constructed using the Hungarian algorithm to globally and simultaneously optimize all possible pairings of molecules between consecutive frames, rather than by sequentially pairing molecules based on spatial proximity[18]. A diffusion coefficient was calculated for each track based on the molecule's mean squared displacement (MSD) during each time lapse τ. Assuming homogenous Brownian

motion, *D* can be obtained from the slope of the MSD curve through the Einstein-Smoluchowski relation in two-dimensional space ($\langle x^2 \rangle = 4D\tau$), where τ is the time tag. A schematic representation of the procedures for calculating diffusion coefficients is given in **Figure A.2**. Only tracks lasting for $\tau \geq 5$ or longer were analyzed; MSDs at higher values of τ were averaged over only a few overlapping displacements and were therefore more error-prone[19]. Based on literature values, FPs typically emit ~10^5 photons before photobleaching[20]. By taking into account electron losses associated with the following—the collection cone of light (~50%), band-pass filters (~75%), quantum yield of the EMCCD (~93%), and experimental noises—and dividing by the photostability of fluorophore (~10-20 imaging frames), photon detection rate equates to ~10^3 photons/frame for my optical setup. In the limit of low background noise, the localization error for a given pixel size and PSF is estimated by this relation,

$$\text{localization error} \sim \frac{1}{\sqrt{number\ of\ photons}},$$

which results in ~30 nm for FPs. Other groups have pushed this localization error down to 10 nm in live cells[21,22]. This theoretical localization error is comparable to the ~50 nm localization error I get from fitting the PSF. Based on localization precision from fitting and a 40 ms integration time, the smallest *D* that can be attributed to real protein motion is 0.012 μm^2/s from this calculation ($\frac{0.05\ \mu m^2}{4 \times 0.04 s}$). However, by taking in account that *D* is a function of τ and $\tau = 5$ in my setup, from this calculation ($\frac{0.012\ \mu m^2/s}{5}$) I get 0.003 μm^2/s. Based on an experiment done in fixed bacterial cells, the apparent motion of PAmCherry molecules was determined to also be 0.003 μm^2/s.[23]

In order to gain statistics for the distribution of diffusion coefficients, I performed bootstrap error analysis in which trajectories of all movies were resampled with replacement 100

times, each generating a data set from which a distribution of diffusion coefficients are calculated. The distribution of D is then fit by a two-term log-normal distribution function to obtain the contributing weights of both populations and their associated diffusion coefficients D_{slow} and D_{fast}. The day-to-day variability in measuring D_{slow} and D_{fast} for the bacterial strains in different growth conditions is accounted by calculating the mean and variation from the distributions of D_{slow} and D_{fast}. The variance in D and populations from day-to-day measurements are reported for the errors in Chapter 2 instead of the smaller variance obtained from bootstrap error analysis.

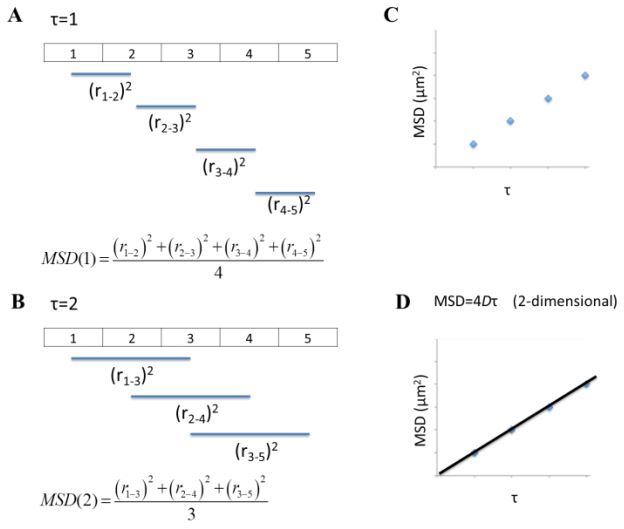

Figure A.2 Schematic representation of the procedures for calculating MSD from a five-frame movie. Only time lag of $\tau = 1$ (A) and $\tau = 2$ (B) is shown here, but $\tau = 3$ and $\tau = 4$ can be calculated in a similar way to generate the points in (C). Using the Einstein-Smoluchowski relation ($MSD = 4D\tau$), a diffusion coefficient is obtained from the MSD vs. τ plot.

A.2 Other related experiments that are not reported in this thesis

A.2.1 *V. cholerae*

- By introducing PAmCherry to the end of the *tcpP* gene, I caused a shift in the open-reading frame that inhibited the transcription of the *tcpH* gene. TcpH plays an accessory role in stabilizing TcpP by preventing TcpP from being degraded[24]. By making the TcpP-PAmCherry protein fusion at the C-terminal end, this resulted in the protein becoming hyper stabilized which prevented this protein fusion from proteolysis by regulate intramembrane proteolysis (RIP)[25]. I have shown that RIP does not work on TcpP-PAmCherry by overexpressing the tail-specific protease (Tsp) in this strain. Because proteolytic activity by Tsp occurs in the periplasmic domain of TcpP, a fluorescent label in this periplasmic region prevents residues TcpPA172 and TcpPI174[26]. By immunoblot against TcpP antibodies, I did not detect the TcpP* fragment—the product of TcpP proteolysis[26].
- To add back TcpH into the endogenous O395 *tcpP-pamcherry* strain, I cloned in a pBAD18:*tcpH* plasmid into this background (CS62). I showed by immunoblot against TcpH antibody that I had successfully added back TcpH into the bacteria. When I imaged this strain on the microscope, I found that TcpP-PAmCherry dynamics were increased when TcpH is overexpressed. Though TcpH stabilizes TcpP interaction to the *toxT* promoter in a wildtype strain[27], this fast TcpP-PAmCherry may be associated with TcpH destabilizing the interaction of TcpP to the promoter due to sterics. Because the mechanisms for TcpH have yet to be elucidated, it is unclear whether or not TcpH interacts with just TcpP or also interacts with other elements of the ToxR regulon.

- Because C-terminal labeled TcpP-PAmCherry cannot be proteolyzed by RIP, I asked if the locations of this fluorophore provided too much steric hindrance for Tsp to locate the site-1 protease. Therefore, I obtained an internally tagged TcpP-Citrine construct (CS13) from Eric Krukonis and tested this protein fusion stability by overexpressing Tsp in this strain. I found that again Tsp was unable to degrade this fluorescently fused TcpP independent of the labeling site. I did not proceed further with this strain as it would not have allowed me to image proteolysis in real-time.
- I also imaged a *V. cholerae* strain where I plasmid-expressed dCas9-mCitrine from an IPTG-inducible promoter. Independent of whether or not I expressed single guide RNAs that targeted the *toxT* promoter, I saw too much expression of dCas9-mCitrine to see any noticeable foci formation at the promoter. Though I had made efforts to clone in dCas9-mCitrine into an exogenous location on the chromosome, this has not yet proven to be a success; part of the problem was related to the size of dCas9-mCitrine fragment. Because I typically do homologous recombination into *V. cholerae* through a suicide vector intermediate, the *dcas9-mcitrine* gene fragment is twice the size of the pKAS32 vector, and so made cloning challenging.
- To generate mutants in *V. cholerae*, I also used a helper plasmid pRK2013[28] (CS85). Though it seemed that the helper plasmid marginally increased the efficiency of getting the suicide plasmid into *V. cholerae*, it did not increase the likelihood of knocking in or knocking out genes.

A.2.2 *E. coli*

- I aimed to elucidate the relationship of Curli Csg proteins and lipoprotein biosynthesis pathways in *E. coli*. Curli is a bacterial amyloid, thus it represents a unique model system to study amyloid fiber formation, along with bacterial protein secretion and macromolecular assembly. The major curli subunit protein CsgA is nucleated into a fiber by CsgB. CsgE, F, and G facilitate secretion and assembly of CsgA into a fiber. Curli is required during initial stages of biofilm development, most likely in attachment phase. I have imaged a DH5α plasmid-expressed C*sgE-PAmCherry* strain and discovered that CsgE localizes at the cellular membrane. Though I saw foci formation, it was unclear whether this was due to overexpression or a relevant phenomenon.

A.3 Strain constructions

Throughout my graduate studies, I have constructed many mutants in various organisms. Table A.1 lists all of the strains that I have both acquired and made in my study.

Table A.1 List of strains in CS-strain box. Strains in red were constructed during this thesis.

Strain	Description of strain	Organism	Resistance
CS1	*Vibrio cholerae* O395 (wild-type)	*V. cholerae*	Strep
CS2	DH5α pGEMT-Easy:*toxR-mcitrine* (linker region) insert	*E. coli*	Amp
CS3	O395 Δ*toxR* Δ*tcpP* pBAD18:*tcpP-pamcherry*	*V. cholerae*	Strep, Kan
CS4	DH5a pMMB66EH (Empty plasmid)	*E. coli*	Amp
CS5	Δ*toxR* pMMB66EH:*toxR-mcitrine*, Δ*tcpP* pBAD18:*tcpP-pamCherry*	*V. cholerae*	Strep, Kan, Amp
CS6	*E. coli* SM10 λ pir	*E. coli*	Kan
CS7	*E. coli* Pir1 (Invitrogen)	*E. coli*	none
CS8	pBAD18 (empty plasmid)	*E. coli*	Kan
CS9	SM10 pKAS32	*E. coli*	Amp

CS10	SM10 pKAS32 (Tamayo)	*E. coli*	Amp, Kan
CS11	DH5α pUCIDT:*toxR-pagfp* (linker region)	*E. coli*	Amp
CS12	DH5α pUCIDT:*tcpP-pamcherry*	*E. coli*	Amp
CS13	O395:*tcpP-citrine* #1 (Krukonis)	*V. cholerae*	Strep
CS14	RY1+pSK:*tcpPH-citrine* #2 (Krukonis)	*V. cholerae*	Strep
CS15	RY1+pSK:*tcpPH-citrine* #2 PREP4 (Krukonis)	*E. coli*	Amp, Kan
CS16	DH5α pGEMT-Easy:*toxR-pagfp* (linker region)	*E. coli*	Amp
CS17	DH5α pGEMT-Easy:*tcpP-pamcherry*	*E. coli*	Amp
CS18	*E. coli* dam$^-$ dcm$^-$	*E. coli*	
CS19	SM10 pKAS32: *toxR-pagfp* (linker)	*E. coli*	Amp, Kan
CS20	SM10 pKAS32:*tcpP-pamcherry*	*E. coli*	Amp, Kan
CS21	SM10 pKAS32:*tcpP-pamcherry*	*E. coli*	Amp, Kan
CS22	SM10 pKAS32:*tcpP-pamcherry*	*E. coli*	Amp, Kan
CS23	SM10 pKAS32:*tcpP-pamcherry*	*E. coli*	Amp, Kan
CS24	O395 Δ*toxR* (parent RA25)	*V. cholerae*	Strep
CS26	O395 Δ*toxRS* (parent RA26)	*V. cholerae*	Strep
CS27	O395 Δ*tcpP* (parent RA67)	*V. cholerae*	Strep
CS28	0395 Δ*tcpH* (RA1376)	*V. cholerae*	Strep
CS29	O395 Δ*toxS* (parent EK 0656)	*V. cholerae*	Strep
CS30	O395 Δ*tcpP* Δ*toxT* (promoter) (parent EK1647)	*V. cholerae*	Strep
CS31	SM10: pKAS32:Δ*toxR* (parent 1647)	*E. coli*	Amp, Kan
CS32	SM10: pKAS32: Δ*toxT* (promoter) (parent EK1645)	*E. coli*	Amp, Kan
CS34	O395:*toxR-pagfp* (chromosome)	*V. cholerae*	Strep
CS35	0395:*toxR-pagfp* (chromosome) in CS-23	*V. cholerae*	Strep
CS37	O395 Δ*toxT* (parent RA 1791)	*V. cholerae*	Strep
CS39	O395:*toxR-pagfp*, *tcpP-pamcherry* (2 color)	*V. cholerae*	Strep
CS41	DH5α pDB110:*toxR-mcitrine* (CTD fusion)	*E. coli*	Amp
CS42	DH5α pBD110:*toxR-mcitrine* (CTD fusion)	*E. coli*	Amp
CS44	DH5α pBD110:*toxR-pagfp* (CTD fusion)	*E. coli*	Amp
CS45	SM10 pKAS32:*toxR-mcitrine* (CTD)	*E. coli*	Amp, Kan
CS46	SM10 pKAS32:*toxR-mcitrine* (CTD)	*E. coli*	Amp, Kan
CS48	SM10 pKAS32:*toxR-pagfp*	*E. coli*	Amp, Kan
CS49	SM10 pKAS32:*toxR-pagfp* (CTD)	*E. coli*	Amp, Kan
CS50	SM10 pKAS32:*toxR-pagfp* (CTD)	*E. coli*	Amp, Kan
CS51	O395:*tcpP-pamcherry*, *toxR-mcitrine* (CTD)	*V. cholerae*	Strep
CS52	O395:*tcpP-pamcherry*, *toxR-mcitrine* (CTD)	*V. cholerae*	Strep
CS53	O395:*tcpP-pamcherry*, *toxR-mcitrine* (CTD)	*V. cholerae*	Strep
CS54	O395:*tcpP-pamcherry*, *toxR-mcitrine* (CTD)	*V. cholerae*	Strep
CS55	O395:*tcpP-pamcherry*, *toxR-mcitrine* (CTD)	*V. cholerae*	Strep
CS57	SM10 pKAS32:*toxR-pamcherry* (internal)	*E. coli*	Amp, Kan
CS58	SM10 pKAS32:*toxR-pamcherry* (internal)	*E. coli*	Amp, Kan
CS59	SM10 pKAS32:*toxR-pamcherry*	*E. coli*	Amp, Kan
CS60	SM10 pKAS32:*toxR-pamcherry*	*E. coli*	Amp, Kan
CS61	DH5a pBAD18:*tcpH*	*E. coli*	Kan
CS62	O395 pBAD18:*tcpH* in CS23	*V. cholerae*	Strep, Kan
CS68	DH5α pBAD18:*tcpH*	*E. coli*	Kan
CS69	DH5α pBAD18:*tcpP*	*E. coli*	Kan
CS70	O395 pBAD18:*tcpH* in CS23	*V. cholerae*	Strep, Kan
CS76	KSK 180 Ron Taylor 0395	*V. cholerae*	Spec, Strep
CS78	KSK 1415 *E. coli* S17 pir pKAS154	*E. coli*	Kan

CS79	pKAS 154 *E. coli*	*E. coli*	Kan
CS81	KD515 pCVD442 EV	*E. coli*	Amp
CS82	S17-1 pir	*E. coli*	Kan
CS83	S17-1 pir pKAS32	*E. coli*	Amp, Kan
CS84	S17-1 pir pKAS32	*E. coli*	Amp, Kan
CS85	MB101 pRK 2013	*E. coli*	Kan
CS120	BW25113 pBAD18:*tcpP-pamcherry*	*E. coli*	Kan
CS121	BW25113 pBAD18:*tcpP-pamcherry*	*E. coli*	Kan
CS122	DH5α pGEMT-Easy:*tcpP*	*E. coli*	Amp
CS123	DH5α pBAD18:*tcpP* (no label)	*E. coli*	Kan
CS124	DH5α pBAD18:*tcpP* (no label)	*E. coli*	Kan
CS125	DH5α pBAD18:*tcpP* (no label)	*E. coli*	Kan
CS126	DH5α pBAD18:*tcpP* (no label)	*E. coli*	Kan
CS127	O395 pBAD18:*tcpP* (no label) in CS-23	*V. cholerae*	Strep, Kan
CS128	O395 pBAD18:*tcpP* (no label) in CS-23	*V. cholerae*	Strep, Kan
CS129	O395 pBAD18:*tcpP* (no label) in CS-23	*V. cholerae*	Strep, Kan
CS130	DH5α pGEMT-Easy:*tcpP-pamcherry*	*E. coli*	Amp
CS131	DH5α pGEMT-Easy:*tcpP-pamcherry*	*E. coli*	Amp
CS132	DH5α pGEMT-Easy:*tcpP-pamcherry*	*E. coli*	Amp
CS133	DH5α pGEMT-Easy:*tcpP-pamcherry*	*E. coli*	Amp
CS134	MG1655 pMMB66EH:*tcpP*-pamcherry	*E. coli*	Carb
CS135	MG1655 pMMB66EH:*tcpP-pamcherry*	*E. coli*	Carb
CS136	MG1655 pMMB66EH:*tcpP*-pamcherry	*E. coli*	Carb
CS137	O395 Δ*tcpP* empty pMMB66EH	*V. cholerae*	Strep, Carb
CS138	O395 Δ*tcpP* pMMB66EH:*tcpP-pamcherry*	*V. cholerae*	Strep, Carb

A.4 References

1. Gustafsson, M. G. L. Nonlinear Structured-Illumination Microscopy: Wide-Field Fluorescence Imaging with Theoretically Unlimited Resolution. *Proc. Natl. Acad. Sci. U. S. A.* **2005**, *102,* 13081-13086.

2. Hein, B.; Willig, K. I.; Hell, S. W. Stimulated Emission Depletion (STED) Nanoscopy of a Fluorescent Protein-Labeled Organelle Inside a Living Cell. *Proceedings of the National Academy of Sciences* **2008**, *105,* 14271-14276.

3. Grotjohann, T.; Testa, I.; Leutenegger, M.; Bock, H.; Urban, N. T.; Lavoie-Cardinal, F.; Willig, K. I.; Eggeling, C.; Jakobs, S.; Hell, S. W. Diffraction-Unlimited all-Optical Imaging and Writing with a Photochromic GFP. *Nature* **2011**, *478,* 204-208.

4. Betzig, E.; Patterson, G. H.; Sougrat, R.; Lindwasser, O. W.; Olenych, S.; Bonifacino, J. S.; Davidson, M. W.; Lippincott-Schwartz, J.; Hess, H. F. Imaging Intracellular Fluorescent Proteins at Nanometer Resolution. *Science* **2006**, *313,* 1642-1645.

5. Hess, S. T.; Girirajan, T. P. K.; Mason, M. D. Ultra-High Resolution Imaging by Fluorescence Photoactivation Localization Microscopy. *Biophys. J.* **2006**, *91,* 4258-4272.

6. Rust, M. J.; Bates, M.; Zhuang, X. Sub-Diffraction-Limit Imaging by Stochastic Optical Reconstruction Microscopy (STORM). *Nat. Methods* **2006**, *3,* 793-795.

7. Manley, S.; Gillette, J. M.; Patterson, G. H.; Shroff, H.; Hess, H. F.; Betzig, E.; Lippincott-Schwartz, J. High-Density Mapping of Single-Molecule Trajectories with Photoactivated Localization Microscopy. *Nat. Methods* **2008**, *5,* 155-157.

8. Dempsey, G. T.; Vaughan, J. C.; Chen, K. H.; Bates, M.; Zhuang, X. Evaluation of Fluorophores for Optimal Performance in Localization-Based Super-Resolution Imaging. *Nat. Methods* **2011**, *8,* 1027-1036.

9. Tuson, H. H.; Biteen, J. S. Unveiling the Inner Workings of Live Bacteria using Super-Resolution Microscopy. *Anal. Chem.* **2015**, *87,* 42-63.

10. Chudakov, D. M.; Matz, M. V.; Lukyanov, S.; Lukyanov, K. A. Fluorescent Proteins and their Applications in Imaging Living Cells and Tissues. *Physiol. Rev.* **2010**, *90,* 1103-1163.

11. Shaner, N. C.; Campbell, R. E.; Steinbach, P. A.; Giepmans, B. N. G.; Palmer, A. E.; Tsien, R. Y. Improved Monomeric Red, Orange and Yellow Fluorescent Proteins Derived from *Discosoma* Sp. Red Fluorescent Protein. *Nat. Biotechnol.* **2004**, *22,* 1567-1572.

12. Shaner, N. C.; Steinbach, P. A.; Tsien, R. Y. A Guide to Choosing Fluorescent Proteins. *Nat. Methods* **2005**, *2,* 905-909.

13. Verkhusha, V. V.; Lukyanov, K. A. The Molecular Properties and Applications of Anthozoa Fluorescent Proteins and Chromoproteins. *Nat. Biotechnol.* **2004**, *22*, 289-296.

14. Subach, F. V.; Patterson, G. H.; Manley, S.; Gillette, J. M.; Lippincott-Schwartz, J.; Verkhusha, V. V. Photoactivatable mCherry for High-Resolution Two-Color Fluorescence Microscopy. *Nat. Methods* **2009**, *6*, 153-159.

15. Biteen, J. S.; Thompson, M. A.; Tselentis, N. K.; Shapiro, L.; Moerner, W. E. Superresolution Imaging in Live *Caulobacter Crescentus* Cells using Photoswitchable Enhanced Yellow Fluorescent Protein. *Proc. SPIE* **2009**, *7185*, 71850I.

16. Magde, D.; Wong, R.; Seybold, P. G. Fluorescence Quantum Yields and their Relation to Lifetimes of Rhodamine 6G and Fluorescein in Nine Solvents: Improved Absolute Standards for Quantum Yields. *Photochem. Photobiol.* **2002**, *75*, 327-334.

17. Durisic, N.; Laparra-Cuervo, L.; Sandoval-Álvarez, Á; Borbely, J. S.; Lakadamyali, M. Single-Molecule Evaluation of Fluorescent Protein Photoactivation Efficiency using an *in Vivo* Nanotemplate. *Nat. Methods* **2014**, *11*, 156-162.

18. Liao, Y.; Schroeder, J. W.; Gao, B.; Simmons, L. A.; Biteen, J. S. Single-Molecule Motions and Interactions in Live Cells Reveal Target Search Dynamics in Mismatch Repair. *Proc. Natl. Acad. Sci. U. S. A.* **2015**, *112*, E6898-E6906.

19. Michalet, X. Mean Square Displacement Analysis of Single-Particle Trajectories with Localization Error: Brownian Motion in an Isotropic Medium. *Phys. Rev. E: Stat. , Nonlinear, Soft Matter Phys.* **2011**, *82*, 041914.

20. Kubitscheck, U.; Kueckmann, O.; Kues, T.; Peters, R. Imaging and Tracking of Single GFP Molecules in Solution. *Biophys. J.* **2000**, *78*, 2170-2179.

21. Bates, M.; Huang, B.; Dempsey, G. T.; Zhuang, X. Multicolor Super-Resolution Imaging with Photo-Switchable Fluorescent Probes. *Science* **2007**, *317*, 1749-1753.

22. Biteen, J. S.; Thompson, M. A.; Tselentis, N. K.; Bowman, G. R.; Shapiro, L.; Moerner, W. E. Super-Resolution Imaging in Live *Caulobacter Crescentus* Cells using Photoswitchable EYFP. *Nat. Methods* **2008**, *5*, 947-949.

23. Liao, Y.; Li, Y.; Schroeder, J. W.; Simmons, L. A.; Biteen, J. S. Single-Molecule DNA Polymerase Dynamics at a Bacterial Replisome in Live Cells. *Biophys. J.* **2016**, *111*, 2562-2569.

24. Carroll, P. A.; Tashima, K. T.; Rogers, M. B.; DiRita, V. J.; Calderwood, S. B. Phase Variation in *tcpH* Modulates Expression of the ToxR Regulon in *Vibrio Cholerae*. *Mol. Microbiol.* **1997**, *25*, 1099-1111.

25. Matson, J. S.; DiRita, V. J. Degradation of the Membrane-Localized Virulence Activator TcpP by the YaeL Protease in Vibrio Cholerae. *Proc. Natl. Acad. Sci. U. S. A.* **2005**, *102*, 16403-16408.

26. Teoh, W. P.; Matson, J. S.; DiRita, V. J. Regulated Intramembrane Proteolysis of the Virulence Activator TcpP in Vibrio Cholerae is Initiated by the Tail-Specific Protease (Tsp). *Mol. Microbiol.* **2015**, *97*, 822-831.

27. Beck, N. A.; Krukonis, E. S.; DiRita, V. J. TcpH Influences Virulence Gene Expression in *Vibrio Cholerae* by Inhibiting Degradation of the Transcription Activator TcpP. *J. Bacteriol.* **2004**, *186*, 8309-8316.

28. Figurski, D. H.; Helinski, D. R. Replication of an Origin-Containing Derivative of Plasmid RK2 Dependent on a Plasmid Function Provided in Trans. *Proc. Natl. Acad. Sci. U. S. A.* **1979**, *76*, 1648-1652.